2019-01-01

Bioprinted Mcf7 Breast Cancer Cells, An In Vitro Model For Drug Discovery

Aleli Campbell
University of Texas at El Paso

BIOPRINTED MCF7 BREAST CANCER CELLS, AN *IN VITRO* MODEL FOR DRUG DISCOVERY

ALELI CAMPBELL
Doctoral Program in Biomedical Engineering

APPROVED

Thomas Boland, Ph.D, Chair

Armando Varela-Ramirez, Ph.D

Wei Qian, Ph.D

Alexander Philipovskiy, M.D.,Ph.D

Stephen Crites, Ph.D
Dean of Graduate School

Dedication

To my beloved ever patient husband, Ron, and my children, Kevin and Deanna.

BIOPRINTED MCF7 BREAST CANCER CELLS, AN *IN VITRO* MODEL FOR DRUG DISCOVERY

by

ALELI CAMPBELL, M.S.

DISSERTATION

Presented to the Faculty of the Graduate School of
The University of Texas at El Paso
in Partial Fulfillment
of the Requirements
for the Degree of

DOCTOR OF PHILOSOPHY

Metallurgical, Materials and Biomedical Engineering
THE UNIVERSITY OF TEXAS AT EL PASO
December 2019

Acknowledgements

I would like to thank my PhD advisor, Dr. Thomas Boland, for his guidance and support during the PhD program. I am very grateful to Dr. Boland for giving me the opportunity to be a part of his research team and for giving me the freedom to pursue the PhD topic I am passionate about. He also provided very insightful information about research and always encouraged me to think more independently about my experiments and results. I have learned so much from you!

I am very thankful to Dr. Varela-Ramirez for his patience and scientific advice during cell culture and cell testing. He was my primary resource for answering questions related to lab experiments. Also, Dr. Philipovskiy who always provided me with challenging questions which helped me pay attention to details. I know I have to do more listening and less talking! I also have to thank Dr. Qian for his helpful advice and suggestions in general, I am very grateful to have him in my committee. Special thanks to Luis Solis and Jonathon Mohl for your invaluable advice.

To my lab mates, Beu, Michael, Carlos, Sorour and Huda thanks for your understanding these last couple of years; I wish you all the best of luck. I must also thank Ralph Loya, whom I would go to when I needed special requests. I know he will miss me for he won't have me to bother him anymore. I also want to thank Zeina Nahleh for being very supportive, she was an inspiration and a role model; Dr. Vines, Dr. Joddar, Bea Tarango, Silvia Balli, Gladys Almodovar, Denisse Gutierrez and Alondra for their helpfulness during this research. Also, many thanks to my friend, Rose Heydarian, who was also very supportive and always had generous words of encouragement and

advice. I am truly blessed to be surrounded by such supportive personalities, in one way or another I have learned from each of you. My mom, Aurora, who was also always very caring and loving. To my sister in law, Kay Merchant and my sisters, Ofelia, Emma, Lupita and Carolina for encouraging me to reach for the stars!

This study was supported by the National Institute of General Medical Sciences of the National Institutes of Health under linked Award Numbers RL5GM118969, TL4GM118971, and UL1GM118970, and NIH-NIMHD-RCMI Grant No. 5G12MD007592 (BRB). Grants 5G12MD007592 and 5U54MD007592 from the National Institute on Minority Health and Health Disparities (NIMHD), a component of the National Institutes of Health (NIH), to Border Biomedical Research Center (BBRC) at UTEP.

Abstract

Current breast cancer treatments are successful in eradicating this disease in the majority of patients, though there are quite a few cases where relapse or recurrence follow, which may lead to continued cancer therapy or death. Thermal inkjet bioprinting (BP) is a novel technique that is used to bioprint biomaterials or diverse cellular organisms to engineer tissue or organ models *in vitro*. In this dissertation, we investigated the molecular effect of BP MCF7 breast cancer cells (BCC), cell survival of the cells when exposed to FDA approved systemic therapy alone and in combination with radiation and lastly, the ability of the cells to form tumors in immunodeficient mice. In the Phospho-MAPK array, a total of 21 kinases were phosphorylated in the BP MCF7 cells, whereas 9 were phosphorylated in the manually seeded controls. The RNA sequence analysis of the BP MCF7 cells identified a total of 12,235 genes, of which 9.7% were statistically differentially expressed. Using a *q-value* ≥ 0.05 and a ± 2 fold change as the cutoff value for the number of upregulated and downregulated genes, a total of 266 and 206 respectively were observed, with 5 genes uniquely expressed in the BP cells: NRN1L, LUCAT1, IL6, CCL26, and LOC401585. When Bioprinted MCF7 BCCs were challenged with Tamoxifen, we observed an 8-10% cell viability higher than MS BCCs at 10μM, 90μM and 110μM concentrations with a statistical significance and similar results were obtained when cells were exposed to palbociclib + letrozole at 10μM, 50μM, 100μM and 150μM. Statistical significance was observed at 10μM, 100μM and 150μM concentrations of palbociclib, $p < .05$. Results from the tissue we analyzed of the implanted BP MCF7 BCCs appeared to contain some hyperplasia with carcinoma in situ, whereas in the tissue from the manually seeded implants we were unable to identify cancerous cells. In the phosphoMAPK array, bioprinted MCF7 cells showed increased levels of phosphorylation in analytes that have been identified as key players in activating critical pathways that, when dysregulated, are associated with biological aggressive oncogenic properties. RNA data suggest that thermal inkjet bioprinting is stimulating large scale gene alterations that could potentially be used for drug discovery. These biological investigations will change the approach to future drug discovery in vitro when applying thermal inkjet bioprinting. Furthermore, this technique could also be applied to bioprint autologous samples nor only with MCF7 breast cancer cells but with any other cancer cells to predict with higher certainty whether a potential treatment regimen will work effectively in cancer patients.

Table of Contents

List of Tables

List of Figures

Chapter 1

1.1 Introduction

Breast cancer is an asymptomatic and complex disease. It accounts for nearly 25 percent of all cancers in women of all ethnicities [7]. There are at least 75 histological classifications of tumors of the breast recognized by the World Health Organization (WHO)[7]. Incident rates of breast cancer are higher for women in ages 39 to 69 [7, 8]. Per the Center for Disease Control (CDC), the breast is the top cancer site identified for females, and it includes all ethnicities: Whites, Asians, Native Americans, African-Americans, and Hispanics in the United States in 2016, where the incidence is approximately 127 per 100,000 [9]. One in eight women will develop cancer in their lifetime in the U.S. and one in six women, globally[10, 11]. Furthermore, 41,760 women are projected to die from breast cancer in 2019 in the US. Additionally, approximately 268,600 new breast cancer cases are estimated to be diagnosed in 2019 [10, 12].

Breast cancer originates in the mammary parenchymal epithelium at either the lobular or ductal unit, but its development is not well understood[1]. Cancer, as defined by the medical dictionary, is not one but a large group of approximately 100 diseases; characteristics include uncontrolled growth of cells in the human body which are capable of migrating from its original site of development to distant sites in the body. Each cancer type is named after its anatomic site in the body, e.g. lung cancer for cancer in the lungs, breast cancer for cancer in the breast, etc.; additionally, the majority of cancers can take decades to develop and it can go undetected due to their asymptomatic nature [3].

In vitro testing is a crucial step during target and phenotypic based drug discovery. These type of studies provide overall knowledge on the efficacy of a drug in the molecular phenotype of cellular organisms [13]. *In vitro* models that use the two dimensional (2D) approach lack the pharmacokinetic response that the *in vivo* testing provides[14, 15]. Results from *in vitro* experiments, however, contribute with information that can later be used *in vivo* through the study of animal models [16]. Options for selecting a drug test model can range from the conventional 2D cell culture in a petri dish, to the very complex three-dimensional (3D) approach [16, 17]. Despite the many options available, there is no standard way of using one method versus the other. 3D *in vitro* models are typically used to study cellular behavior in an environment that can simulate models *in vivo* [18]. One of the advantages of using *in vitro* experiments is that they provide reasonable data on how these models will behave when subjected to new test environments, whether these are of chemical or physical nature. Another advantage is that, initially, these tests can be performed without having to experiment in animals or humans. Though as more knowledge is gained, scientists are able to more accurately predict cellular functions in their native microenvironments during drug discovery, which in turn helps develop more effective drugs.

In an effort to address this issue, a series of experiments are proposed to develop *in vitro* tumor models for drug discovery. This research is subdivided into three aims: aim one consists of developing and analyzing this model *in vitro*. In this aim, we will evaluate the model through a differential nucleotide assay, RNA sequential analysis, and identify the relative levels of phosphorylation of Mitogen-Activated Protein Kinases and other serine / threonine kinases (phospho-MAPK) through a human phospho-MAPK

assay. Aim two involves testing the *in vitro* models with commercially available drugs, such as tamoxifen and palbociclib + letrozole concurrently with or without radiation therapy. Tamoxifen is an FDA approved estrogen modulator that is used to treat and prevent breast cancer in premenopausal and post-menopausal women. Palbociclib plus letrozole have been approved to treat late-stage breast cancer [19]. Though the combination of these three treatments, palbociclib, letrozole and radiation, has not been approved to treat breast cancer patients. Finally in aim three, we will test the biological response of the bioprinted tumor models *in vivo*. This will be accomplished by implanting bioprinted MCF7 breast cancer cells in immunocompromised mice (SCID). The implants will be grafted subcutaneously in the ventral area near the mammary fat pads.

1.2 Breast Cancer

There are over 70 histological classifications of tumors of the breast recognized by the World Health Organization (WHO) [7]. Incident rates of breast cancer are higher for women in ages 39 to 69 [7, 8]. Per the Center for Disease Control (CDC), the breast is the top cancer site identified for females and includes all ethnicities: Whites, Asians, Native Americans, African-Americans, and Hispanics in the United States in 2015. The National Vital Statistics Report recorded a slight decrease in mortality rates ranging from 3.9 per 100,000 population to 3.7 per 100,000 from 2005 to 2015 of malignant neoplasms in November 2017 and a significant decrease was observed from 1999 to 2005 (7.7 per 100,000) [8]. Despite the fact that breast cancer mortality rates have decreased, morbidity remains high. The pain and suffering breast cancer patients are

subjected to throughout the entire treatment affects not only patients, but also family members and society as a whole.

The majority of breast cancers originate in the mammary epithelium, specifically in the terminal duct lobular units (TDLU) [20]. Laterality of breast cancer is slightly higher in the left side than the right side and between 50 – 60 % of the tumors appear in the upper outer quadrant of the breast (near the axilla) [21]. Breast tumors are classified according to the type of biomarkers they express. Receptor positive breast cancers respond to endocrine therapy and nearly 70% of all breast malignancies fall under this category, in contrast to receptor negative breast cancers that do not [22]. In particular, triple negative breast cancer is associated with worse outcomes [23]. To date, a total of eight different endocrine drugs have been approved in the US (megestrol, tamoxifen, goserelin, anastrozole, letrozole, toremifene, exemestane and fulvestrant).

Breast cancer does not typically presents symptoms. Though the most frequent method of detection when there are symptoms, are breast lumps with or without pain [20]. Some of the systemic symptoms include, loss of appetite, weight loss, and fatigue, other symptoms include urinary difficulties, change of bowel patterns and skin symptoms [24, 25]. Early detection of breast cancers is associated with better outcomes.

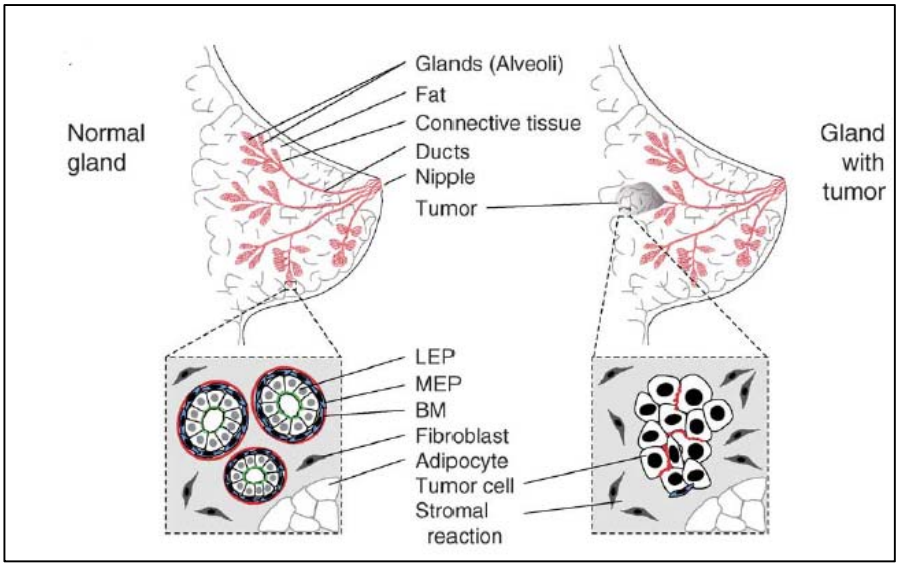

Figure 1.1: Architecture of the breast (Normal versus cancerous Gland) [1]

1.3 Etiology

Root causes associated with this heterogeneous disease are not well established. However, the following factors have been linked with the risk of developing breast cancer: genetics, early menarche, late childbearing, hormonal imbalance, high consumption of red meats and alcohol, exposure to ionizing radiation, higher body weight, and lack of physical activity [26]. Additionally, in this fast-paced society, lifestyle and eating habits, play an important role in hormone regulation and this could increase the risk of developing abnormalities that may lead to cancer. Alcoholic beverage consumption is another risk factor for the development of breast cancer [27]. On the other hand, some risks that cannot be changed includes genetics. In these cases, early genetic testing and surveillance play a key role in detecting it at an early stage, which may improve prognosis outcome [28, 29].

1.4 Stages of Breast Cancer

There are two categories for staging breast cancer: the anatomic stage group and the prognosis stage group. The American Joint Committee for Cancer (AJCC) began the TNM staging for breast cancer in 1956 [30]. TNM Staging of Breast cancer stage is based on **T**umor size, lymph **N**ode involvement and cell **M**etastasis and it also includes clinical and pathological staging [31, 32]. Prognosis tumor (T) staging is comprised of eight levels and eight sublevels, ranging from T**x**, where the tumor cannot be assessed to T4d, where the tumor has been evaluated as an inflammatory carcinoma that may have crossed the chest wall or has invaded other areas, see table 1 [31, 33, 34]. Lymph Node (N) staging is based in two stages as well (pretreatment and post-treatment), clinical and pathological (cN,pN). Within these stages there are five main levels: NX, N0, N1, N2 and N3, with six sub-classifications for the clinical stage and eleven for the pathological stage, see table 2 below[35, 36]. M staging has two levels, cM0, cM1 and pM1, and one sublevel, cM0(i+), see Table 1.3 for additional details.

Table 1.1 Tumor categories, reproduced from Amin MB, Edge SB, Greene FL, et al, eds. AJCC Cancer Staging Manual. 8th edition, New York: Springer; 2017.

T Level	**Criteria**
TX	Primary tumor could not be assessed
T0	No evidence of primary tumor
Tis (DCIS)[a]	Ductal carcinoma in situ (DCIS)
Tis (Paget)	Paget disease of the nipple NOT associated with invasive carcinoma and/or carcinoma in situ (DCIS) in the underlying breast parenchyma. Carcinomas in the breast parenchyma associated with Paget disease are categorized based on the size and characteristics of the parenchymal disease, although the presence of Paget disease should still be noted.
T1	Tumor ≤ 20mm in greatest dimension
-T1mi	Tumor ≤ 1mm in greatest dimension
-T1a	Tumor > 1mm but ≤ 5mm in greatest dimension (round any measurement from > 1.0-1.9mm to 2mm)
-T1b	Tumor > 5mm but ≤ 10mm in greatest dimension
-T1c	Tumor > 10mm but ≤ 20mm in greatest dimension
T2	Tumor > 20mm but ≤ 50mm in greatest dimension
T3	Tumor > 50mm in greatest dimension
T4	Tumor of any size with direct extension to the chest wall and/or to the skin (ulceration or macroscopic nodules); invasion of the dermis alone does not qualify as T4
-T4a	Extension to the chest wall; invasion or adherence to pectoralis muscle in the absence of invasion of chest wall structures does not qualify as T4
-T4b	Ulceration and/or ipsilateral macroscopic satellite nodules and/or edema (including peau d'orange) of the skin that does not meet the criteria for inflammatory carcinoma.
-T4c	Both T4a and T4b are present
-T4d	Inflammatory carcinoma (see "Rules for Classification")

Table 1.2. Lymph node categories, reproduced from Amin MB, Edge SB, Greene FL, et al, eds. AJCC Cancer Staging Manual. 8th edition, New York: Springer; 2017.

N Stages	**Characteristics**
cNX[b]	Regional lymph nodes cannot be assessed (eg, previously removed)
cN0	No regional lymph node metastases (by imaging or clinical examination)
cN1	Metastases to movable ipsilateral level I and II axillary lymph node(s)
-cN1mi[c]	Micrometastases (approximately 200 cells, larger than 0.2mm, but no larger than 2.0mm)
cN2	Metastases in ipsilateral level I and II axillary lymph nodes that are clinically fixed or matted; or in ipsilateral internal mammary lymph nodes in the absence of axillary lymph node metastases
-cN2a	Metastases in ipsilateral level I and II axillary lymph nodes fixed to one another (matted) or to other structures
-cN2b	Metastases only in ipsilateral internal mammary lymph nodes in the absence of axillary lymph node metastases
cN3	Metastases in ipsilateral infraclavicular (level III axillary) lymph node(s) with or without level I and II axillary lymph node involvement; or in ipsilateral internal mammary lymph node(s) with level I and II axillary lymph node metastases; or metastases in ipsilateral supraclavicular lymph node(s) with or without axillary or internal mammary lymph node involvement
-cN3a	Metastases in ipsilateral infraclavicular lymph node(s)
-cN3b	Metastases in ipsilateral internal mammary lymph node(s) and axillary lymph node(s)
-cN3c	Metastases in ipsilateral supraclavicular lymph node(s)

Table 1.3. Lymph node categories, reproduced from Amin MB, Edge SB, Greene FL, et al, eds. AJCC Cancer Staging Manual. 8th edition, New York: Springer; 2017.

M Stages	**Characteristics**
M0	No clinical or radiographic evidence of distant metastases
-cM0(i+)	No clinical or radiographic evidence of distant metastases in the presence of tumor cells or and no deposits no greater than 0.2mm detected microscopically or by using molecular techniques in circulating blood, bone marrow, or other nonregional lymph node tissue in a patient without symptoms or signs of metastases
M1	Distant metastases detected by clinical and radiographic means (cM) and/or histologically proven metastases larger than 0.2mm (pM)

In the newly revised edition of breast cancer staging, hormonal status, estrogen receptors (ER), progesterone receptors (PR) and Human Epidermal Growth Factor Receptor 2 (Her2/neu) expression, histological features, ductal or lobular and tumor grade also are included in the prognostic staging of the AJCC staging manual [31, 33].

In anatomic staging, breast tumors are classified mostly based on physical attributes, such as tumor size, lymph node involvement and metastasis. Anatomic staging provides quantitative information over the primary tumor size, regional lymph nodes and metastasis [33, 37]. In addition, anatomic staging is used to report treatment outcomes and to maintain a common language with countries without means to report on pathobiological markers[37]. Refer to table 1.4 for details of anatomic staging.

Table 1.4. Anatomic stages, reproduced from Amin MB, Edge SB, Greene FL, et al, eds. AJCC Cancer Staging Manual. 8th edition, New York: Springer; 2017.

ANATOMIC STAGES / PROGNOSTIC GROUPS			
When T is…	**And N is…**	**And M is…**	**Then The Group Stage is…[b]**
Tis	N0	M0	0
T1	N0	M0	IA
T0	N1mi	M0	IB
T1	N1mi	M0	IB
T0	N1	M0	IIA
T1	N1	M0	IIA
T2	N0	M0	IIA
T2	N1	M0	IIB
T3	N0	M0	IIB
T1	N2	M0	IIIA
T2	N2	M0	IIIA
T3	N1	M0	IIIA
T3	N2	M0	IIIA
T4	N0	M0	IIIB
T4	N1	M0	IIIB
T4	N2	M0	IIIB
Any T	N3	M0	IIIC
Any T	Any N	M1	IV

Ductal Carcinoma in Situ (DCIS) is a cancer in its very early stage (T0), cancer cells are typically found locally within a breast quadrant and cancer cells are scattered throughout as opposed to tightly packed forming a small tumor [35, 38].

1.5 Breast Cancer Detection Methods

Per the Society of Breast Imaging and the American College of Radiology, women 40 years of age and older qualify for yearly mammograms or anyone who is high risk (e.g., family history of cancers) also qualifies for early screening [35, 39]. Several detection methods exist, ranging from self-examinations to yearly clinical exams done by a clinical provider, to mammography, ultrasound (US) and in some cases, breast Magnetic Resonance Imaging (MRI), and rarely used is Positron Emission Technology (PET)[39, 40]. The approved method of choice by the Breast Imaging Commission of the American College of Radiology (ACR) for breast cancer detection though, is through mammography [39]. With the advancement of new technologies, however, adjunctive methods are being used, such as Ultrasound, breast MRIs, and PETs [41]. These detection methods are supplemental to mammography and are used for corroboration when suspicious masses are detected and are used as the second “opinion” for validation [42, 43]. Some of these methods have been approved only for women with high risk (> 20 %) [35, 39].

Due to the asymptomatic nature of this disease, it is recommended to perform self-examinations habitually. Self-examination is often recommended three to four days after monthly menstrual period ends, which include manually palpating each breast trying to detect a lump or an abnormality and completing self-examination with a slight squeeze of the nipple to check for fluid discharge [40]. Additionally, the clinical provider will also perform a similar examination during yearly checkups. A mammogram is a form of X-ray imaging that is taken of the area in question. Each breast is compressed

and scanned in three different positions with intention to detect abnormal masses, figure 1.2 [44, 45].

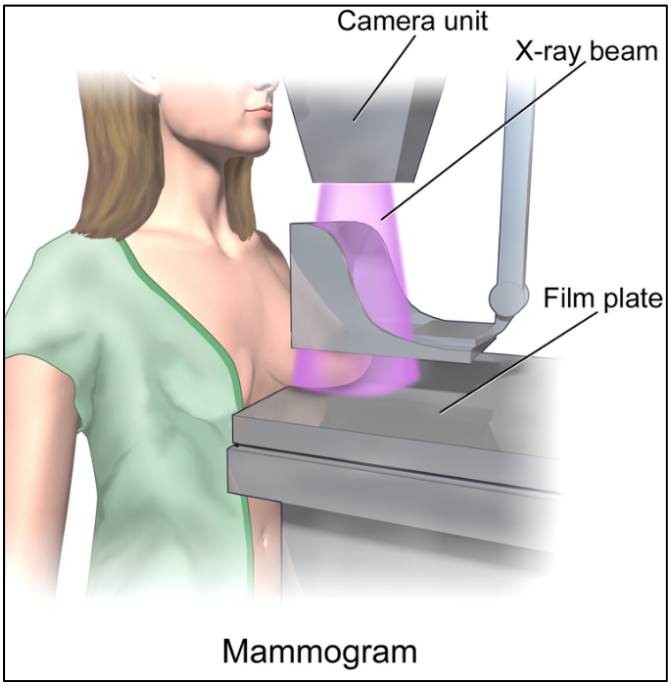

Figure 1.2: Mammography Imaging Technique [2, 46]

Ultrasound produces imaging as well and it uses ultrasound waves to detect masses or other suspicious areas during a scan [41, 47]. Breast MRIs though less common is also used to aid in the detection of breast cancers. This technology uses the nuclear magnetic resonance of atoms within the body to create imaging to also detect abnormal masses [47, 48]. Even though MRI does not have exposure to ionizing radiation, it is rather expensive and some precautions are required for its use, such as the removal of foreign implanted material including metal objects [45, 49, 50]. More importantly, there have been cases where MRI has failed to detect Ductal Carcinoma In-Situ (DCIS) [39, 47, 51]. Another detection method also available but not often used is Positron Emission Tomography (PET). PET is another imaging modality that involves

radioactive tracer isotopes, which are injected intravenously; this procedure is a reliable method to determine metastasis of cancer, yet it also is very expensive and exposes patients to radiation [39, 45, 49]. Finally, molecular imaging enables visualization of the cellular function and the follow-up of the molecular process in living organisms without altering them. However, this type of imaging uses probes known as biomarkers to help image particular targets or pathways and it is an ex-vivo process [50, 52, 53]. The process is typically used post-biopsies to identify biomarkers present in tumor samples. In addition, the results are next used to determine the type of treatment regimen a patient will receive.

The cost associated with treating one breast cancer patient can range from approximately 70k to 185k in a 24 month period [54, 55]. This cost does not include patient copays or transportation-related costs. After the initial treatment (surgery and chemotherapy) is completed, some breast cancer patients may be required to continue hormonal treatment for up to ten years depending on the type and stage of their cancer [56, 57]. In addition, follow up visits to the oncologist could range from every three to six months depending on the biological characteristics of the cancer. Furthermore, ongoing tests that are required prior to each visit may include blood work, CT-Scans, Ultrasound, MRI and mammograms, as necessary [58].

1.6 Breast Cancer Treatment Options

Staging and other factors play a role in determining the type of treatment a breast cancer patient will receive [58]. Oncologists have several treatment options when treating breast cancer patients as they follow guidelines set out by the National

Comprehensive Cancer Network (NCCN) [56, 59]. Per NCCN guidelines, the cancer parameters identified above are used to determine the type of treatment each breast cancer patient will receive [56]. Factors associated with treatment options are stage (also classified as TNM), tumor grade and hormonal status (estrogen receptors, progesterone receptors) [33, 56].

Additionally, cancer therapies follow a set of predetermined standard procedures as defined by NCCN/ASCO guidelines [56, 60]. Another option for chemotherapy treatment for stage II and III breast cancer, consists of neoadjuvant treatment, if the patient meets criteria [56, 61]. This treatment lasts typically from three to six months. The step after neoadjuvant chemotherapy surgery proceeds next (tumor excision) followed by 2-4 weeks or recovery time [19, 60]. Continued treatment with chemotherapy is a possibility, and may be followed by radiotherapy[56]. In some cases, chemotherapy may not be an option this is based on each patient's biological tumor markers[56]. Then, once the patient has completed both therapies and based on hormonal status each patient may be given Hormonal Therapy (HT) for five to ten years [56]. Early-stage breast cancer patients may receive surgery and radiation or just surgery, which really depends on each patient's biomarkers [35, 55, 56].

1.7 Breast Cancer Cell Characteristics

Established breast cancer cell types are cultured to represent specific tumor types, e.g., ER+/-, PR+/-, Her2/neu+/- [61]. These biomarkers are used in the clinical setting because they impact the type of treatment that a patient will receive. In the biomedical research setting, the molecular classification is also utilized, see *Table 1.5 (adapted*

from 61). MCF7 breast cancer cells are classified as Luminal A (or ER/PR +, Her2/neu -) while MDA-MB231 claudin-low cancer cells (or triple negative breast cancer cells for their biomarkers, ER/PR/Her2/neu -) from metastatic adenocarcinoma, and MDA-MB-468 basal type cancer cells (aka triple negative breast cancer cells) [22]. During target drug discovery these cell lines are typically used; this approach provides a basic understanding of breast cancer biology [22, 62].

Table 1.5.Breast cancer cells:molecular and clinical classifications (adapted from [22, 63])

Molecular Classification	**Clinical profile**	**Additional characteristics (Mutations)**	**Example cell lines**
Luminal A	ER^+, $PR^{+/-}$, $HER2^-$	Ki67 low, endocrine responsive, often chemotherapy responsive	MCF-7, T47D, SUM185, HCC1428, MDA-MB-175-VII
Luminal B	ER^+, $PR^{+/-}$, $HER2^+$	Ki67 high, endocrine, variable to chemotherapy. $HER2^+$ are responsive to trastusumab	BT474, ZR-75
Basal Like	ER^-, PR^-, $HER2^-$	$EGFR^+$ and/or cytokeratin $5/6^+$, Ki67 high, (associated with BRCA1/2 gene mutations), TP53, PTEN, etc., nonresponsive to endocrine, often responsive to chemotherapy	MDA-MB-468, SUM190, HCC2157, HCC38, CAL851, HCC70, HCC1599, HCC1937, HCC1143,
Claudin-low	ER^-, PR^-, $HER2^-$	Ki67, E-cadherin, claudin-3, claudinin-4 and claudinin-7 low, PIK3CA, HRAS, RB1, PTEN, TP53, BRCA1, CDKN2A, KRAS, PDGFRA, NF1. Intermediate response to chemotherapy	BT549, MDA-MB-231, MDA-MB-157, MDA-MB-436, HS578T, SUM1315, CAL-51, CAL-120
HER2	ER^-, PR^-, $HER2^+$	Ki67 high, responsive to trastusumab and chemotherapy	SKBR3, MDA-MB-453
ER, estrogen receptor; PR, progesterone receptor; HER2, human epidermal growth factor receptor 2; EGFR, epidermal growth factor receptor; -, negative; +, positive.			

Cancer cells have been observed to have the ability to display both, a paracrine and autocrine system, and as a result, this may lead to uncontrollable cell replication [64,

65]. In the paracrine signaling system that functions normally, a growth factor receptor only triggers a signal into the cytoplasm when a ligand is bound to it, *figure 1.3* [3]. However, when the genes that encode such receptors are mutated, signal firing is independent of ligand binding and can continuously emit signals. This is defined as autocrine signaling, which is observed in cancer cells [3]. Autocrine signaling can also be a result of receptor overexpression or of receptors that are also truncated, also due to genetic mutations, *figure 1.4*. An increased number of ligand-independent receptors in the cell surface may cause collisions which lead to receptor dimerization and a continuous signal emission inducing to cell proliferation [3]. The ability of cancer cells to emit independent signaling is what leads to cellular conglomeration resulting in cancer development.

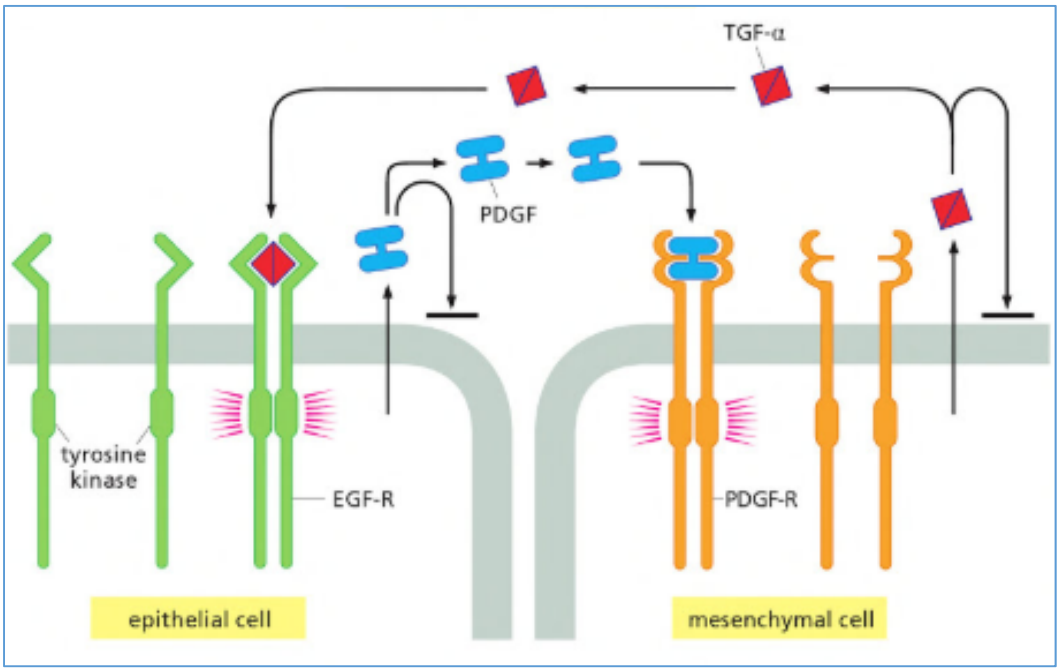

Figure 1.3 Example of a normal paracrine signaling [3].

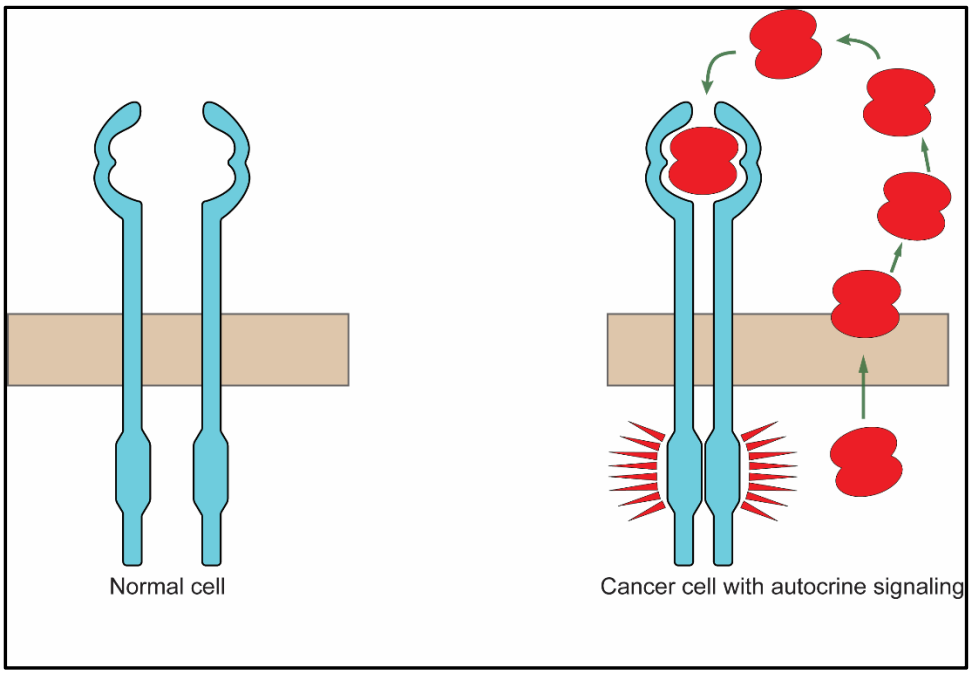

Figure 1.4 Autocrine signaling, behavior encountered in cancer cells [3]

Chapter 2

2.1 *In Vitro* Studies Review

In vitro models for drug development continue to improve due to the introduction of genomics, proteomics, pharmacodynamics, bioinformatics and automated High Throughput Screening (HTS) [66]. Target based drug design using appropriate cell assays is not only progressing in identifying new targets but is also conducted in combination with virtual testing aka "*in silico*" testing, which applies software computer-based methods for drug simulations[66, 67]. *In silico* methods provide rapid and inexpensive techniques for quick verification. In addition, assay efficiency has also undergone significant improvement by increasing the well of the well-plates from 96-wells to 384, 1536, and even 3456 wells, which have been developed to optimize the use of resources, figure 2.1 below [4, 68]. Well plates with > 1500 wells require the use of minute volumes at the micron level thus they are rarely used as this requires specialized tools [4, 69].

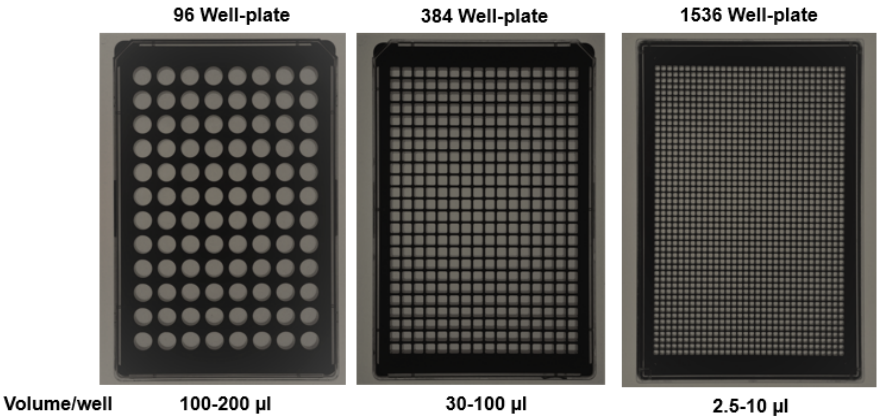

Figure 2.1 Types of Micro-well plates developed [4]

Pharmaceutical companies continue to develop and test new drugs in spite of numerous challenges encountered when bringing a new drug to market. Yet drug development and drug approvals remain challenging with almost all of them failing from the initial *in vitro* testing of drugs, to animal testing studies, to clinical trials [70, 71]. In addition, the regulatory environment leaves it at the pharmaceutical's responsibility to conduct and follow the preclinical studies and to provide clinical study outcomes before a drug can be brought to market [72]. This process is time-consuming and it can take up to 15 years for market approvals. Additionally, the cost is estimated at 1.2 billion dollars [73]. In some instances, when drug testing *in vitro* and in animal models do not agree in either clinical phase I or clinical phase II studies, drug companies have to abort testing altogether and start over [74, 75]. Despite all of these struggles, pharmaceutical companies continue to make strides towards new breast cancer therapies; to date, 13 new breast cancer drugs have been approved since 2008 [60].

There are three characteristics of the drug discovery phase: 1. Demonstration of target protein expression (mRNA) in involved cell types or in affected tissue in animal models or subjects. 2.The revelation that modulation of the targeted cell systems results in anticipated functional effects. And 3. Demonstration that the target is a contributing factor in conveying the disease / phenotype in animal models or in subjects [76].

In vitro testing is crucial in target and phenotypic based drug development for it provides basic knowledge on the effects that targeted drugs will have and also of the phenotypic changes in cellular response [13]. Even though *in vitro* models provide information on how cells will react when first exposed to different drugs, which can later be used in animal models, most of them are conducted using standard 2D cell culture methods,

which lack the pharmacokinetic response that the *in vivo* environment provides [77] . To overcome this issue, the conventional 2D cell culture in a petri dish, has been improved with several 3D cell culture approaches ranging from a simple layer-by-layer approach to the very complex hanging drop method; rationalizing that these models can better mimic *in vivo* models for the study of cellular behavior [18, 78]. One of the advantages of using *in vitro* experiments is that they provide reasonable data on how these models will behave when subjected to new test environments, whether these are of chemical or physical nature. Another advantage is that, initially, these tests can be performed without having to experiment on animals or humans [78, 79] . As more discoveries are accomplished with *in vitro* models, scientists are better able to predict cellular functions in their native microenvironments during drug discovery, which in turn supports the development of more effective drugs [4].

Nevertheless, one of the main barriers of *in vitro* studies pertains to pharmacokinetics / pharmacodynamics. Pharmacokinetics is associated with the *in vivo* response to Absorption, Distribution, Metabolism, and Excretion (ADME) [80]. This is true as the main purpose of pharmacokinetics is to establish how a drug is absorbed and depleted throughout the body and how the human body reacts in response to such drugs [78]. Throughout the *in vivo* drug discovery process, adverse events are also monitored, as wells as any drug interactions particularly, when administered concomitantly with other medications, generally prescribed to cancer patients [80]. *In vitro* study results, once refined, are then advanced to the next level, through animal studies and then followed by Phase I clinical trials for the purpose of toxicity testing [72].

Despite all the shortcomings of *in vitro* testing, these manually seeded models continue to be used for drug development because they provide cost-effective solutions and has been the conventional method of choice for preclinical research [1]. The cellular response of these *in vitro* models is not yet fully understood but these models offer scientists with a general idea of the toxicity of a targeted drug [4]. *In vitro* models not only provide specific tissue characteristics but they also provide, specific to the regional milieu of the human body being studied. In the case of breast tumors, cellular polarity and cellular interactions with its surrounding Extracellular Matrix (ECM) are necessary for reliable drug testing [1]. In order to replicate a response of real functions of *in vivo* environments, an *in vitro* model simulating the actual environment, including an extracellular matrix, with fibroblasts, epithelial and cancer cells should be investigated [1]. These tactics could evolve into an extension of the results presented in this dissertation considering the fact that the study of bioprinted cancer cells at the molecular level is unknown. It is imperative to identify and understand the intrinsic phenotypic differences between bioprinted and manually seeded cancer cells in a basic environment. Once these permutations are revealed and well established, a more suitable model can be further developed, which include the introduction of the variables mentioned above. Results from the investigations in this dissertation will lay the groundwork for the development of more efficacious *in vitro* cancer models for drug discovery.

2.2 Tissue and Tissue Biofabrication

A diverse variety of natural and synthetic tissue constructs have been engineered for regenerative medicine. Naturally occurring biomaterials include agarose, gelatin,

alginate, hyaluronic acid, fibrinogen, and collagen [81]. One of the key characteristics often desired in synthetic material development is biodegradation, which is the breakdown of compounds and materials yielding products that can be digested by cellular organisms [82, 83]. Mainly, biomaterials used for tissue engineering are anticipated to stimulate cellular and tissue metabolic processes such as proliferation, differentiation and adhesion. Although natural biomaterials have some variability due to their structural complexities, recent developments have substantially improved the properties of these biomaterials [82]. In essence, these biomaterials can be structured to promote and simulate the body's natural homeostasis [84].

Diversified tissue biofabrication techniques have extensively been devised and established, from the traditional techniques such as, freeze drying, solvent casting, gas foaming, etc. [17], to the bioprinting techniques like extrusion, inkjet bioprinting, laser assisted printing and others [17, 85]. These methods and technologies are aimed to replicate scaffolds capable of mimicking the cellular physiological milieu of *in vivo* enronments. Few of the scaffolds developed *in vitro* have been tested *in vivo* with promising outcomes, figure 2.4 [5, 18, 86]. A functional biomaterial for *in vitro* testing must be porous and biocompatible with cells and other living organisms.

Lyophilisation (freeze drying) consists of freezing a scaffold or other material, subjecting it to low pressure and then removing the ice by sublimation. Though this method may lack key features of genuine tissues such as permeability or porosity [87]. Porosity is a desired property to allow for vascular development post cell seeding [80].

Solvent casting is another technique that creates a cast with a mixture of an organic solvent, like alginic acid, with a crosslinker such as calcium chloride (in the case of alginate) or other particles to produce a semi-solid gel like structure (membrane) [81]. Any such approach has its own advantages and disadvantages that scientists take into account during scaffold development.

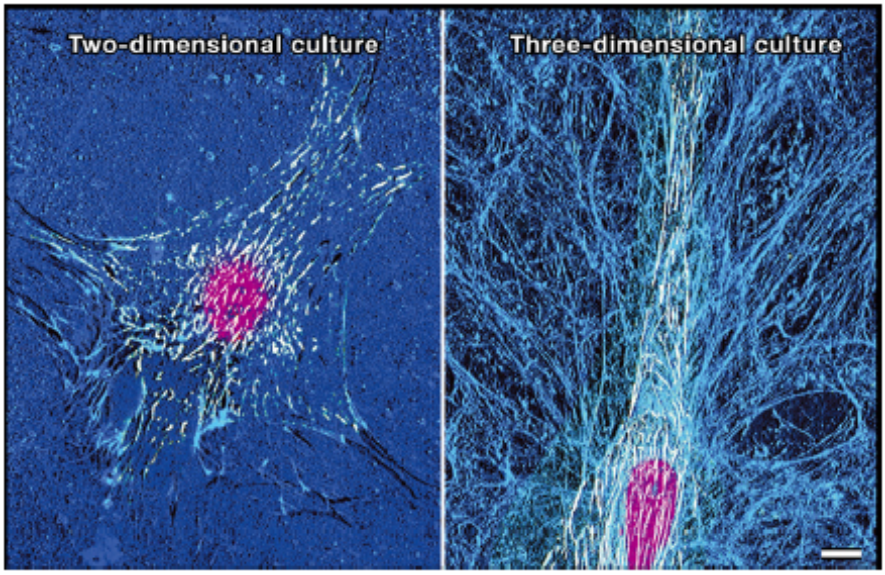

Figure 2.4 2D and 3D cell culture [5].

2.3 Tissue Engineering Processes

Biomedical tissue printing technology has been around for over a decade and it is still an underutilized technology with promising opportunities. Multifaceted tissue constructs have been devised, developed, and tested with successful results [88, 89]. Bioprinted skin cells designed into a scaffold have been applied and proven to do better than commercially available bioengineered skin in animal models. Yanez, et al., were able to obtain a 17% skin contraction improvement when compared to apligraf. Apligraf is FDA approved for skin grafting, which is used to treat patients with ulcers or diabetes [88, 90, 91].

3D tissue biofabrication *in vitro* has progressively developed to mimic *in vivo* environments. To date, several approaches for 3D tumor modeling exist, from the multi-layer multi-cell culture, to single Block-Cell (BloC) bioprinting, to inkjet printing [16, 92-94]. Human Tissue harvesting from biopsies is another approach to developing tumor models in vitro though this approach tends to have a limited lifecycle, and drugs tested this way may provide results that cannot be generalized for the entire population with similar biomarkers [95]. Several 3D tissue models have been developed, a layer-by-layer (LBL) engineered tissue approach, inkjet-based printing, the hanging drop, spheroids methods among others have been used [93, 96].

LBL tissue constructs developed and tested by Catros, et al., where they used a laser-assisted bioprinting (LAB) technique to pattern cells [97]. The authors mixed approximately 50 million cells/mL in 1 % alginate to form a gel and deposited drops of cells that were generated by heating the back of the gel. The drops were deposited onto a substrate that was 100 μm thick electrospun polycaprolactone (PCL). This experiment tested two different tissue models, a stacked substrate with cells seeded by the standard method versus the LBL model using a cell pattern. The LBL model showed a higher cell quantity when compared to the stacked substrate model when similar quantity of cells was initially applied using these two methods [93].

Inkjet bioprinting, identified as a non-impact printing technology, where ink drops are discharged from a pen or ink cartridge onto a substrate have also been used to generate tissue models. [6, 96, 98-101]. The purpose of the substrate, which is a gel is to provide some sort of support or shock absorption for the cells that are being bioprinted, which may acquire a speed close to 1 m/s [100, 102-104]. Tissues

bioprinted in this publication contained stem cells, muscle cells and aortic endothelial cells. This model has been successfully tested in vivo displaying promising results when angiogenesis development was observed 8 weeks following implantation in mouse models [99].

Figure 2.5 Modified Inkjet printer [6]

The hanging-drop method is another procedure that has been widely used in spheroid shaped models [105, 106]. However, this method appears to be time-consuming and is not very repetitive [106, 107]. There are some limitations in this method such as transportation and handling restrictions, which may result in environmental gradients possibly producing phenotypic changes in cells [108]. Additionally, because it is necessary to wait for cells to settle, there is a chance one could introduce contaminants. The rating given to this method by Moroni, et al., is low to very low for the Resolution/time for Manufacturing ratio [17].

The Resolution/time for Manufacturing (RTM) ratio is a quantitative rating tool introduced to evaluate the process of specific bioprinting technologies [17]. The RTM presents with an overall idea of how long each bioprinting process will take to complete.

Having an overall idea of the time it takes to design and develop a bioprinted tissue when using one technique versus another provides the researcher with the option for planning and determining a new design. It is always desirable to have a basic notion of the resolution and timeframe when planning tissue development.

Moroni, et al., elucidate a complete overview of the different processes for biofabrication of tissue engineering. In this guide, the authors very nicely summarize in a table the main features of the different biofabrication techniques that have been developed and tested to date. Not only do the authors provide a concise explanation of biofabrication techniques conducted but they also provide ratings regarding minimum feature widths and limitations that each biofabrication technique possesses.

Chapter 3

3.1 – Introduction

In vitro testing for drug discovery is continually improving with the introduction of genomics, proteomics, pharmacodynamics, bioinformatics and automated high throughput screening (HTS) [66, 109]. Target-based drug design using appropriate cell assays, is not only progressing in identifying new targets, but it is also conducted in combination with virtual testing aka "*in silico*" testing, where software computer-based methods for drug simulations are applied [66, 67]. *In silico* methods provide rapid and inexpensive techniques for quick tests verification then proceed with *in vitro* cell testing which is normally done in the early stage of drug discovery [110]. *In vitro* studies and assay development are critical steps of drug discovery (DD) [13, 79]. Previous studies have suggested that bioprinting can be used to model tissues for drug discovery and pharmacology [109, 110]. Peng et al., suggests that 3D bioprinting can help reduce the attrition rate in drug discovery by creating more realistic models through manipulation of pattern/shape constructs to form porous structures ensuring adequate delivery of nutrients and vascularization as normally required for cells *in vivo*. The molecular effect of bioprinting through a modified thermal inkjet printer on bioprinted (BP) breast cancer cells is unknown. By bioprinting realistic models, we mean to employ tissue/cells based on target characteristics or specific areas of interest such as bone, cardiac, or cancer cells.

While it is important to understand the viability and physiological changes of bioprinted cells, it is critical to understand the molecular changes within bioprinted (BP) cells in order to identify triggering mechanisms associated with cellular functions and behaviors.

To our knowledge, Analysis of MCF7 cells bioprinted by a thermal inkjet printer, through phosphorylation, RNA Seq analysis, have not been published before. Zhao, et al., tested a 3D extrusion-based bioprinted model of Hela cells and found the following: 'morphological differences, increased Matrix Metalloproteinase (MMP) protein expression and higher cell proliferation when compared to the 2D standard cell culture model.' For *in vitro* studies, gross anatomical and interactive cellular alterations are important to be able to predict close approximations to external stimuli, whether they are of biological or synthetic nature during drug discovery. However, understanding the cellular response of BP MCF7 breast cancer cells (BCC) or any other cells at the molecular level is crucial to determine and potentially predict drug efficacy, toxicity, and safety.

Bioprinting technology has been widely used to develop tissue engineering for a range of clinical applications, e.g., skin grafting, tissue regeneration, cartilage repair, and others [88, 111-114], yet it has never been used to develop tumor models *in vitro* for drug discovery. In a recent publication Chen et al., developed a bioprinting system where mass spectrometry was conducted in single printed cells [115]. In another publication, Phamduy et al., [116] used laser direct-write cell bioprinting process to print MDA-MB-231 and MCF7s directly onto *ex vivo* rat mesentery tissue where they were able to monitor cell viability, proliferative and migratory properties. In that experiment, they successfully observed cell attachment and cell invasion within 2 - 5 days. The literature analyzing molecular and physiological changes in thermal inkjet bioprinted MCF7 BCCs is long overdue. Here we report viability, apoptosis, kinase

phosphorylation, and RNA sequencing (RNA seq) analysis of BP MCF7 BCCs. In this investigation, a modified HP thermal inkjet printer was used to bioprint the cells.

3.2 Materials and Methods

3.2.1 Cell Culture and Bioprinting Process

Cell culture: In this study, MCF7 (ATCC® HTB-22™) breast cancer cells were used for the in vitro experiments. Eagle's minimum essential medium (EMEM), supplemented with 0.01 mg/L Human recombinant insulin and 10% fetal bovine serum (referred to as media), trypsin 0.25% EDTA, and sterile phosphate-buffered saline (PBS) solution were used [117]. Briefly, MCF7 cells were cultured per ATCC's cell protocol, a 75 cm flask with 8-10 ml of media were incubated in a humidified incubator maintained at 37°C with 5% CO2 until 80-90% confluency was reached cells were split and passaged to ensure cell stability.

3.2.2 Bioprinting Process

In preparation for bioprinting, MCF7 cells growing around 80 – 90% of confluency were gently rinsed with PBS (to remove dead cells and debris) and detached with trypsin harvested and centrifuged at 800 rpm for 5 mins. The supernatant was removed, and the cell pellet was next rinsed in PBS. Then the cells were counted with trypan blue and a hemocytometer. Modified inkjet cartridges adapted for a modified HP thermal inkjet printer were used to for bioprinting purposes [6, 118]. Next, 100 µL of PBS-cell solution (approximately 1.6x106 cells/mL) was added and printed into a tissue culture treated petri dishes (100x15 mm) or a Falcon, 96-well black/clear, tissue culture treated plate,

flat bottom with lid. Following the bioprinting process, the cell viability analysis was conducted at 24 and 48 h utilizing two approaches: by using the Invitrogen™ Countess™ automated cell counter and through manual count by two different lab members using trypan blue and a hemocytometer. In these series of experiments, three independent measurements were accomplished, each performed in triplicate. Collected data are depicted as an average and standard deviation.

3.2.3 Examination of the apoptosis/necrosis pathway via flow cytometer

MCF7 Cells were bioprinted at a density of approximately 600,000 cells/dish in 6 ml of media. After 24 and 48 h post-bioprinting, cells were collected as above ad double-stained by using the Annexin A5- FITC/propidium iodide (PI) staining kit, which is typically used to discern whether the cells are dying via apoptosis or necrosis pathway in the Beckman Coulter flow cytometer. The total percentage of apoptotic cells is depicted as the sum of both early and late stages of apoptosis (Annexin A5-FITC positives), whereas the cells stained only with PI, were considered as the necrotic cell population [119]. Data acquisition and analysis were performed by using the Gallios flow cytometer (Gallios Beckman Coulter: Miami, FL.) and the Kaluza software version 3.1. (Beckman Coulter) as previously detailed [120].

3.2.4 Stain Process

Morphological characteristics of the BP and MS MCF7 cells were evaluated with laser-confocal microscopy. 24 h post-bioprinting, cells were stained as explained elsewhere [121]; briefly, cells were fixed in 4% formalin for 20 minutes, washed and incubated in 0.1% v/v Tween 20 in PBS for 10 mins at room temperature (RT), washed twice more

with permeabilizing solution, incubated again in 200 µl of 5% w/v in bovine serum albumin (BSA; sigma) dissolved in tris-buffered saline solution containing 0.5% v/v Tween 20 for 1 h at RT on a rocker platform. The cells were next stained with the primary antibody Neu (sc-33684, dilution: 1:50) overnight in a rocker platform at 5^{o}C. The cells were next washed three times with permeabilizing solution and a 1:50 v/v dilution of secondary antibody goat anti-mouse IgG conjugated with Alexa Fluor^{TM} 568 (Invitrogen) was added and then incubated for 1 h on a rocker platform at RT. They were rinsed three more times with permeabilizing buffer and posteriorly they were co-stained with 0.165 µM of Phalloidin Alexa Fluor^{TM} 488 (Invitrogen), and 5 µg/ml of 4′,6-diamidine-2′-phenylindole, dihydrochloride (DAPI, Invitrogen) for 1 h on a rocker platform; rinsed three more times with 0.1% v/v Tween 20 in PBS and leaving 200 µl in the wells at the end. Finally, using an inverted confocal-laser-scanning microscope (model LSM 700: Zeiss; New York, NY) assisted by the Zen 2009 software (Zeiss), to acquire high-quality digital in three fluorescence channels (Alexa 568, Alexa 488 and DAPI). The enhanced contrast Plan-Neofluar 40x/1.3 oil immersion, differential interference contrast objective was used. The parameters to capture the high resolution images were consistently maintained; single-plane images were consecutively scanned for each fluorescence channel setting the pinhole at 1 Airy Unit.

3.2.5 Phospho-MAPK Antibody Array (BP cells)

The antibody array phospho-mitogen-activated protein kinase (phospho-MAPK) (R&D Systems #ARY002B) was used to analyze the phosphorylation levels of 26 kinases, which includes 9 MAPKs, ERK1/2, JNK1-3 and p28 isoforms in order to understand how the relative phosphorylation levels are affected by the bioprinting process. A collective

sample of BP MCF7 BCC was harvested at 12, and 24 h post-bioprinting. Samples were processed as per the kit's protocol. Briefly, cells were solubilized in lysis buffer, diluted, mixed with detection antibodies, and incubated overnight in a rocking platform at 5^{o}C with the phospho-MAPK array membranes. The membranes were washed the next day and detection reagents were applied. Upon completion of the reagent detection step, the iBright^{TM} FL1000 Imaging System (Invitrogen Thermo Fisher Scientific) was used to develop the membranes. Microarray data was obtained by pixel density values, which were normalized, analyzed, and quality controlled by using Invitrogen^{TM} iBright^{TM} imaging software v.3.0 (Thermo Fisher).

3.2.6 RNA Extraction and Sequencing

RNA sequencing was conducted in BP MCF7 BCCs at 2, 12, and 24 h post-bioprinting with the intention of identifying genes that were upregulated or downregulated by this process. Samples for RNA sequencing were prepared following the same bioprinting protocol as mentioned above. BP MCF7 BCCs were next gently detached with a cell sweeper to avoid exposure to influencing solutions, centrifuged at 800 rpm for 5 mins and collected at 2, 12 and 24 h. RNA extraction was conducted for each sample with the PureLink RNA mini kit from Thermo Fisher and used per manufacturer's protocol. RNA concentration was evaluated with a Nano-drop 2000 spectrometer (Thermo Fisher Scientific). RNA Integrity Number equivalent (RINe) was assessed for each sample and ranged from one to ten. RNA seq data was analyzed for data summarization, normalization and quality control using Trimmomatic (version 0.36) [122], Bowtie2 (version 2.2.5)[123] and Cufflinks (version 2.2.1) [124]. Differentially expressed genes were selected by using threshold values of >2 and <-2 fold change and a *q-value* ≤ .05.

The *q-value* is used in genome-wide expression data, this statistical method is used to filter the proportion of the false positives from a collection of p values > .05.

STRING was used to map pathways of upregulated and downregulated differentially expressed genes. Cytoscape, v.3.7.1., was next used to compare both network samples. Finally, Network analysis to identify protein-protein interactions (edges or protein-protein connections) was extracted from Cytoscape. The number of connections or interactions are important parameters when targeting specific proteins associated with a disease. Genes with a > 2 fold and < -2 fold (upregulated and downregulated genes) and a *q-value* < .05 were further classified by their gene ontology (GO) terminology. Upregulated and downregulated genes in the BP cells were divided into 3 groups, by their associated biological processes (bp), molecular functions (mf) and cellular components (cc). We also used STRING to create a protein network and compared the results of the MS to the BP MCF7 cells. We further mapped the protein pathways associated with genes expressed only in the BP cells. RNA and DNA information/analysis were compiled from: STRING, Panther, and Cytoscape 3.7.1 the following websites were also used to extract protein/gene connections: SMART, gene ontology, UniProt, and the Online Mendelian Inheritance in Man®.

3.2.7 Statistical Analysis

Continuous variables for cell response to bioprinting were summarized using means and standard deviation (SD) of triplicate samples. In this experiment, 3 independent samples at 2 different time frames (24 and 48 h) were used to calculate viability and a one-way ANOVA analysis was conducted to compare the means for each time frame of

the BP and manually seeded MCF7 BCCs, negative controls were also conducted. For the antibody array assay, data was centered, normalized and clustered utilizing the iBright^{TM} Analysis software version 3.0. All statistical analysis were completed using Minitab 18 and IBM SPSS Statistics 25.

and quality control using Trimmomatic (version 0.36) [122], Bowtie2 (version 2.2.5)[123] and Cufflinks (version 2.2.1) . Differentially expressed genes were selected by using threshold values of > 2 and < -2 fold change and a *q-value* ≤ .05. A second analysis using the Log2 transformation was also conducted, same threshold values as before > 2 and < -2 fold change and a *q-value* ≤ .05, were considered statistically significant. The *q-value* is used in genome-wide expression data, this statistical method is used to filter the proportion of false positives from a collection of *p-values* < .05. STRING was used to map pathways of upregulated and downregulated genes. Cytoscape, v.3.7.1., was next used to compare both network samples. Finally, network analysis to identify protein-protein interactions (edges or protein-protein connections) was extracted from Cytoscape (Tables 3.1 and 3.2). The number of connections or interactions are important parameters when targeting specific proteins associated with a disease.

Genes with a > 2 fold and < -2 fold (upregulated and downregulated genes) and a *q-value* < .05 were further classified by their gene ontology (GO) terminology. A Venn diagram was used to group genes as classified by their GO term, biological process (bp), molecular function (mf) and cellular component (cc). These GO terms are explained elsewhere (geneontology.org), bp (biological process) terms describe the "biological programs" or bigger processes that are fulfilled by several molecular events, such as DNA repair or response to oxidative stress. Mf (molecular function) refers to

events occurring at the molecular level by gene components, depicts events that can be conducted by single gene products such as vitamin D response element or calcitriol binding, to name a few. However, there are also some functions fulfilled by sets of molecular entities consisting of multiple gene outcomes such as DNA-binding transcription factor activity or toll-like receptor binding. Cc (cellular component) denotes the location with respect to cellular structures where the gene performs an activity for instance, cytosol, mitochondrion or nucleus. Upregulated and downregulated genes in the bioprinted cells were divided into 3 groups, by their associated biological processes, molecular functions and cellular components. We further mapped the 266 and 206 genes in STRING to create a protein network and compared the MS cells to the BP MCF7 cells. We also mapped the protein pathways associated with genes expressed only in the BP cells. RNA and DNA information/analysis were compiled from: STRING, Panther, and Cytoscape 3.7.1 (an open-source program); the following websites were also used to extract protein/gene connections: SMART, gene ontology, UniProt, and the Online Mendelian Inheritance in Man® (OMIM).

3.3 Results

3.3.1 Post-bioprinting Cell Viability and Apoptosis

The cell viability results from the manual cell count process of the BP cells ranged from 60% to 87% tested at 24 and 48 h intervals. The average percentage cell viability for MS (non-printed) cells was 98.6%. The average percentage cell viability from the automated cell countess of the BP cells at 24 and 48 h was 76.7% and 72.8%, respectively. In the flow cytometer, for samples collected at 2 and 24 h post-bioprinting, the percent rate of live cells was 70% and 30%, respectively. Apoptosis rates at these

time frames were 30% and 69%, respectively and are shown in *Figure 1*. Previous reports of BP cells have indicated viability rates ranging from 70% to 90% respectively (Figure 3.1).

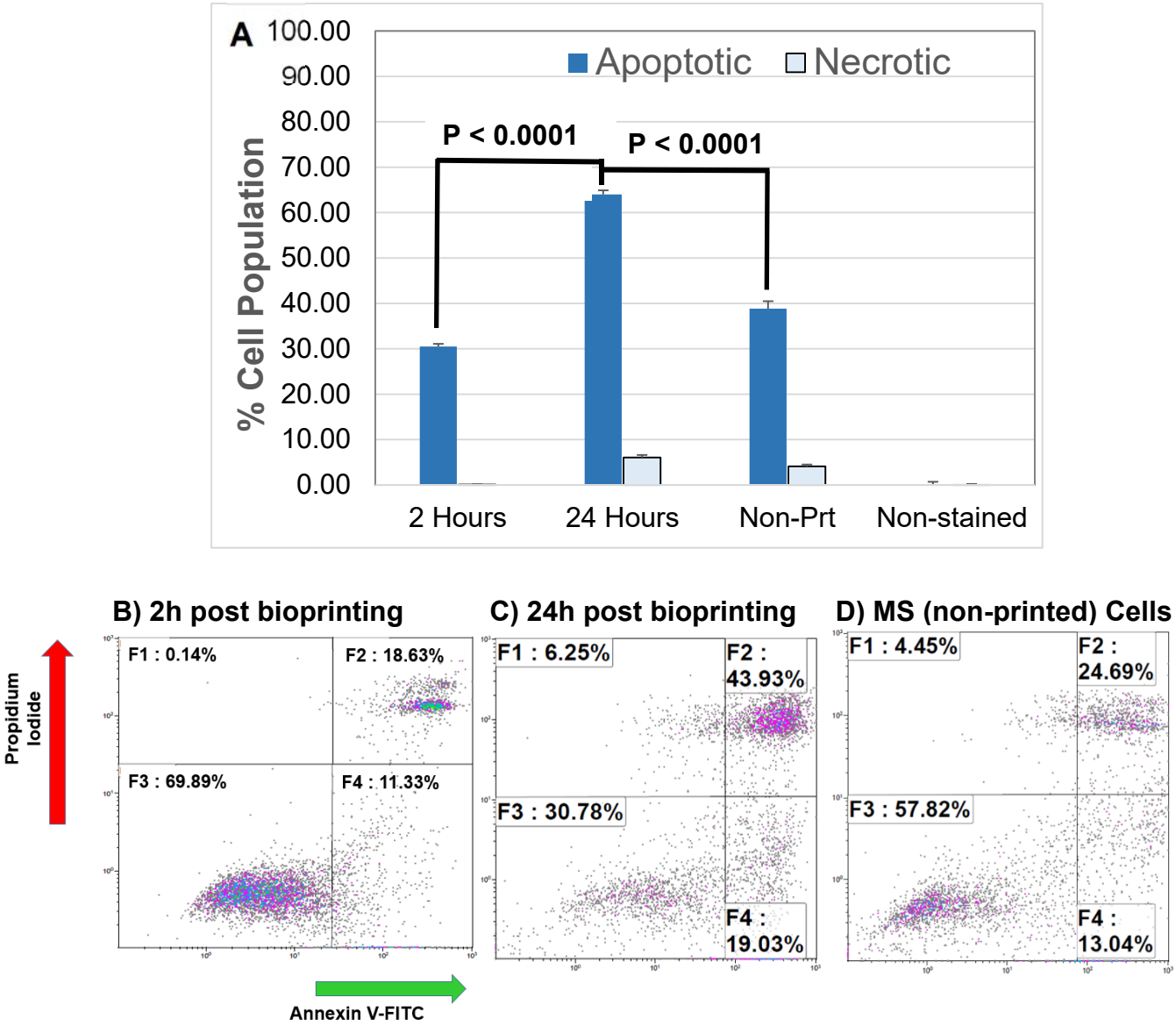

Figure 3.1 Percentage of Apoptotic MCF7 breast cancer cells post-bioprinting. A) Annexin A5-FITC kit used for this analysis. Cells were collected post-bioprinting at 2 and 24 h. Cells were bioprinted onto a petri dish with EMEM, and cells were incubated immediately post-bioprinted. The Annexin assay was conducted in all cells, no media changes were made. The total percentage of the apoptotic cell population is expressed as the sum of early and late apoptosis percentage (F2+F4), dark blue bars. Light blue

bars depict necrotic cells, cells stained with PI. Each bar represents the average of triplicates. Controls used were live cells stained, unstained and dead cells (not shown). Error bars represent the standard deviations. B) Dot plot graphs depict results at 2 h post-bioprinting. Graph C) displays results at 24 h post-bioprinting. And graph D) are the results from manually seeded (non-printed) MCF7s cells. P-values are from a two-tailed student t-test for independent tests. 10,000 events were obtained per sample.

3.3.2 Cell Morphology Results

Comparing the morphology of both cells (*Figure 3.2*), BP and MS MCF7 cells, it appeared that the MS MCF7 cells displayed distorted nucleus as compared with BP cells. The nucleus of the BP cells seemed less delineated and possibly pricked in some areas whereas in MS cells the limits of the nucleus looked well defined and intact as observed in both, the blue and red channels. Additionally, staining results with the Neu antibody to quantify protein expression on both cells samples, the fluorescence intensity measurements was significantly higher by 3 fold in MS cells than in the BP cells ($p < .001$). Fluorescent parameter settings in that channel, Alexa 568, was the same for both samples. Visually, the fluorescence intensity in BP cell samples was markedly weak compared to the MS cells.

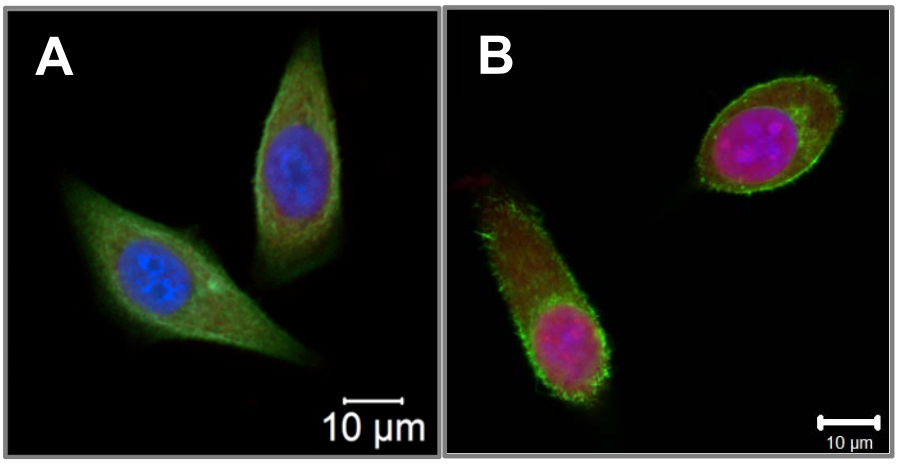

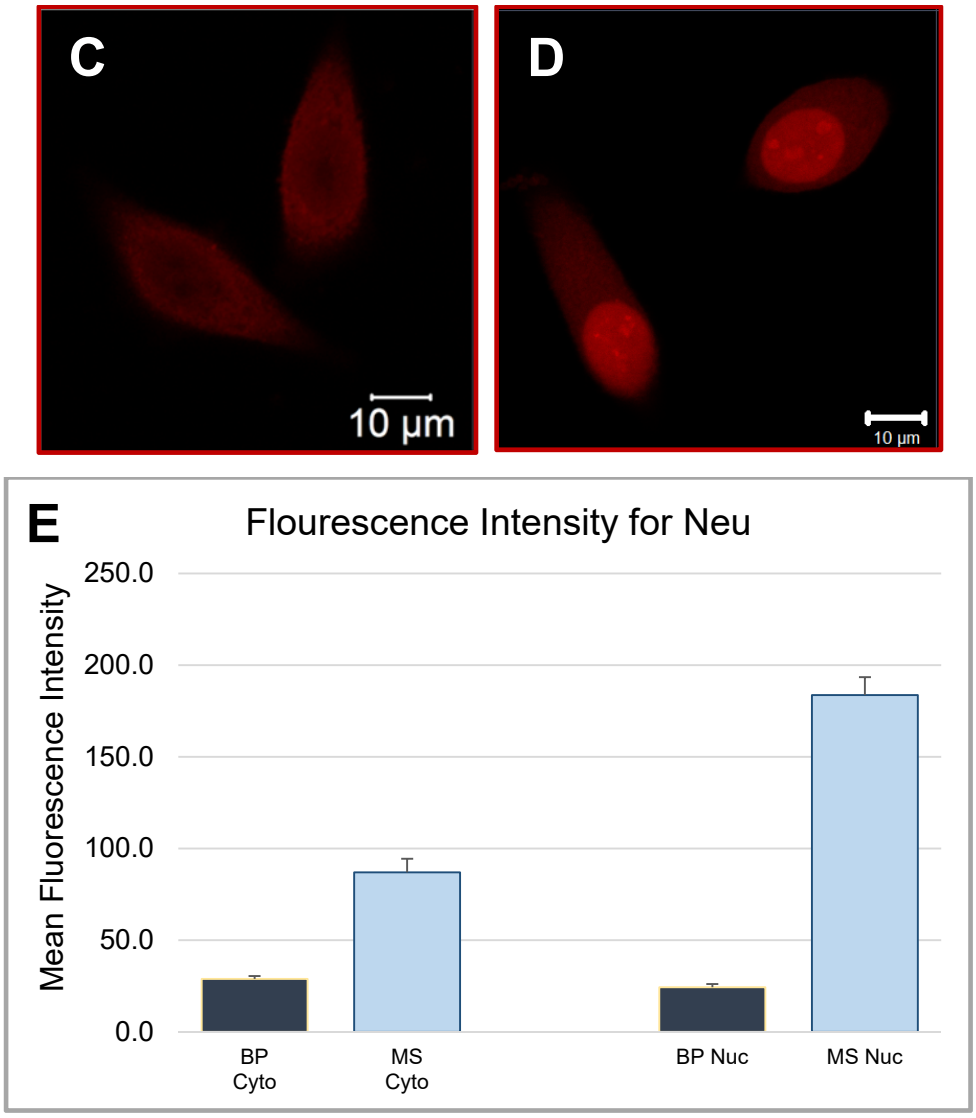

Figure 3.2 A) Bioprinted MCF7 cells 24 h post-BP. Image showing in all three channels. B) Manually Seeded MCF7 fixed at 24 h post-seeding. C) Bioprinted MCF7 Cells and D) manually seeded MCF7 cells, single-channel image, stained with Neu (sc-33684) primary antibody and goat IgG anti-mouse secondary conjugated with Alexa 568 channel. The same parameter settings were used for both cell samples. Fluorescent Intensity measurements were significantly different between the two samples, cytosol and nucleus were measured separately. In panel E) Mean intensity measurements for the cytosol and the nucleus of the BP cells were 28.9 (1.6) and 24.3 (1.7), respectively. The mean intensity measurements for the cytosol and nucleus of MS cells were 87.0 (7.4) and 183.6 (9.8), respectively (BP Cyto = Bioprinted Cytosol, MS Cyto = Manually Seeded Cytosol, MS Nuc = Manually Seeded Nucleus, BP Nuc = Bioprinted Nucleus).

3.3.3 Phospho-MAPK Array Results

The BP MCF7 cells phospho-MAPK array revealed a total of 21 highly phosphorylated sites, whereas the MS cells revealed 11 phosphorylated sites. Of those phosphorylated targets in the MS cell samples, six analytes appeared > 1.6 fold stronger phosphorylation level than the BP cells, (targets: p70S6 Kinase, CREB, ERK2, ERK1, Akt1, and Akt2), though no statistical significance was observed (p = .272, *Figure 3.3*). On the other hand, the BP MCF7s displayed 21 phosphorylated sites of which 12 did not show in the MS cells, (targets were: RSK1, HSP27, p38δ, p38β, MSK2, p53, MKK6, TOR, MKK3, p38γ, RSK2, and JNK2). Phosphorylated targets above the threshold were further investigated to associate the targets with key biological processes (bp), molecular functions (mf), and cellular components (cc) in the cells and to correlate with RNA sequencing results (*Figure 3.4*). Network analysis to determine the number of edges (protein-protein interactions) showed MAPK1, CREB1, TP53, MAPK3, MAPK8, AKT1, HSPB1, MAP2K3, and AKT2 with > 10 direct edges in the BP cell sample group (*Figures 3.3, 3.4, and 3.5*).

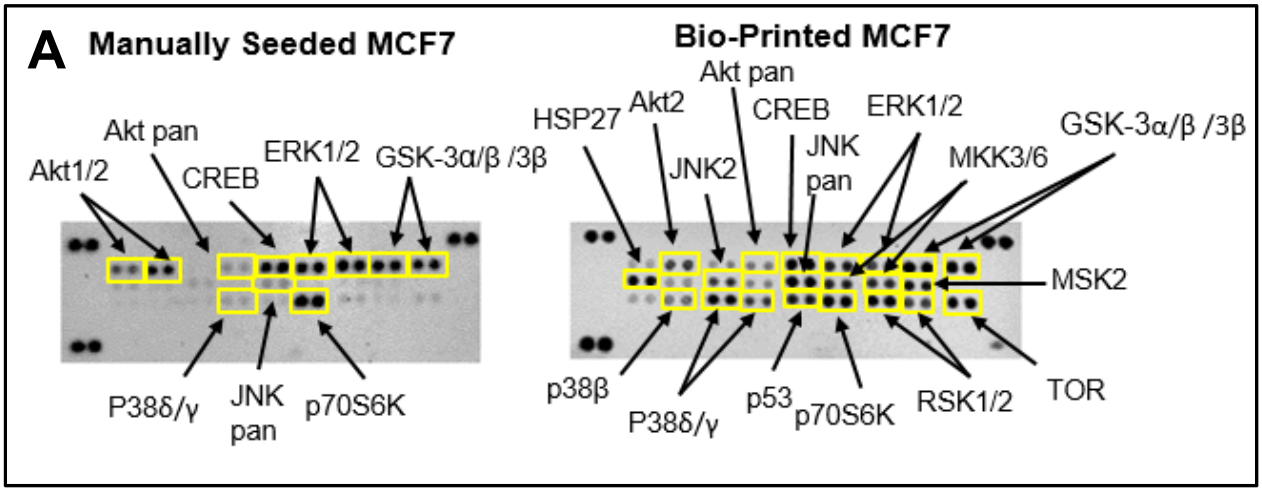

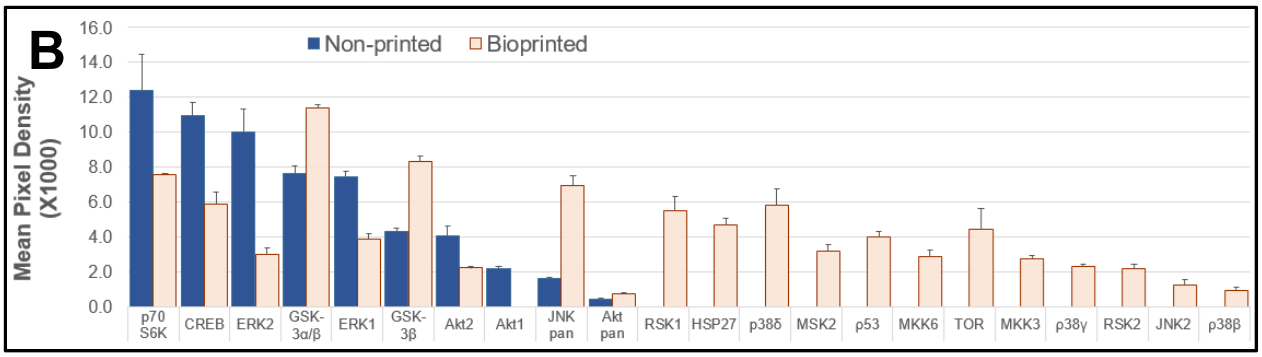

Figure 3.3. Activation of cellular kinases by thermal inkjet bioprinting. Chemiluminescent images in iBright FL1000 of a Proteome Profiler Human Phospho-MAPK Array (Catalog # ARY002B). **A)** Membranes of manually seeded and BP MCF7 breast cancer cells. Membrane arrangement: LEFT = manually seeded (MS) MCF7 cells, RIGHT = BP MCF7. Signal for each kinase is represented by a pair of duplicate spots; three reference pairs are shown in three upper/lower corners. B) Histogram profiles for selected analytes were generated by quantifying the mean spot pixel density exposure in the iBright FL1000 and Invitrogen™ iBright™ Analysis Software v.3.0. Kinases that show increased levels of phosphorylation are identified. The mean pixel density for the analytes is shown in the bar graphs. 21 kinases appeared phosphorylated in the BP samples, whereas 10 kinases showed in the manually seeded. Of the MS cells 6 kinases were strongly phosphorylated by > 1.6 fold as compared to the BP cells.

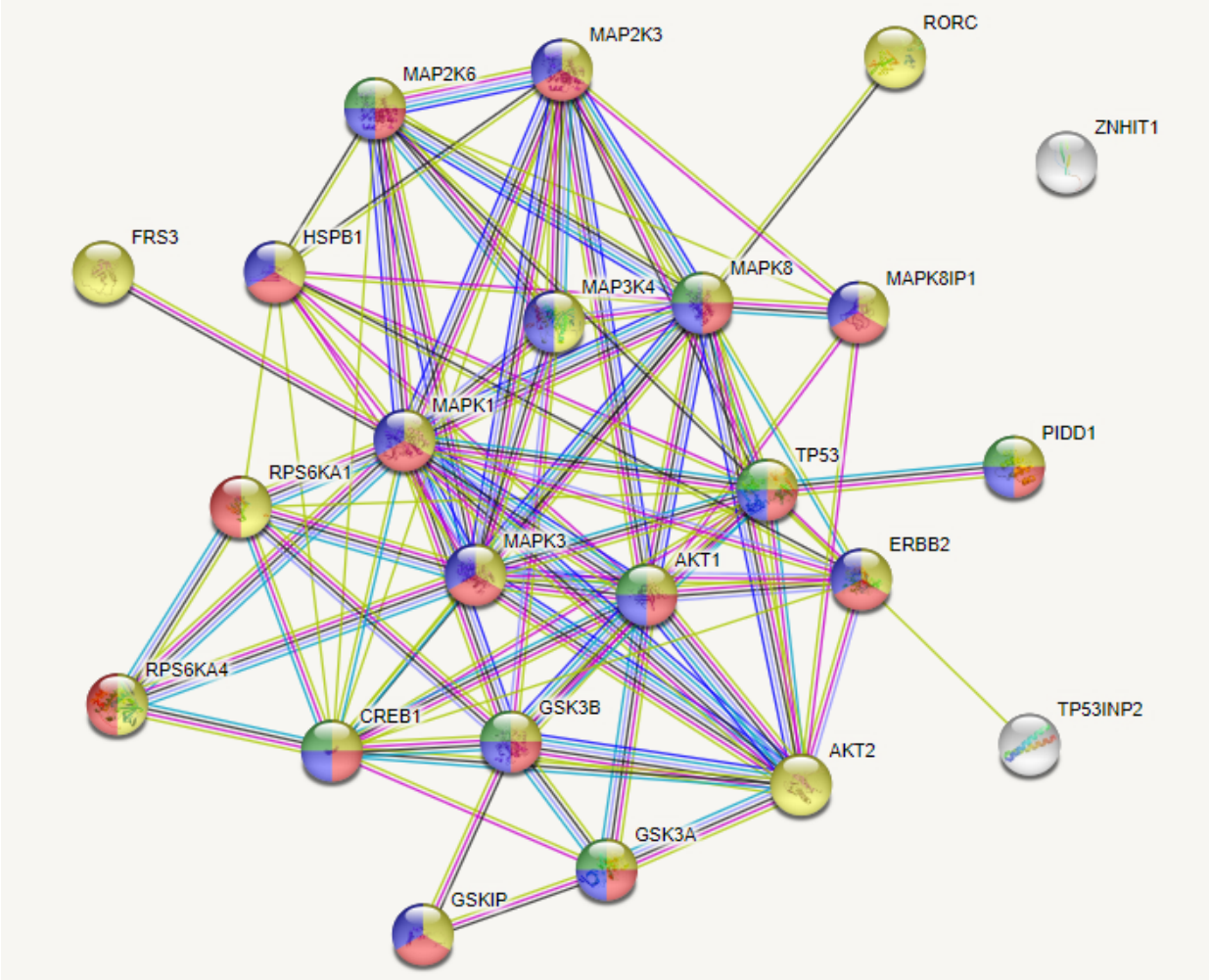

Figure 3.4. The network of analytes phosphorylated in BP MCF7 breast cancer cells. Functions selected in this network were the regulators of apoptosis (green, 8), response to stress (red, 17), intracellular signal transduction (yellow, 21) and signal regulators (blue, 16). This network depicts functional interactions among BP BC predisposed genes. In this network of phosphorylated sites, there are significantly more interactions than expected ($p \leq .001$).

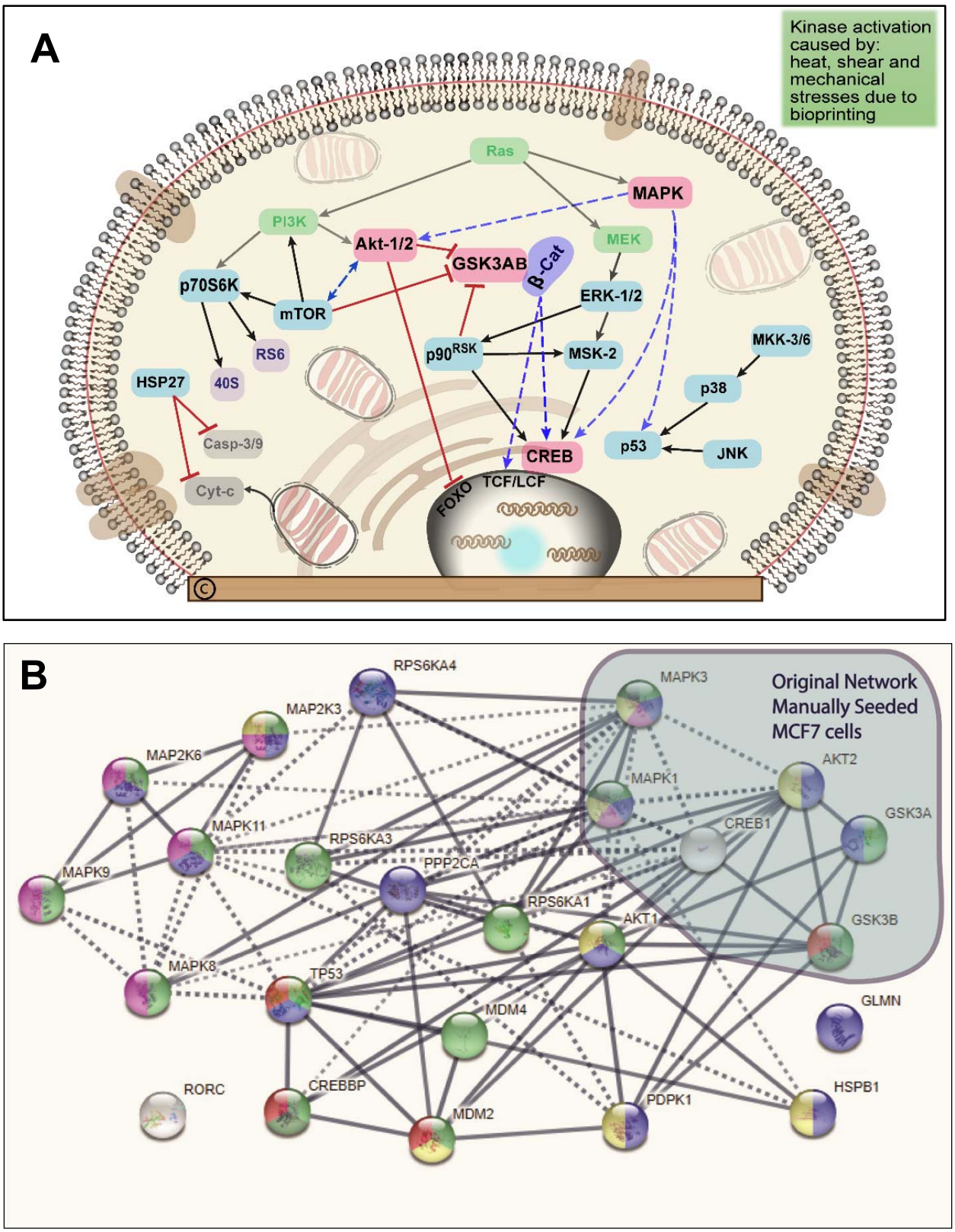

Figure 3.5. A) Schematic summary of the intracellular pathways activated by bioprinting MCF7 cells. B) Representation of the critical kinases and their pathways in the cell.

Green ovals not included in the phosphorylated kinases but they represent key signals to kinases shown, pink ovals represent overlapping kinases, present in both, MS and BP cells. Blue ovals represent kinases phosphorylated only in BP cells. Blue lightning bolt represent insults to the cell, due to either heat or mechanical stresses caused to bioprinting. Red connector lines ending in a perpendicular line mean the originating kinase blocking signaling activity or deactivation. – B) Network with links classified based on curated evidence in STRING. Biological functions selected are p53 binding process (red, 4), regulation of phosphorylation (blue, 14), stress activated protein kinase signaling cascade (pink, 7), regulation of cellular response to heat (dark green, 4) and cellular response to stress (light green, 16). These nodes have a significant number of interactions, as expected due to phosphorylated targets were extracted. The interaction score was set at 0.7 with k-mean clustering set at 5. Thus only links that have a high confidence probability are displayed ($p < .001$). A total of 24 targets were observed from the phosphorylated targets in Bioprinted cells, whereas for manually seeded cells, 6 phosphorylated sites were observed in this network. Despite the complexity of this network, we observed that MAPK1, TP53, CREB1, MAPK3, MAPK8, AKT1, HSPB1, AKT2 and MAP2K3 proteins display more than ten protein-protein interactions.

3.3.4 RNA Results

RNA seq analysis conducted in bioprinted MCF7 cells produced a total of 12,235 genes, of which 1,187 (9.7 %) were significant (*q-value* ≤ .05). Using a cutoff value of a ± 2 fold change for the number of upregulated and downregulated genes, a total of 266 and 206, respectively, were selected. Furthermore, the Log2 transformation of expression values, a total of 65 genes were significant (*q-value* ≤ .05), with 5 genes expressed only in the BP cells (NRN1L, LUCAT1, IL6, CCL26, and LOC401585). The five genes only expressed in the BP cells were analyzed by their gene ontology (GO) classification in Panther 14.1, under Molecular Function (mf), 4 GO terms were identified (GO:0005488, GO:0098772, GO:0003824, and GO:0060089). Under the biological process (bp), four GO terms were found (GO:0065007, GO:0009987, GO:0051179, and GO:0050896). Finally, under cellular component (cc) 2 GO terms were obtained (GO:0005623 and GO:0005576).

The following 4 genes, EFCAB11, FAM117B, FAM46B, and RBM43 were downregulated < -2 fold and the following 3 genes, GCLM, MOB3C, and VDR were upregulated > 2 fold. No significant connections were found among those genes. EFCAB11 contains 11 nodes and 11 edges, but there was no statistical significance, with an interaction score set at 0.4. Recent publications have associated this gene with hepatocellular carcinoma. Genes that were upregulated with > 10 protein to protein interactions included: CYP1A1, CYP1B1, IL6, UGT1A6, and EGFR (see Tables 3.1 and 3.2). Downregulated genes in BP cells with ≥ 10 protein interactions included: TP53, FOS, JUN, EGR1, HIST2H2AC, and FOSB (see Table 2). A complete list of gene analysis is available in appendix I.

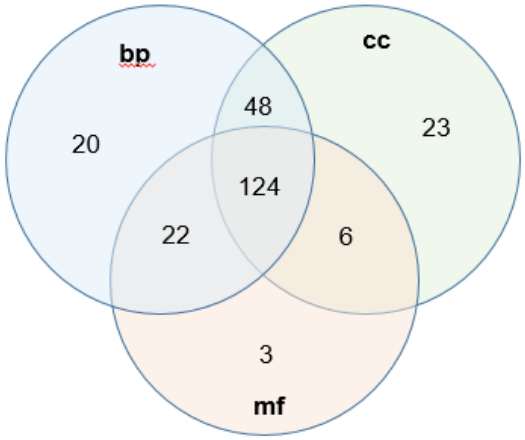

Figure 3.6 Venn diagram of number of genes with upregulated gene expression in the BP MCF7 BCCs > 2 fold. Criteria used to depict each group was by gene ontology (GO). There are 3 characteristics associated with the GO terms: bp=biological process, cc=cellular component, and mf=molecular function, explained above. B) Venn diagram of downregulated gene expression in the BP MCF7 BCCs. (< -2 fold and *q-value* < *.05* was used to classify them by their GO terms. The total number of upregulated genes (> 2 fold) in the bioprinted cell samples was 266, whereas the total number of downregulated genes (< -2 fold) was 206. In the molecular function taxonomy, there were 4 genes (EFCAB11, FAM117B, FAM46B, and RBM43) that were downregulated in the (< -2 fold) group and 3 genes in the upregulated group (> 2 fold), GCLM, MOB3C, and VDR. No significant connections were found among those genes. When we entered the genes individually in STRING we found that EFCAB11 contains 11 nodes

and 11 edges (connections/interactions) but there was no statistical significance, the interaction score set at 0.4. Recent publications have associated this gene with hepatocellular carcinoma. In the RNA seq analysis, this gene is located in chromosome 14. FAM117B produced 5 nodes with 10 edges and resulted in 2 GO terms under biological processes. This network has been associated with negative regulation of activation-induced cell death in T-cells and response to osmotic stress, for additional information search GO:0070236 and G:0006970. This gene was downregulated in the BP cells and was located in **chr2**. FAM46B's network contains 2 nodes (minimum interaction score set *p* = *.7*, high confidence), yet no significant interaction associated with this gene was found in STRING. Additionally, not much information was found regarding RBM43 other than being identified as a motif protein 43, a protein RNA-binding protein 43 located in **chr2**. In the > 2 fold results, GCLM, located in chr1, and the protein encoded by this gene has been identified has been associated with several biological processes such as a negative regulator of the extrinsic signaling pathway, aging, apoptotic mitochondrial changes, and with the first step of the sub-pathway that synthesizes glutathione from L-cysteine and L-glutamate. MOB3C was also found in chr1 and it was overexpressed in the bioprinted MCF7 cells 2.5 fold higher than non-printed MCF7 cells. The protein encoded by this gene is involved with metal ion binding and has been involved with regulating the activity of kinases. Finally, VDR was found in STRING, with an interaction score set at 0.7, with 11 nodes and 40 associated edges (protein connections). This gene is upregulated by 2.2 fold in the BP MCF7 cells and it is located in chr12. The complete list of upregulated/downregulated genes expressed in the BP MCF7 cells and MS cells is in Appendix I

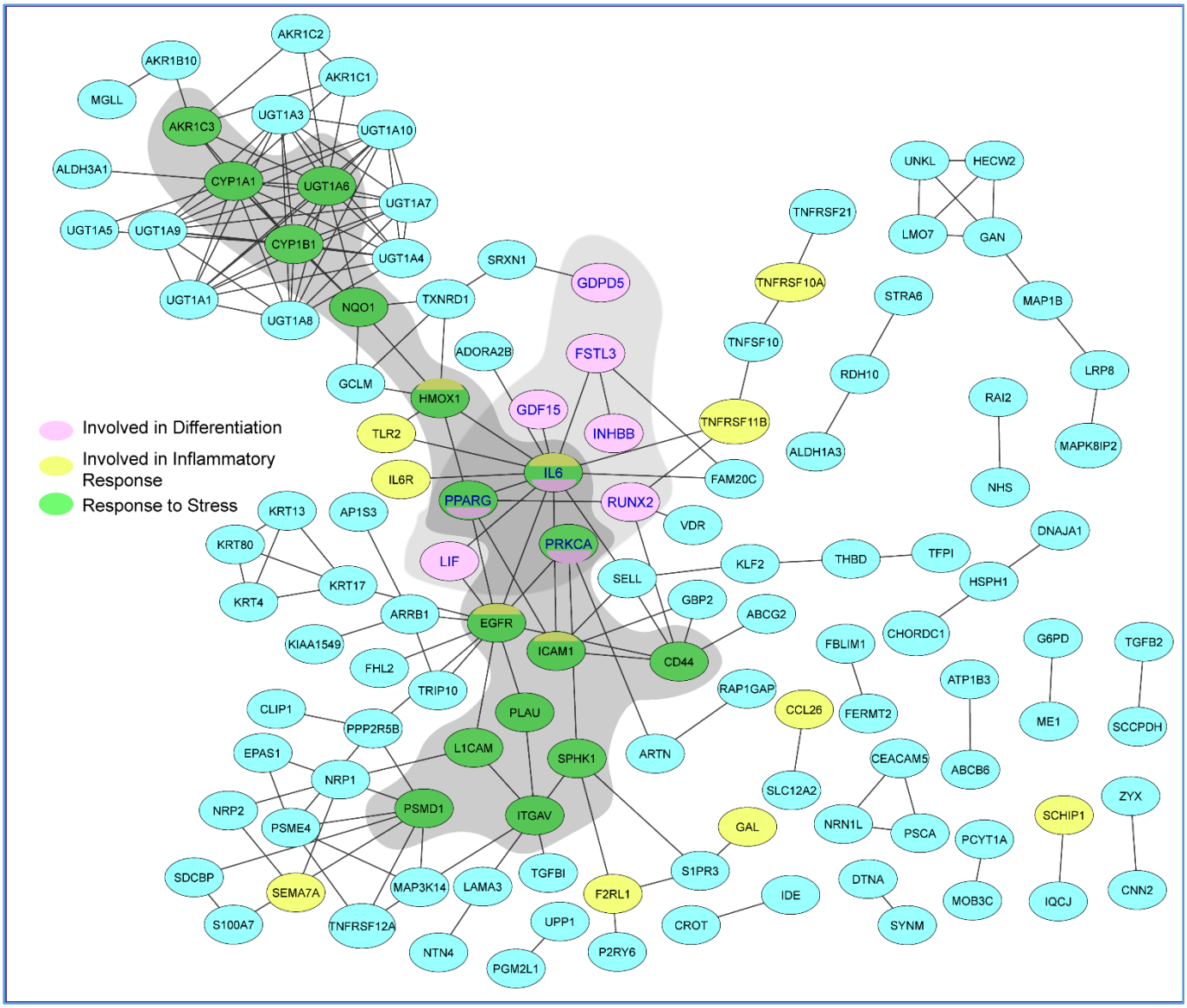

Figure 3.7. Network diagram of upregulated genes in RNA seq analysis, protein-protein network interaction, with organic layout, slightly re-arranged for better readability. Genes with > 10 edges are observed for CYP1A, IL6, UGT1A6, EGFR and CYP1B1, (see *Table 3.1*). Ovals with pink fill were found to be involved in cell differentiation, ovals with yellow fill are involved in inflammatory response and ovals with green fill were identified as responsive to stress.

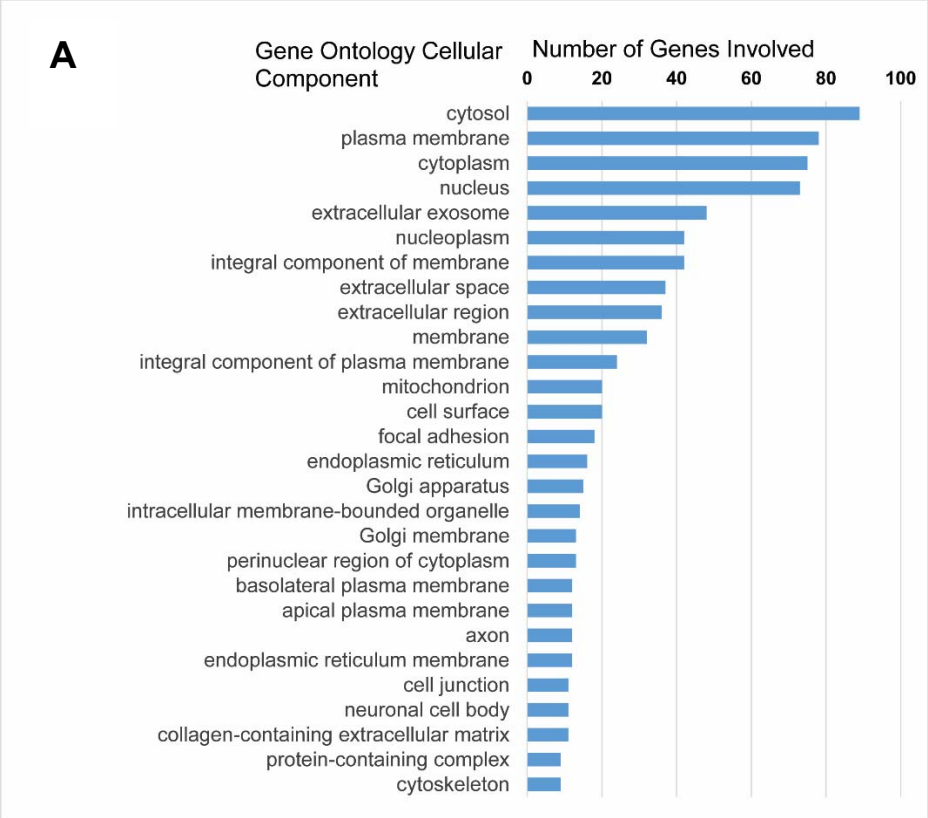
A
Gene Ontology Cellular Component
Number of Genes Involved
0
20
40
60
80
100
cytosol
plasma membrane
cytoplasm
nucleus
extracellular exosome
nucleoplasm
integral component of membrane
extracellular space
extracellular region
membrane
integral component of plasma membrane
mitochondrion
cell surface
focal adhesion
endoplasmic reticulum
Golgi apparatus
intracellular membrane-bounded organelle
Golgi membrane
perinuclear region of cytoplasm
basolateral plasma membrane
apical plasma membrane
axon
endoplasmic reticulum membrane
cell junction
neuronal cell body
collagen-containing extracellular matrix
protein-containing complex
cytoskeleton

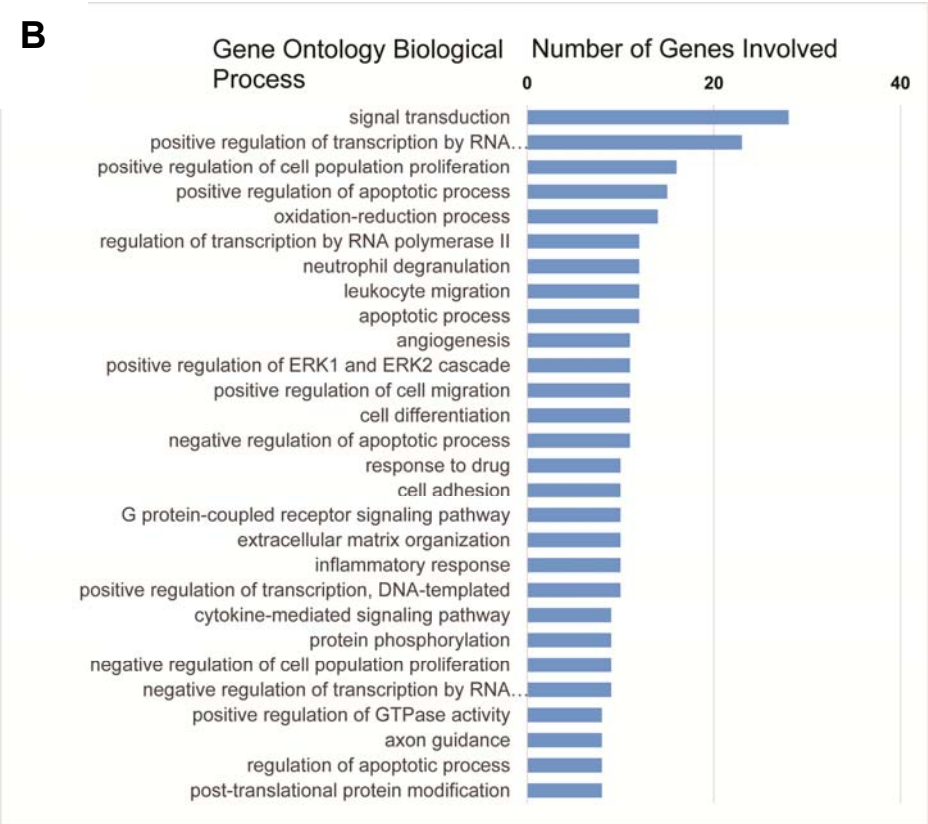
B
Gene Ontology Biological Process
Number of Genes Involved
0
20
40
signal transduction
positive regulation of transcription by RNA...
positive regulation of cell population proliferation
positive regulation of apoptotic process
oxidation-reduction process
regulation of transcription by RNA polymerase II
neutrophil degranulation
leukocyte migration
apoptotic process
angiogenesis
positive regulation of ERK1 and ERK2 cascade
positive regulation of cell migration
cell differentiation
negative regulation of apoptotic process
response to drug
cell adhesion
G protein-coupled receptor signaling pathway
extracellular matrix organization
inflammatory response
positive regulation of transcription, DNA-templated
cytokine-mediated signaling pathway
protein phosphorylation
negative regulation of cell population proliferation
negative regulation of transcription by RNA...
positive regulation of GTPase activity
axon guidance
regulation of apoptotic process
post-translational protein modification

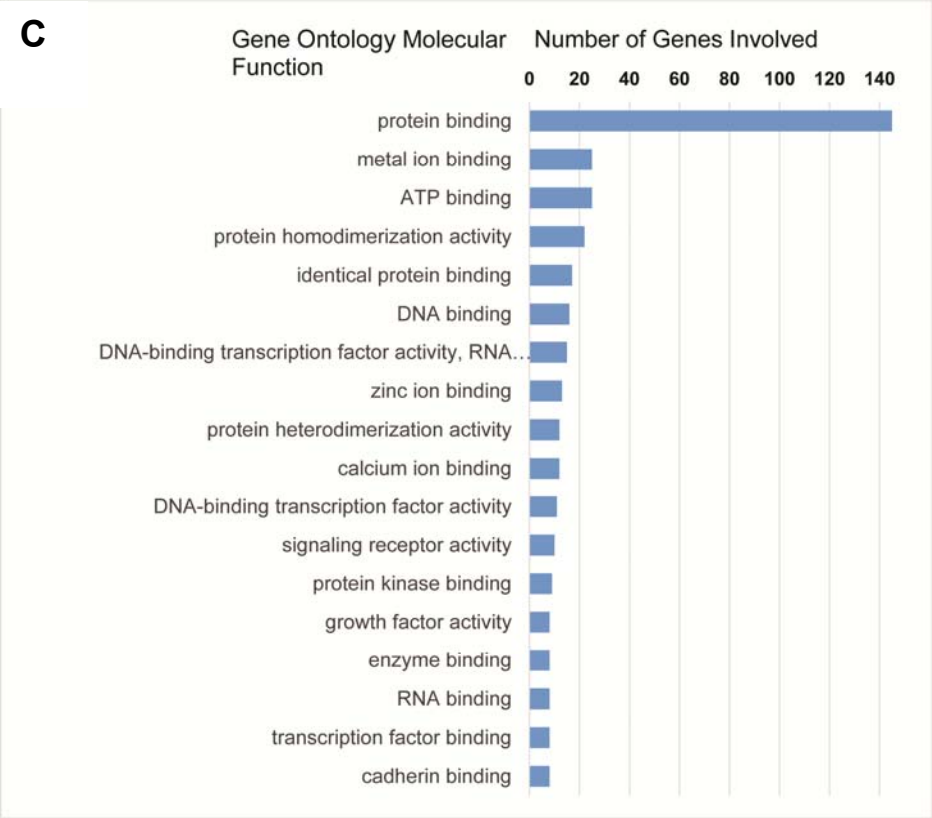

Figure 3.8 Bar graphs depicting the frequency of the different molecular functions or sites associated with the GO terms in the differentially expressed genes (upregulated). The bars indicate the number of times a function or component is repeated, graph A) displays the data connected to the biological processes, B) molecular functions, and C) cellular components. Data set is shown for > 8 repeated ontologies with *q-values* ≤ *.05*. The top three biological processes involved molecular signaling from the outside of the cell to the inside, inducing transcription and cell proliferation, which could be the cellular response to the stress these cells were exposed to due to bioprinting.

Table 3.1. List of genes extracted from the upregulated genes (greater than 2 fold) in the bioprinted MCF7 cells RNA seq analysis, this table contains only genes with ≥ 5 number of edges, network diagram depicted in figure 11. The number of edges represents the interactions among the proteins, this table was extracted from Cytoscape v.3.7.1.

GENES	Closeness Centrality	Degree	Number Of Directed Edges
CYP1A1	0.22222222	14	14
IL6	0.34024896	13	13
UGT1A6	0.22162162	13	13
EGFR	0.33744856	12	12
CYP1B1	0.22102426	12	12
UGT1A3	0.18594104	9	9
UGT1A4	0.18594104	9	9
UGT1A10	0.18594104	9	9
UGT1A8	0.18594104	9	9
UGT1A9	0.18594104	9	9
UGT1A1	0.18594104	9	9
UGT1A7	0.18594104	9	9
PSMD1	0.22465753	7	7
AKR1C3	0.18594104	6	6
NQO1	0.25867508	6	6
HMOX1	0.29927007	6	6
ITGAV	0.23563218	6	6
CD44	0.27152318	6	6
PSME4	0.22343324	5	5
ICAM1	0.26537217	5	5
PPARG	0.32156863	5	5

Table 3.2. List of genes extracted from the downregulated genes (< - 2 fold) in the bioprinted MCF7 cells RNA seq analysis, this table contains only genes with ≥ 5 number of edges, network diagram depicted in figure 12. The number of edges represents the interactions among the proteins, this table was extracted from Cytoscape v.3.7.1

GENE	Betweenness Centrality	Closeness Centrality	Degree	Number Of Directed Edges
TP53	0.62411488	0.50420168	20	20
FOS	0.27122411	0.46875	15	15
JUN	0.10417137	0.45112782	12	12
EGR1	0.12483051	0.43478261	12	12
HIST2H2AC	0.16229755	0.37037037	11	11
FOSB	0.03096045	0.37735849	10	10
MYC	0.12	0.42253521	9	9
EGR2	0.03934087	0.36144578	8	8
KIF20A	0.08163842	0.28037383	6	6
ATF3	0.01900188	0.4	5	5
HMMR	0.04887006	0.27906977	5	5
NR4A1	0.00951977	0.40268456	5	5
CTGF	0.09722222	0.39473684	5	5

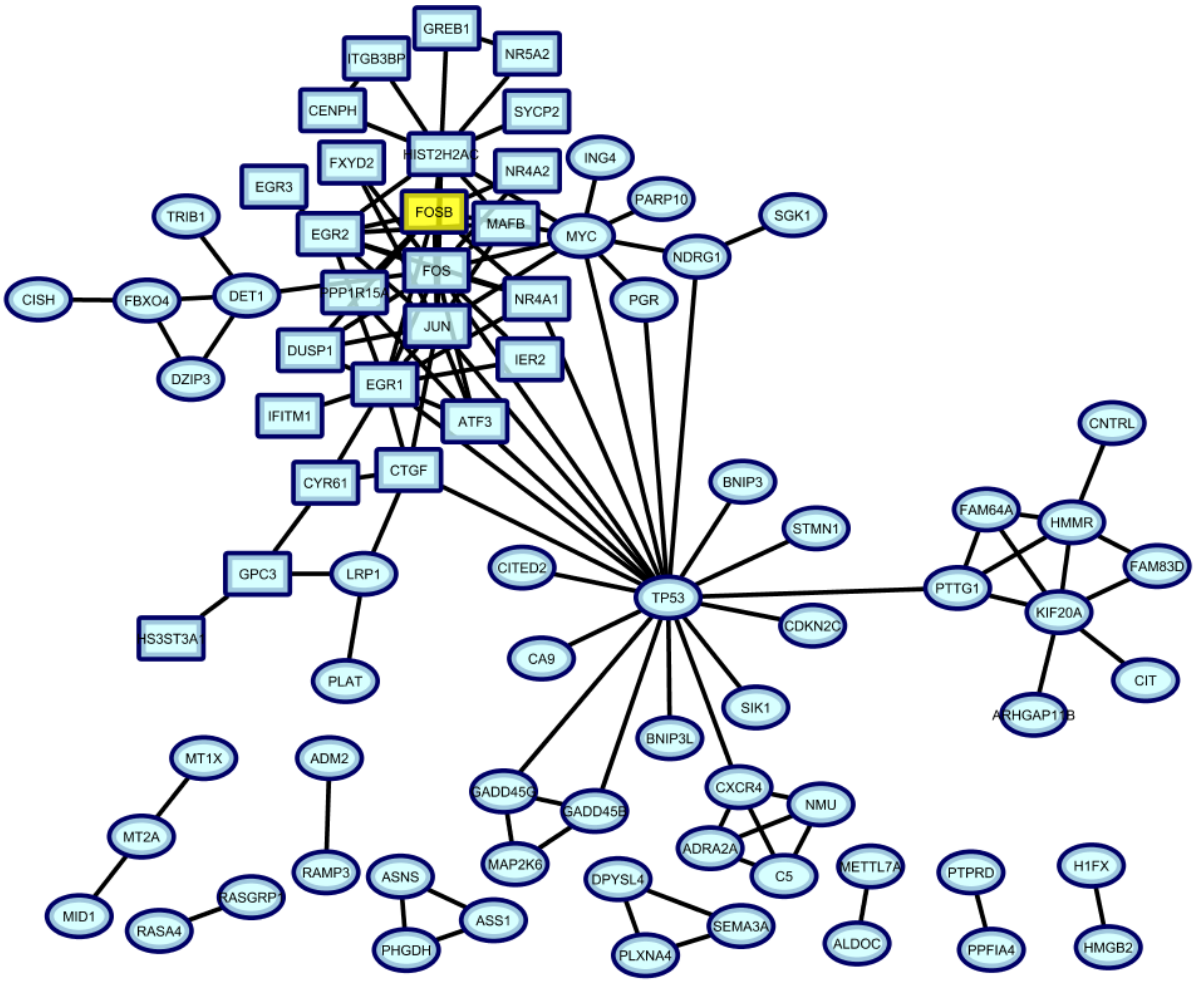

Figure 3.9 Network diagram of downregulated genes in RNA seq analysis of BP MCF7 BCCs, protein-protein network interaction, layout selected was organic layout, slightly re-arranged for better readability. This network contains only the genes defined in STRING. Genes with > 10 edges are observed for TP53, FOS, JUN, EGR1, HIST2H2AC, and FOSB, (see *Table 3.2*).

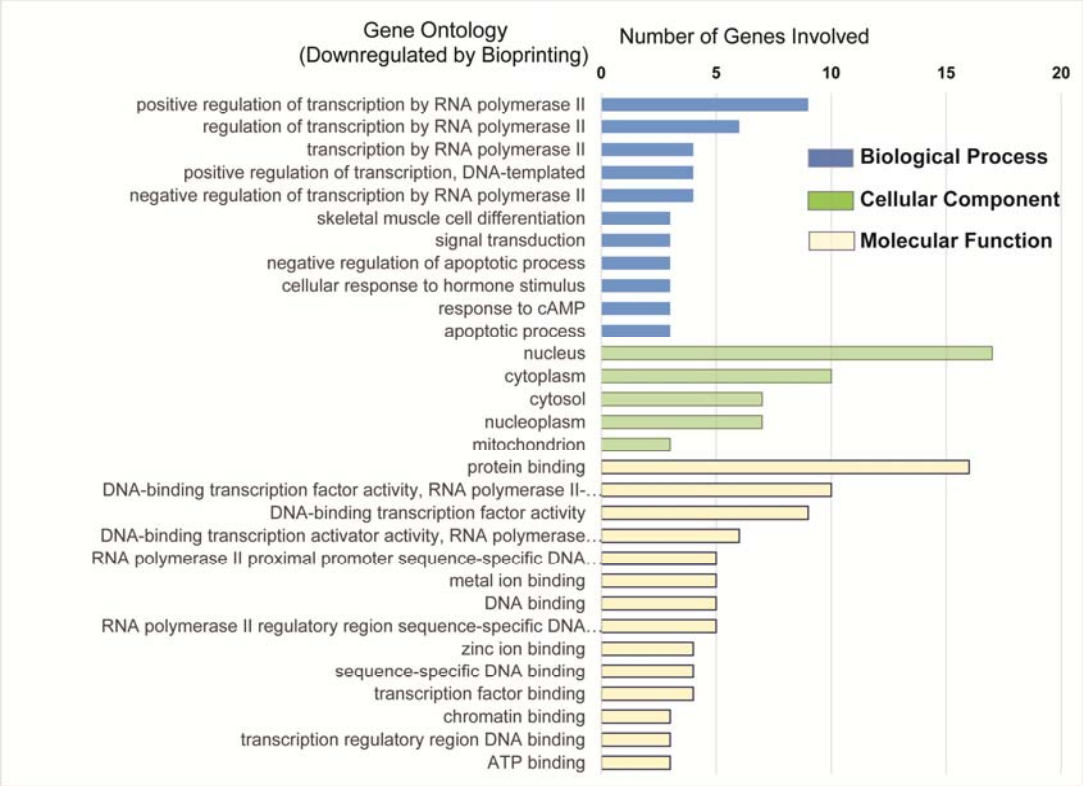

Figure 3.10 Bar graph depicting the frequency of the different molecular functions or sites associated with the GO terms in the differentially expressed genes (downregulated). The bars indicate the number of times a function or component is repeated, data connected to the biological processes, molecular functions, and cellular components. Data set is shown for > 3 repeated ontologies with *q-values* ≤ .05. Fewer ontologies under biological process were observed in downregulated genes due to bioprinting, which is what we expected to find.

3.4 Discussion

The present study evaluated morphology, viability, apoptosis and necrosis, phosphorylation of MAPK array, exosome, and RNA seq analysis of BP MCF7 BCCs. The cellular morphology of BP cells was compared to the MS cells. The BP cells appeared to have blebs, and non-spherical and distorted bulky features when compared to the MS cells (Figure 3.2). These protrusions may be caused by shear and

mechanical stresses during bioprinting. Wickmann, et al. identified blebbing as one of the distinctive characteristic of apoptosis [125]. This apoptotic morphological feature was confirmed by performing the Annexin A5-FITC necrosis/apoptosis assay, where after several hours following bioprinting, a number of cells appeared in the early and late apoptosis phases (Figure 3.1).

BP cells were interrogated with the neu antibody. Neu is a glycoprotein expressed in approximately 30 % of the cancers, yet not highly expressed in MCF7 cells. Neu (HER2) was probed in the BP and MS MCF7s to test the hypothesis that bioprinting would induce the expression of the HER2/neu protein. However, results were contradicting, during microscopy analysis using the laser-scanning confocal, utilizing the same parameter settings to both samples, intensity measurements were extracted from several cells and were compared. A remarkable difference between intensity measurements of the two cell samples was observed, statistical significance was found (Figure 3.2, $p < .0001$).

3.4.1 Viability, Apoptosis, Necrosis

Viability results from this experiment were conducted at 24 and 48 h post-bioprinting with 3 repeated measurements each using an automated counter and a hemocytometer with 2 lab associates conducting cell counts. These results were comparable to other published results which indicate a > 70 % viability [99, 126]. Others have reported higher cell viabilities ranging from 90 % to 98 %[99, 127] 24 h post bioprinting [77]. Chang et al., reported that bioprinted HepG2 cells' viability in a multi-syringe nozzle was between 70-80 % [128]. Though, in that study, the bioink used to bioprint cells was

sodium alginate crosslinked with $CaCl_2$. In our experiment, the viability of the bioprinted cells ranged from 60 % to 87 % tested at both, 24 and 48 h intervals. Additionally, in this setup, no media replenishments were applied which could additionally impact cell survival. In brief, during this process, cells are discharged from the modified print cartridge at approximately 2.5 μm/s [129], they pass through a heated filament where the temperature is briefly (μsecs.) raised close to 300^{o}C [130, 131]. Therefore, bioprinted cells in a thermal inkjet printer are briefly heated as they pass through the printing filament and literally tossed onto the biopaper. In this experiment a petri dish with pre-incubated cell media at a pH of 7.2 was used [98, 101, 131]. It is worth noting that during cell count preparation, most of the cells that did not survive bioprinting may have been discarded during the prep process because those cells were already detached from the petri dish. When centrifuged and the supernatant was gently decanted some of the floating cells might have been removed, leaving mostly live cells in the pellet.

Moroi et al. found that tumor cells exposed to a 43^{o}C water bath for 30 minutes quickly entered apoptosis depending on the localization of the tumor cells [17]. In addition, they observed that necrosis did not change immediately but it gradually increased within 3-6 h, ($p < .01$) [132]. Measurements of results from the Annexin VA analysis at 2 h post-bioprinting, resulted in an apoptotic rate of 30.5 % with a necrotic rate of 0.1 %. At 24 h, it indicated a 45 % apoptotic rate with a necrotic rate of 6 % following bioprinting. The percentage of live cells in this assay was 69 % and 30 % at 2 and 24 h, respectively, suggesting that bioprinting causes damage to the cells. On average, 12 % and 19 % of the bioprinted cells evaluated at 2 and 24 h post-bioprinting appeared in the early

apoptotic cycle. As sampling collection time was increased post-bioprinting, a 2.4 fold increase in the late apoptosis stage was observed 24 h later and a 1.15 fold increase at 48 h. In another study, Catros, et al. reported a mortality rate of endothelial cells embedded in sodium alginate solution bioprinted with a Laser Assisted Bioprinter (LAB) between 37-60 %, which was dependent upon on the thickness of the Matrigel™ (bioink) used and the laser energy applied, which varied between 20 μm to 100 μm and from 8 μJ to 24 μJ, respectively [97]. They observed a lower mortality rate in thicker gels (80 μm-100 μm) when higher laser energy was applied [97]. However, the actual mortality rate was not directly measured, it was concluded from observed images. Bioprinting may be causing thermal and mechanical stress to the cells resulting in a high number of stressed and weak cells that when subjected to the Annexin A5-FITC assay, they just became apoptotic, instead of fully convalescing. This is important when considering drug tests, bioprinted cells shall be allowed recovery time with at least one media change prior to adding any drugs.

3.4.2 Phospho MAPK array – phosphorylated analytes in BP MC7 BCCs

3.4.2.1 GSK-3α/β

GSK-3β – regulated by the Ras signaling pathway, stimulates cell proliferation [133]. GSK-3α,a Ser/Thr kinase, was identified as a deactivator of Glycogen Synthase and a regulator of other cellular functions, e.g. cancer cell survival and proliferation [134]. Some phospholipids also contain an inositol group (inositol – resides in the cell's membrane attached to the hydrophilic head of those phospholipids and it is a water-soluble carbohydrate molecule) [3]. This Inositol's moiety can be changed by adding a phosphate group, or by several distinct kinases. When this occurs, the resulting

phosphoinositol is next cleaved from the hydrophobic portion of the phospholipid molecule [135]. As a result, the hydrophilic portion, aka phosphoinositol (IP_3) scatters away into the membrane operating as an intracellular hormone to send signals from the plasma membrane to other parts of the cell. These types of hormones are referred to as second messengers [3, 135, 136]. The byproduct of the separation is a diacylglycerol (DAG), which activates a key signaling kinase in the cell, the ser/thr kinase, aka protein kinase C (PKC) [3]. When this activation occurs, it triggers other signaling cascades that have been associated with inhibition of apoptosis, stimulation of cell proliferation, cell cycle progression, and stimulation of protein synthesis. Inhibition of apoptosis was also observed during initial drug tests (tamoxifen). This phenomenon is known as the hormesis effect [137]. In that study bioprinted cells developed some resistance to tamoxifen at higher drug concentrations (> 90 μM) but this effect was not observed in MS cells.

In another arrangement, GSK-3β was found to phosphorylate β-catenin, cyclin-D1, and Myc, through what is known the canonical Wnt pathway, which causes –β-catenin's degradation [3, 138]. If however, GSK-3β is deactivated, β-catenin translocates to the nucleus where it binds Tcf/Lft Transcription Factors (TF) and stimulates expression of various genes including genes related to cell proliferation [3]. GSK-3β is deactivated via phosphorylation by Akt/PKB; this inhibition prevents cells from entering apoptosis [138].

GSK3 works as a multifunctional downstream switch that influences the output of several signaling pathways [136, 139]. GSK3 α/β isoforms are architecturally alike but their functionality is not similar [140, 141]. GSK-3α is abrogated by phosphorylation at

ser211 by Akt and other kinases [141]. GSK-3α & GSK-3β share approximately 85 % of amino acid identity. Dysregulated GSK-3 has been implicated in several diseases including type II DM, Alzheimer's, Bipolar disorder and cancer [3, 139, 142]. GSK-3α/β is highly phosphorylated in both cell sample conditions, yet in the BP cells, phosphorylation was 1.6 fold higher than in MS cells. GSK3α/β are encoded by GSK3A and GSK3B, respectively. In the RNA seq analysis, both genes were expressed, where expression of this gene was upregulated in the BP cells by 1.2 fold, though no statistical significance was found (*q-values* > *.05*) for both. Through the protein-protein network analysis we observed that this protein contains 9 interactions, which activate or de-activate other signaling pathways that may stimulate cancer progression as is the case of β-catenin.

3.4.2.2 JNK pan

The c-Jun is a member of the MAPK (mitogen-activated protein kinase) family that emits signals from the extracellular domain to the nucleus and cytoplasm of the cell [143, 144]. Three types of MAPKs have been identified: p38Kinases, ERKs, and JNKs (encoded by gene MAPK8). JNKs are small proteins, 45-55kDa, and product of three genes which, through different splicing, create up to 10 isoforms [143, 145]. Some of the phosphorylation sites for MAPKs include p53, cMYC, ATF2 and c-Jun [146]. JNKs translocate to the nucleus when stimulated by inflammatory cytokines and environmental stresses, there they regulate the process of various TFs, comprising the c-jun element of AP-1 and ATF-2, the AP-1/c-jun complex was found to act as a signal-transducing transcription regulator [3, 144]. This kinase has been implicated in several biological processes such as cell migration, differentiation, proliferation, transformation

and programmed cell death [3, 147]. It has been shown that JNK/SAPK, p38 can be activated by environmental stresses, like heat shock, osmotic shock and others [148] as we believe to be the case in BP MCF7s. Phosphorylation levels of JNK in BP cells were 4.4 fold higher than in the MS cells. Expression levels of this gene in the RNA seq analysis changed slightly, BP cells exhibit a downregulated expression by 0.17 fold than in MS cells, though no statistical significance was found (*q-value* > *.05*). We believe that phosphorylation of JNK by bioprinting may be inducing Activating Protein-1 (AP-1), which has been implicated in antiestrogen resistance in breast cancer.

3.4.2.3 RSK1/2

RSK1, also known as ribosomal S6 kinase 1 is encoded by gene RPS6KA1. It is also referred to as P90RSK1 (90kDa RSK1) or MAPKAPK 1a (MAPK-activated protein kinase 1a). It is a broadly expressed component of the RSK consort of growth factor-regulated ser/thr kinases [149]. RSK proteins contain two known isoforms (RSK2/3); each of which contains two distinct kinase catalytic domains, a C-terminal and an N-terminal [150]. RSKs activate and mediate activation of mitogen-activated kinase (MAPK) cascades and stimulate cell proliferation and differentiation [151]. RSK1 is phosphorylated by ser/thr ERK kinase, which is upstream in the MEK-ERK signaling cascade [151, 152]. RSK1 has been found to phosphorylate several substrates associated with apoptosis, e.g. CREB, and c-Fos [3, 150] and it is a key mediator of the MEK-MAPK cell survival signaling [150, 151, 153]. RSK1/2 appeared highly phosphorylated in BP cells but not in MS cells (*Figure 5*). RPS6KA1 is highly upregulated in BP MCF7 cells by 1.6 fold, as compared to MS cells with a statistical significance of *q-value* = *.001*. Both, the Phospho-MAPK array and RNA seq, results

confirm this finding. This suggests that MCF7 cells surviving the bioprinting process may become more resilient which makes this *in vitro* model a great candidate to test drug immunity.

3.4.2.4 HSP27

HSPs have been identified to belong to a large family of stress response proteins and they function as molecular chaperones by assisting with the folding/unfolding of other cellular proteins, have a primary role in protein repair and keeping substrate aggregation [154, 155]. HSPs are normally expressed at low levels but under heat shock they hyper-phosphorylate [154, 156] as was observed in BP MCF7 cells. Elevated levels of HSPs has been found in ischemia/reperfusion, cancer, and chronic heart failure [157] [155]. HSP27 also functions as an anti-apoptotic molecule, regulating apoptosis through direct interaction of key components of the apoptotic pathway, this occurs in cooperation with HSP70 [157, 158]. HSP27 inhibits cytochrome c released from the mitochondria. Cytochrome c is required for the activation of caspases, which are associated with apoptosis [159]. This suggests that HSP27 is engaged with preventing the activation of procaspase-9 and procaspase-3, which negatively affect apoptosis [155, 158, 159]. Phosphorylation for this analyte was observed in BP cells only, and it was not shown in MS cells. In the RNA seq analysis of the BP MCF7 cells, expression levels are higher than in MS MCF7 cells although no statistical significance was found ($q\text{-}value > .05$). Unregulated levels of heat shock proteins might trigger a cell survival mechanism in cancer cells.

Heat Shock Proteins (HSPs) are known to play a key role in response to cellular stresses [160-162]. This assay confirms one of our hypotheses that thermally bioprinted BCC stimulate Heat Shock Proteins (HSPs), in this case HSP27. Additionally, HSPs activate the angiogenic pathway that leads to VEGF expression, vessel formation, and accelerated tumor formation in host tissues [162, 163]. Thermal inkjet bioprinting exposes cells to heat pulses during the bioprinting process [98, 99], which explains HSP27 strong phosphorylation and upregulation by the bioprinting process.

3.4.2.5 p38 family

The p38 MAPKs, a group of 4 related Ser/Thr kinases (alpha, beta, gamma, and delta), are stimulated by proinflammatory cytokines, environmental stresses, hypoxia and osmotic shock [164, 165]. All p38 elements are phosphorylated by MKK3 and/or MKK6 at two Thr and Tyr positions within the phosphoacceptor sequence Thr-Gly-Tyr [166]. p38α, aka SAPK2α and MAPK14, were initially purified as kinases, which are vital to the signaling cascade connecting IL-1 to MAPKAPK-2 and HSP27 [167]. Collectively expressed, p38α is twice phosphorylated by MKK3 and MKK6 at Thr180 and Tyr182. Once stimulated, p38α phosphorylates several targets, which include cytoplasmic kinases MNK4 and PRAK5, the nuclear TFs ATF2, STAT1, and Max [3, 166-168]. The activation of those kinases may act as tumor suppressors and the activation of those TFs is important in cell proliferation and cell survival. In fact, mutated STAT3 has been found in a number of human cancers [3]. Several compounds that inhibit p38α continue to be screened as potential therapies for inflammatory disease and arthritis [169, 170]. In BP MCF7 cells, p38 was highly phosphorylated whereas in MS cells no phosphorylation was observed, which may also be attributable to phosphorylation of MKK3/6 and stress caused by bioprinting. Expression levels in RNA seq are slightly higher in BP cells by 1.2 fold than in MS cells, although no statistical significance was found (*q-value* > .05).

3.4.2.6 MSK2

MSK2 aka RSK-B (Ribosomal S6 Kinase B), has two catalytic domains, an N- and a C-terminal. Both domains have ATP activation [171]. MSK2 activates due to stress-

related signaling by P38a/MAPK and weakly by ERK1 [171]. RSKs are involved with regulation of glycogen metabolism, cell survival, regulation of transcription factors and co-regulators like estrogen receptors, c-Fos and CREB [171, 172]. MSK2 is encoded by the RPS6KA4 gene. RSK-B has been associated with Bardet-Biedl syndrome (obesity) [173]. MSK2 appears phosphorylated in BP cells but it is deactivated in MS cells. Additionally, in RNA seq analysis, the expression is higher in the BP cells (> 1.2 fold) than in MS cells, though no statistical significance was noted (*q-value* > .05). Cancer cells are known to metabolize large amounts of their glucose through the glycolysis cycle, rather than through the citric cycle, meaning that activation of MSK2 in the bioprinted cells may assist with the regulation of glycogen metabolism and cell survival.

3.4.3 Phosphorylated sites in both MS and BP MCF7 BCCs

3.4.3.1 p70S6 Kinase

P70S6 is located in the cytoplasm and controls the activation of cell growth which results in the phosphorylation of the 40S ribosomal protein S6 [174, 175] and is generally expressed in adult human tissues [174, 176]. The PI3K/Akt pathway has been found to control the activation of P70S6 [177]. p70S6K activity increases during the G1 phase by 20 fold when released from the G0 phase [178, 179]. Activation of p70S6K requires consecutive phosphorylations at proline-directed sites in the alleged auto-inhibitory pseudo-substrate domain, along with Thr389, a site that is phosphorylated by phosphoinositide-dependent kinase 1 (PDK1) and it is encoded by the RPS6KB1 gene [174, 176]. P70S6K is highly phosphorylated in MS cells; however, phosphorylation levels decrease by 0.6 fold in BP MCF7 cells, which suggest cell cycle arrest at G0 for the BP cells. Explaining low survival rates post-bioprinting. In the RNA

seq analysis, RPS6KB1 gene is upregulated by 1.4 fold in BP MCF7 cells; however, it is not statistically significant (*q-value* > *.05*).

3.4.3.2 CREB

The cyclic AMP Response Element-Binding Protein (CREB) is part of the bZIP family of TFs. It encloses a simple domain that determines DNA binding, and a leucine zipper domain that enables dimer formation[3]. Once activated, CREB dimers bind cAMP response elements described by the palindromic sequence TGACGTCA [180]. When phosphorylated at ser133, CREB also binds the co-activator CREB binding protein (CBP), increasing transcription by acetylating histones to enable chromatin unfolding [181]. CBP, a widely acting transcriptional co-activator works with β-catenin to induce expressions of essential genes, including gene encoding survivin, an important anti-apoptotic IAP protein, as well as the well-known protein, cyclin-D [3]. CREB is associated with cancer growth and poor clinical outcomes in several types of cancer, including breast cancer [182]. In MS cells, CREB, ERK1/2 were constitutively phosphorylated by 2 and 3.5 fold, respectively, higher than in BP MCF7 BCCs. CREB is encoded by the CREB1 gene and in the RNA seq analysis, CREB1 is slightly overexpressed in BP MCF7 cells but it is not statistically significant (*q-value* > *.9*). The lower phosphorylation levels in the BP cells suggests to participate in cell survival and cell synthesis.

3.4.3.3 ERK1/2

Two isoforms of the ERKs, ERK1 and ERK2, are 84 % similar in sequence and are encoded by MAPK3/MAPK1, respectively [183]. A protein Ser/Thr kinase which is a

member of the EC signal-regulated kinases (ERKs) are activated in response to numerous growth factors and cytokines[183]. ERK1/2 participate in the MAPK signaling cascade. Activation of ERK1 needs both tyr and thr phosphorylation that is mediated by MEK [184]. ERK1 once activated, translocates into the nucleus and phosphorylates several TFs, which regulate apoptosis, translation, cytoskeletal components and other signaling factors [63, 168, 183, 185]. ERK1 is commonly found in tissues with the highest expression occurring in the brain, spinal cord and heart [183, 186], and about half of the ERKs in phosphorylated cells are located in the cytoskeleton [149]. In MCF7 cells, the ERK pathway is activated by estradiol [149]. While ERK1/2s were highly phosphorylated in MS cells, the phosphorylation levels in BP cells is lower by 0.3 and 0.5 fold. In this experiment, the RNA seq analysis expression levels for ERK1 are slightly lower in BP cells (0.35 fold) than in MS cells. For ERK2, the opposite is observed with higher expression levels in BP cells (1.36) than in MS cells, exhibiting no statistical significance (*q-values* > *.05*). Lower phosphorylation levels in the BP cells indicate some signaling is still evident, which may interact with other proteins or stimulate TFs to regulate translation or apoptosis.

3.4.3.4 Akt1/2

A family of ser/thr kinases known as Akt1 and Akt2 regularly triggered downstream of growth factor receptors and PI3 Kinase [3, 187]. These kinases are composed of an N-Terminal pleckstrin homology (PH) domain, a central kinase domain, and a C-terminal regulatory domain and are encoded by Akt1/2 genes, respectively [187]. Amplified Akt2 has been found in ovarian tumors [188]. Akts participate in cell survival and proliferation, cycle progression, vesicle trafficking, glucose transport, metabolism, and

biological processes [189, 190]; Akt activation is believed to have a key function in tumorigenesis [191]. Akt's survival signaling is regulated by several systems in addition to the phosphorylation of the Bad protein[192]. Akts regulate glucose uptake by mediating translocation of SLCA4/GLUT4 glucose transporter to the cell surface [23, 192]. Akt1/2, both appeared phosphorylated in MS MCF7 cells. Phosphorylation of Akt1 is not observed in the BP cells. Phosphorylation of Akt2 was 1.7 fold higher in the MS BCCs. Similarly, in the RNA seq analysis, expression level for Akt1, was slightly higher, 0.025 fold in MS cells than in BP cells, yet no statistical significance was found (*q-value >.05*). AKT2 38 fold, respectively. Lower phosphorylation levels in BP cells suggest that its role as glucose uptake regulator is limited due to the effect of bioprinting.

3.4.3.5 P53

P53 serves as the cell's guardian and regulates its destiny when it receives indications that "something" is wrong, causing it to emit signals to activate apoptosis [3]. p53 is known as a tumor suppressor protein, and it has been found mutated in many types of tumors [193] [194]. A number of events can stimulate increased p53 levels, such as exposure to acidic environments or to nitrous oxide, low oxygen tension, lack of an intracellular group of nucleotides, blockage of DNA or RNA synthesis and other insults in the cells [194, 195]. p53 works in conjunction with the mitochondria, or endoplasmic reticulum[194, 196] and other co-activators to induce apoptosis or cell cycle arrest when DNA repairs are not possible [3, 195, 197]. P53 is encoded by the TP53 gene. Phosphorylation levels were high in the BP cells suggesting p53 to be highly dysregulated in those cells. Normal noncancerous cells typically contain low levels of this protein [3]; it may also indicate that p53 was activated through the JNK signaling as

observed previously. However, in the RNA seq analysis, expression levels for P53 were significantly higher (2 fold, *q-value = .001*) in the MS cells than in the BP cells, suggesting that p53 is mutated as expected in cancer cells, though inactivation of p53 remains unknown at this point. Additionally, it could be that p53 is also being deactivated indirectly via the Akt signaling cascade.

3.4.3.6 MKK6/MMK3

MAP2K6 (MKK6) has a critical role in the MAPK signal transduction pathway [198]. MKK6 is 83% identical to MKK3 and both can activate p38 in vitro and in vivo [198-200]. p38 signaling pathway then leads towards the specific activation of transcription factors, such as ATF2 and Elk1 [201]. ATF2 dysfunction has been linked to cancer metastasis [202]. This protein is encoded by MAP2K6 and MAP2K3 genes. MKK6/MKK3 are present in both the nucleus and the cytoplasm [203]. These proteins are activated by several insults, such as heat shock, UV rays, osmotic shock, cellular DNA damage and their regulation remains obscure [201]. MKK6 is expressed mostly in muscle tissue and the pancreas and the heart, at lower levels [200]. The phosphorylation level of analytes MKK6/MKK3 was observed in the BP cells yet it was not seen in the MS MCF7 cells. Similarly, MAP2K3 was upregulated in the BP cells by 1.38 fold yet no statistical significance was found *q= .18*. Though MAP2K6 expression levels in the RNA seq of BP cells was significantly lower (0.35 fold) than in MS cells (*q-value = .027*). Hyper-phosphorylation of these kinases in BP cells may be attributed to stress caused by bioprinting. This feature may be beneficial as tumor models.

3.4.3.7 TOR

Mammalian Target of Rapamycin (mTOR) a ser/thr protein kinase acts as the main regulator in many important biological processes (bp). A few of which are energy and stress signals, cellular metabolism, growth factors and nutrients, growth and survival in response to hormones, autophagy and cytoskeletal re-organization among others [204-207]. It is part of two signaling complexes, mTORC1 and mTORC2 [208, 209]. When active, mTOR phosphorylates 4E-BP1 and p70S6K. 4E-BP1 releases EIF4 which leads to RNA transcription resulting in protein synthesis [208]. mTOR was found to prevent autophagy through phosphorylation; directly through the phosphorylation of a ULK1 and indirectly through DAP1 [210]. TOR and mTOR are encoded by genes TOR1A and MTOR, respectively. This analyte, very similar to MKK6/MKK3, appears phosphorylated in the BP MCF7 cells but not in the MS MCF7 cells, which suggests that newly bioprinted cells may be inducing cell proliferation. Expression levels for TOR1A and MTOR in the RNA seq analysis were 1.2 and 1.3 fold higher in the BP cells, no statistically significant (*q-value* > *.05*).

3.4.4 RNA Sequence Analysis

For decades, preclinical and clinical evidence has shown that cancer cells exhibit significantly higher sensitivity to hyperthermia than normal cells, intratumoral temperature ranging from 42 – 45^{o}C [211]. Cellular exposure to 45^{o}C for 30 min specifically, altered the expression of key mitotic regulators and halted G2/M phase progression in breast cancer cells, including the MCF7 cell line [206]. Thus through RNA seq analysis, we sought to explore the differences in gene expression of the MS and BP MCF7 cells since bioprinting exposes them to heat as well.

The non-protein coding gene Lung Cancer Associated Transcript 1 (LUCAT1) was among the genes found differentially and significantly overexpressed in the BP cells, as compared to the MS MCF7 cells; yet expression levels found in breast cancer stem cells (BCSCs) is higher than in normal BCCs [212]. Upregulated LUCAT1 has been implicated in BCC proliferation and shorter overall survival and progression-free survival [210]. LUCAT1 is a member of the long intervening noncoding RNAs (lincRNAs) class that seems to function downstream on the nuclear factor erythroid 2–related factor 2 (NRF2) [207]. NRF2 controls gene expression that regulates oxidative stress protection in airway epithelial cells [213]. Thus, it is likely that the LUCAT1's overexpression increases resistance to death in the BP MCF7 cells *via* NRF2, which is a developing regulator of cellular resistance to oxidants [214]. LUCAT1, expressed only in BP MCF7 BCCs, suggests that bioprinting may be differentially selecting more specifically BCSCs. It is also possible that the genes associated with stem cell phenotype are already expressed in few of the cells beforehand and when the cells were bioprinted, it triggered more cell induced cell proliferation of more cells with the stem cell phenotype. LUCAT1 has been identified as a potential target for drug discovery [215, 216].

The C-C motif Chemokine Ligand 26 (CCL26) was also found to be overexpressed in the BP MCF7 cells, as compared to the MS cells. CCL26, also known as Eotaxin-3, is a chemotactic cytokine for eosinophils and basophils and exerts its effect by binding to its receptor CCR3 [217]. It was reported that CCL26 is regulating expression of cancer-associated genes during airway inflammation [218]. Furthermore, the upregulation of this gene, as well as CCL2, IL6 and LOXL2, has been implicated as part of the effects of cancer-associated fibroblasts in promoting progression of hepatocellular carcinoma

cells [219]. These molecules are also responsible for immune cellular conglomerations and for influencing the immune response system [220]. Additionally, the CCL26-CCR3 ligand-receptor structure appears to be involved in inflammatory processes and it is upregulated in cancer progression [211], which highlights the suitability as an in vitro model for anti-cancer drug discovery initiatives.

In the molecular function taxonomy, there were 4 genes (EFCAB11, FAM117B, FAM46B, and RBM43) that were downregulated in the < -2 fold group and 3 genes were upregulated in the > 2 fold group, GCLM, MOB3C, and VDR. In STRING we found that EFCAB11 contains 11 nodes and 11 edges (connections/interactions) but there was no statistical significance, interaction score set at 0.4. Recent publications have associated this gene with hepatocellular carcinoma [221]. In the RNA seq analysis, this gene is located on chr14. FAM117B produced 5 nodes with 10 edges and resulted in 2 GO terms under biological processes. This network has been associated with negative regulation of activation-induced cell death in T-cells and response to osmotic stress, GO:0070236 and G:0006970. This gene was downregulated in the BP cells and was located in chr2. FAM46B's network contained 2 nodes (minimum interaction score set *probability* = *.7*, high confidence), though no significant interactions associated with this gene were found in STRING. Additionally, regarding RBM43 was identified as a motif protein 43, a protein RNA-binding protein 43 located in chr2, https://www.uniprot.org/uniprot/Q6ZSC3. In the > 2 fold results, GCLM was found in chr1, and the protein encoded by this gene has been identified as being associated with several biological processes, e.g., aging, apoptotic mitochondrial changes, negative regulator of the extrinsic signaling pathway, and with the first step of the sub-pathway

that synthesizes glutathione from L-cysteine and L-glutamate, https://www.uniprot.org/uniprot/P48507. MOB3C was overexpressed in the bioprinted MCF7 cells 2.5 fold higher than non-printed MCF7 cells. The protein encoded by this gene is involved with metal ion binding and has been involved with regulating the activity of kinases. Finally, VDR was found in STRING, with an interaction score set at 0.7, with 11 nodes and 40 associated edges (protein connections). Additional information can be found in STRING. This gene was upregulated by 2.2 fold in the BP MCF7 cells, high statistical significance was found (*q-value = .003)*.

NRN1L is a protein-coding gene located both in the Glycosylphosphatidylinositol (GPI) anchored in the cell membrane and also in the secreted form in the ECM [222, 223]. IL6 is released from the bloodstream following muscle contraction. IL6 has been linked to a wide variety of biological processes, such as the increase of the lipid breakdown and the improvement to insulin resistance, see, https://www.uniprot.org/uniprot/P05231. It has a key role in the differentiation of B-cells into Ig-discharging cells (an antibody used to neutralize pathogens) [224] and monocyte differentiation [225]. It has been associated with the induction of myeloma, plasmacytoma growth, and possibly involved in prion's disease [224, 226]. IL6, in this analysis, was found in BP MCF7 BCCs (chr7 - 22765013-22771621). Finally, another gene that was significantly upregulated in the BP cells was CYP1A1. CYP1A1 was observed to be upregulated by more than 300 fold. CYP1A1 encodes cytochrome P450 enzymes. These enzymes catalyze many reactions involved in drug metabolism and synthesis of steroids and lipids [227].

Under normal circumstances, cancer cells can overpass the in vivo removal tactic of the immune system by implementing diverse strategies such as evasion of apoptosis [228].

Those cellular eluding mechanisms include mutations that offer the ability to counteract the immune system, which fails to detect and eliminate. Cancer cells acquire the ability to undergo rapid proliferation without regard to the normal homeostatic system; uncontrolled proliferation is a distinctive characteristic of cancer development and progression (metastasis) [229]. Additional to these mutations, we have observed that cancer cells surviving the bioprinting process, elicit further phenotypic changes, which we believe makes them even more resistant to cancer drugs. Thus we are proposing to use bioprinted cancer cells, which become resilient and hard to kill, to discover a new class of more efficacious and potent cancer drugs. Collectively, these findings contribute with relevant information to affirm that this BP model can mimic a novel tumor model that should be studied further and applied in preclinical studies.

3.5 Conclusion

Results of bioprinted MCF7 BCC at the physiological and molecular levels were evaluated at different time frames following bioprinting in a modified thermal inkjet printer. Despite losing up to 37 % of the cell population 24 h post bioprinting, it is evident that this process induces phosphorylation at several critical sites, which activate a number of key signaling cascades as was observed in the phosphorylation of MKK6/MKK3 and RSK1/2, which have been implicated with cancer metastasis. Collectively, GSK-3α/β, ERK1, Akt1/2, JNK, RSK1/2, HSP27, p38, MSK2, p53, MKK3/6, and TOR when mutated or hyper-phosphorylated are implicated in biologically aggressive behaviors making this *in vitro* BP tumor model an ideal candidate to explore drug discovery. Unregulated levels of heat shock proteins may also be triggering a cell survival mechanism in cancer cells like receptor conglomeration of receptors in the

ECM. In this experiment, bioprinted MCF7 cells showed increased levels of chaperone protein HSP27. It is possible that bioprinting may be stimulating an increased amount of ligand-independent receptors in the cell surface which may cause certain collisions that might lead to receptor dimerization and thereby making them more sensitive in overexpressed genes associated with cellular resistance to intrinsic biological processes and cellular functions.

Furthermore, RNA seq analysis performed in bioprinted cells also provided substantial information by identifying genes involved in response to the bioprinting process. These data clearly demonstrated that thermal inkjet bioprinting is triggering a significant number of gene alterations that could potentially be used for target drug discovery. Additionally, it may be stimulating other conditions like activating pathways implicated in drug immunity, cell motility, proliferation, survival and differentiation such as the expression of NRN1L, LUCAT1, IL6, CCL26, which have been implicated with numerous diseases. This underscores the need to use these thermal inkjet bioprinting tumor models to simulate *in vivo* conditions where, in some cases, tumors develop immunity to chemotherapeutic drugs. [3]. This underscores the need to use these bioprinted models developed by thermal inkjet bioprinting to simulate *in vivo* conditions where, in some cases, tumors develop immunity to stress exposure and drug resistance.

This genomic and proteomic analysis of BP MCF7 cells indicates that BP MCF7 cells may be causing several mutations which enabled cells to become more robust encouraging MCF7 cells to activate key kinases implicated in cancer development, proliferation, metastasis and possibly many other diseases. Furthermore, through the

phospho-MAPK array, we confirmed that bioprinting is activating signaling pathways associated with cellular response to apoptosis, mitosis, cell migration, transcription and other cellular functions. Additionally, it may also be triggering other undiscovered functions in the BP BCCs, such as activation of critical pathways implicated in drug immunity or inducing cell motility, proliferation, survival and differentiation. Moreover, these data suggest that thermal inkjet bioprinting is stimulating large scale gene alterations that could potentially be used with autologous drug tests to confirm drug efficacy prior to initiating cancer therapy. Insights into the cell response after bioprinting have demonstrated that BP cells can potentially improve the in vitro models used for drug discovery, which may lead to a promising model for BC targeted drug discovery.

Chapter 4

4.1 Introduction

Breast cancer is a heterogeneous disease and the majority of the cancers can take years to develop [3] which can go undetected due to their asymptomatic nature in the majority of cases [230]. Early-stage detection has better prognosis than late-stage breast cancers due to more timely interventions in most instances [230-232]. Current breast cancer treatments are successful in eradicating this disease in the majority of patients, though there are quite a few cases where relapse or recurrence occur, which may lead to continued cancer therapy or death [10, 11].

In vitro cell testing is normally done in the early stage of drug discovery [110]. Tissue biofabrication *in vitro* has progressively developed to mimic *in vivo* environments. To date, several approaches for 3D tumor modeling exist, from the multi-layer multi-cell culture, to single Block-Cell (BloC) bioprinting, to inkjet printing [16, 92-94]. Human tissue harvesting from biopsies is another approach to developing tumor models *in vitro* though this approach tends to have a limited lifecycle and drugs tested this way may provide results that cannot be generalized for the entire population with similar biomarkers [95]. Thermal Inkjet Bioprinting is proposed as a potential *in vitro* model for further exploration of drug discovery.

Drug testing on these *in vitro* bioprinted models may be ideal for targeted drug development because it could lead to a better understanding of drug resistance for new and approved drugs. We anticipate that personalized treatments based on autologous bioprinted models, will indicate whether or not a specific treatment will be effective, prior

to initiating a treatment regimen. We hypothesized that a breast tumor model composed of bioprinted breast cancer cells will attain more accurate representations of *in vivo* environments.

Breast cancer patients with metastasis who are on systemic therapy such as palbociclib-letrozole may develop painful metastasis that may require radiation therapy for pain control. Systemic therapy is usually held during radiation therapy. This aim explored concurrent systemic therapy and radiation therapy *in vitro* on BP BCCs. Exposing bioprinted cells to palbociclib followed by radiation therapy will help identify drug response in these tumor models *in vitro.* It has been suggested to evaluate this treatment in combination with radiation although the treatment combination has not been approved for cancer treatment. Here we report findings of treatments with tamoxifen, Palbociclib-Letrozole in conjunction with radiation in BP and MS MCF7 and MDA-MB231 breast cancer cells and normal breast cells MCF10As. Tamoxifen is an endocrine treatment given to patients post-surgery and post-chemotherapy to prevent breast cancer recurrence.

4.2 Material and Methods

4.2.1 Cell Culture and Bioprinting Process

In this study, MCF7 (ATCC® HTB-22™) BCCs, MDA-MB231 basal BCCs, MCF10As normal breast cells, Eagle's Minimum Essential Medium (EMEM) supplemented with 0.1mg/L insulin and 10 % Fetal Bovine Serum (FBS), Complete Growth Medium, Dubbelco’s Modification of Eagle’s Medium (DMEM) supplemented with 10 % FBS and 1 % antibiotic/antimycotic solution, DMEM/ F-12 Medium supplemented with 10 % FBS, 1 % Penicillin-Streptomycin solution, 100 µg/mL Epidermal Growth Factor (EGF), 0.5

μg/mL hydrocortisone, and 10 μg/mL of recombinant human insulin were utilized. Trypsin w/EDTA 0.25 %, and sterile Phosphate-Buffered Saline (PBS) solution were also used. Cells were incubated as before, briefly, MCF7s, MDA-MB231 and MCF10As were cultured per ATCC cell product protocol in a humidified CO_2 incubator maintained at 37°C with 5 % CO_2 until 80 - 90 % confluency was reached. Cells were next trypsinized, and counted. Approximately, $1.2X10^6$ cells/mL were prepared in 1X PBS.

Modified inkjet cartridges were sonicated for 15 minutes and tested in a modified thermal inkjet printer. Next, 100 μL of cell solution (PBS-cells –bioink) was added to a modified sterile inkjet printer cartridge. A previously modified thermal inkjet printer was used to bioprint the cell solution.

4.2.2 Drug Preparation

Tamoxifen was prepared in ethanol (200 proof) in a stock solution of 10 mM. Palbociclib was prepared in Dimethyl Sulfoxide (DMSO) in a stock solution of 1 mM. And Letrozole was dissolved in DMSO in a stock solution of 100 mM. Drugs were serially diluted to determine cell cytotoxicity (CC50) of the BP and MS cell samples.

4.2.3 Tamoxifen Treatment

MCF7 (ATCC® HTB-22™) BC cells were cultured, when 80 – 90 % confluency was observed, cells were trypsinized and counted. Next, 100-200μL of PBS-MCF7 cell solution was added to a modified inkjet printer cartridge. 100 μL of media was added to a 96-well plate and incubated in a CO_2 humidified incubator set at 37°C with 5 % CO_2. A squared pattern was bioprinted over half of the 96-well plate, in the other half, MS cells were added and incubated for 24 h. Bioprinted and Manually Seeded MCF7 BCCs, were next treated with Tamoxifen serially diluted at 5 μM, 10 μM, 50 μM, 90 μM

and 110 μM concentrations. Cytotoxicity was measured 24 h post-treatment with a Differential Nucleotide assay (DNS) in the In-Cell Analyzer Imaging System [233]. Briefly, 24 h post-bioprinting, we exposed cells to Hoechst and Propidium Iodide 22 h after start of treatment to determine cell viability. Treated samples were incubated for 1-2 h prior to doing the analysis in the in-cell analyzer.

4.2.4 Palbociclib-Letrozole and Radiation Treatment Process

Bioprinted and Manually Seeded MCF7, MDA-MB231, and MCF10A cells were incubated for 5 days post-bioprinting with two media changes to allow cells to adapt and grow in their new environment prior to drug exposure and radiation exposure. In the 5^{th} day, a combination of Palbociclib at 10 μM, 50 μM, 100 μM, and 150 μM, with Letrozole maintained constant at 10 μM was incorporated into each well; 12 h later, the cells were exposed to fractionated irradiation of five daily fractions, at 2, 4 (2X), and 5 (2X) Gray (Gy), for a total cumulative dose of 20 Gy. Cells were evaluated at two-time points at 10 Gy and 20 Gy. The DNS assay was applied at 6 h post-irradiation. Cytotoxicity was evaluated at 1-2 h post-exposure to Hoechst and PI in the In-Cell analyzer imaging system 1000 [233]. Positive and solvent controls were also tested in parallel.

Mean (Standard Variation) values are reported for each condition. Statistical relevance was determined using paired T-tests and ANOVA for continuous variables, p-values < 0.05 were considered statistically significant. Minitab and SPSS were used for the calculations.

4.3 Results

4.3.1 Tamoxifen Treatment

Results showed that when exposed to high concentrations of tamoxifen (> 90 µM) cell viability of BP MCF7 BCCs was at 8.2 % (4.81) while for MS cells, cell viability was 0.11 % (0.07). At 5 µM percent mean cell viability was 41.1 % (37.3) and 52.3 % (53.4). At 10 µM the percent cell viability was 81.6 % (11.4) and 68.3 % (21.3) for BP and MS cells respectively.

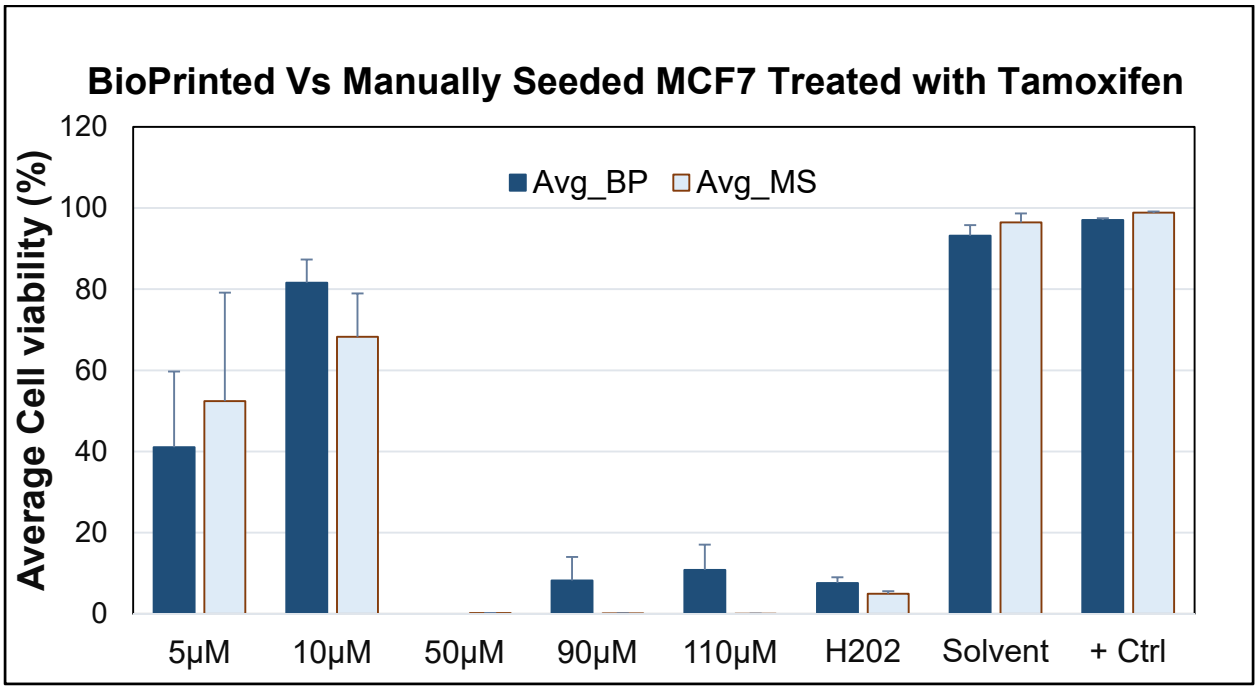

Figure 4.1 Cell viability of bioprinted and manually seeded MCF7 BCCs with 5 concentrations of serially diluted tamoxifen.

The results of the student T-test and of the positive controls were statistically significant at 50 µM and also for the positive control (media). See Table 4.1. In the table, a negative difference means that the percent viability of BP MCF7s was higher and not similar to the MS MCF7 BCCs.

Table 4.1. Student T-test with p-values of the cell viabilities when exposed to tamoxifen, BP= Bioprinted, MS = Manually Seeded, + = positive, EtOH = Ethanol.

Test μ1-μ2=0	T-Value	DF	P-Value	Difference	95% CI for Difference
5μM BP Vs 5μM MS	1.47	2	0.279	45.5	(-87.4, 178.4)
10μM BP Vs 10μM MS	-0.95	3	0.41	-13.3	(-57.7 - 31.1)
50μM BP Vs 50μM MS	4.59	3	**0.019**	0.1957	(0.0600, 0.3315)
90μM BP Vs 90μM MS	0.96	2	0.44	-2.66	(-14.61, 9.30)
110μM BP Vs 110μM MS	-0.03	3	0.976	0.3	(-32.8, 32.1)
Ctrl+ BP Vs Ctrl+ MS	-3.25	4	**0.031**	-1.81	(-3.357, -0.264)
H202 BP Vs H202 MS	-1.69	4	0.166	-2.63	(-6.93, 1.68)
EtOH BP Vs EtOH MS	-0.91	4	0.414	-3.31	(-13.40, 6.78)

4.3.2 Palbociclib-Letrozole in Conjunction with Radiation

4.3.2.1 MDA-MB-231 Breast Cancer Cells

In BP MDA-MB-231 BCCs, we observed a similar trend as the BP MCF7 with the tamoxifen treatment. No statistical significance was observed between the bioprinted and manually seeded MDA-MB-231 BCCs.

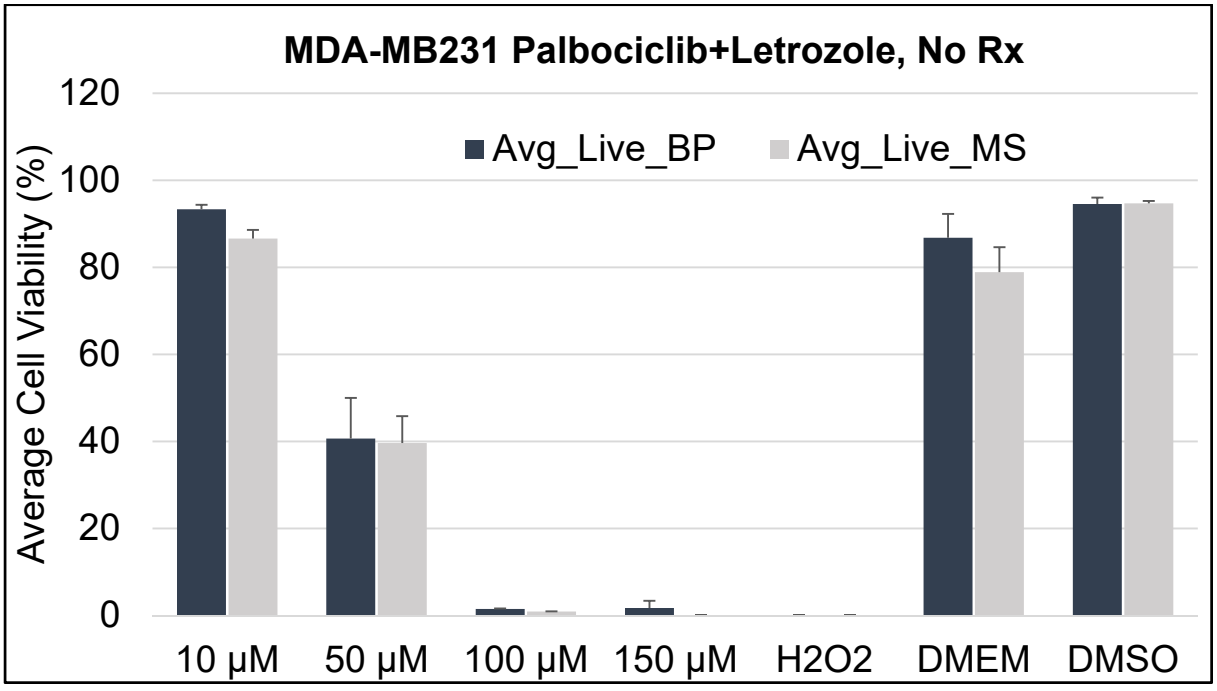

Figure 4.2 – Percent cell viability of MDA-MB321 BCCs when treated with Palbociclib and letrozole.

When cells were treated only with drugs and no radiation (Rx), at 10 μM concentration of palbociclib+10 μM letrozole, the percent average of live cells was 93.4 % (1.05) while the manually seeded cells were 86.6 % 2.0). This result was statistically significant, $p < 0.05$. The BP and MS cells at 50 μM palbociclib+10 μM letrozole was 40.6 % (9.3), and 39.6 % (6.2), respectively and no statistical significance was found. At 100 μM palbociclib+10 μM letrozole, the average for the BP and MS cells was 1.5 % (0.1) and 0.9 % (0.05), respectively and a statistical significance of $p = 0.003$. At 150 μM palbociclib+10 μM letrozole, mean cell viability was 1.7 % (1.7) and 0 % for BP and MS cells, respectively, see table 4.2 below.

Table 4.2 – Paired T-test results from the cell viability of BP and MS MDA-MB-231 cells when treated with palbociclib and letrozole.

				95% C.I. of the Difference				
Concentration	**Mean Diff.**	**Std. Dev.**	**Std. Err Mean**	**Lower**	**Upper**	**t**	**df**	**Sig. (2-tailed) (p-value)**
10μM+Let	6.7	1.9	1.0	3.7	9.8	7.0	3.0	**0.006**
50μM+Let	1.1	10.0	5.0	-14.8	16.9	0.2	3.0	0.8
100μM+Let	0.6	0.1	0.1	0.4	0.8	8.9	3.0	**0.003**
150μM+Let	1.7	1.7	0.8	-0.9	4.4	2.1	3.0	0.1
Media	7.9	5.1	3.0	-4.9	20.6	2.7	2.0	0.1
DMSO	-0.2	1.5	0.9	-4.0	3.7	-0.2	2.0	0.9

When BP and MS MDA-MB-231 cells were treated with the drug combination of palbociclib and letrozole given concurrently with radiation (Rx) therapy of 10 Gy given in 3 fractions, at 10 μM concentration of palbociclib +10 μM letrozole, the percent average of live cells was 91 % (1.6) while the manually seeded cells was 97 % (1.0). This result

was statistically significant, p-value < 0.05. The BP and MS cells at 50 µM palbociclib +10 µM letrozole was 12 % (3.2), and 24 % (4.7), respectively and statistical significance was found p < 0.0001. At 100 µM palbociclib +10 µM letrozole, the average for the BP and MS cells was 6 % (2.7) and 5% (4.3), respectively and no statistical significance was found. At 150 µM palbociclib + 10 µM letrozole, mean cell viability was 0.1 % (0.1) and 0.5 % (0.7) for BP and MS cells, respectively, see *table 4.3*. For H_2O_2, both cell samples did not survive this treatment. The percent average of BP and MS cells only treated with Rx was 86 % (2.3) and 94 % (1.0), respectively. Similar results were observed for cells exposed to the vehicle solution, DMSO in this instance. The percent average of cell viability for BP and MS cells was 96 % (1.0) and 99 % (0.3), respectively though no statistical significance was seen for both, media and DMSO.

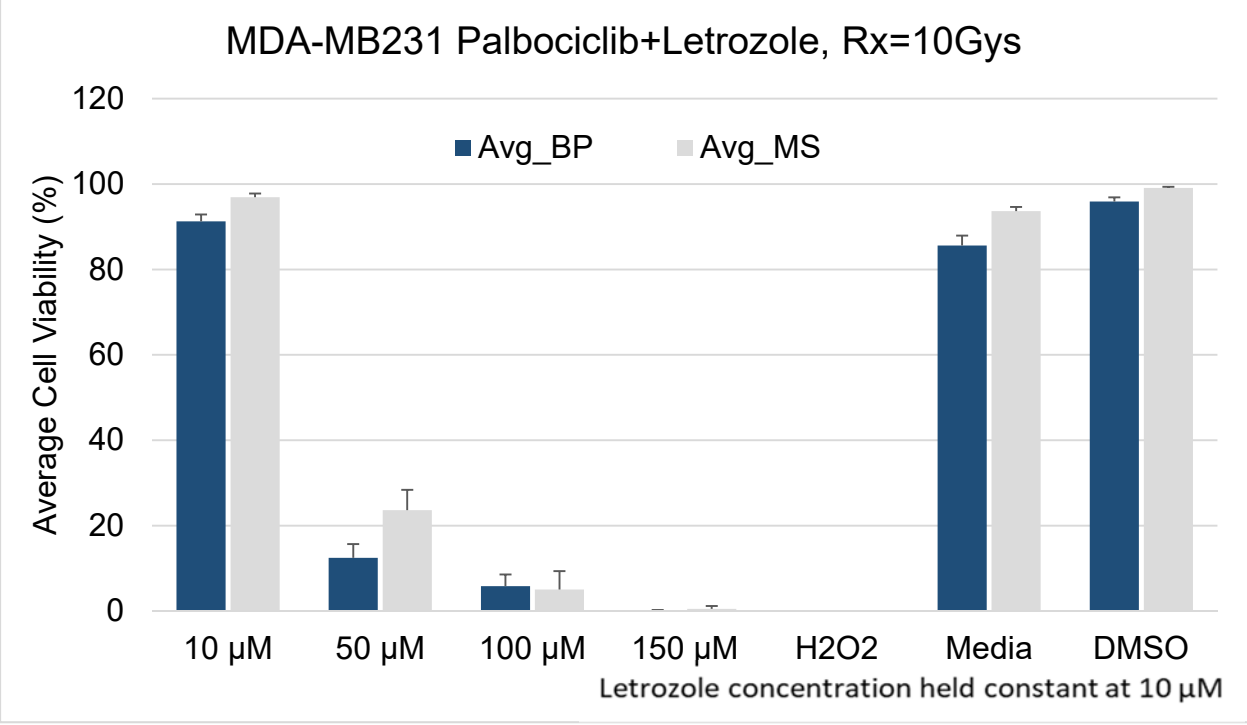

Figure 4.3 Percent cell viability of BP and MS MDA-MB-231 treated with palbociclib and letrozole (maintained at 10 μM) in conjunction with radiation, cells evaluated at 10 grays.

Table 4.3 – Paired t-test results from the cell viability of BP and MS MDA-MB-231 cells when treated with palbociclib and letrozole when exposed to 10 grays.

			95% CI of the Difference				
Mean Diff.	**Std. Dev.**	**Std. Err Mean**	**Lower**	**Upper**	**t**	**df**	**Sig. (2-tailed) (p-value)**
-5.7	2.2	1.0	-8.4	-2.9	-5.8	4.0	**0.004**
-11.2	2.0	0.9	-13.7	-8.7	-12.4	4.0	**<0.0001**
0.8	6.0	2.7	-6.6	8.2	0.3	4.0	0.780
-0.4	0.7	0.3	-1.3	0.5	-1.2	4.0	0.296
-8.1	3.3	1.9	-16.2	0.1	-4.3	2.0	0.051
-3.2	1.3	0.7	-6.3	-0.1	-4.4	2.0	**0.047**

When BP and MS MDA-MB-231 cells were treated with the drug combination of palbociclib and letrozole given concurrently with radiation (Rx) therapy of 20 Gy given in 3 fractions, at 10 μM concentration of palbociclib + 10 μM letrozole, the average cell viability percentage was 57 % (11.4) while the manually seeded cells was 42 % (4.6). The BP and MS cells at 50 μM palbociclib +10 μM letrozole was 1.8 % (0.4), and 16 % (4.2), respectively. At 100 μM palbociclib +10 μM letrozole, the average for the BP and MS cells was 6 % (2.7) and 5 % (4.3), respectively. At 150 μM palbociclib + 10 μM letrozole, the mean cell viability was 0.1 % (0.1) and 0.5 % (0.7) for BP and MS cells, respectively, see *table 4.3*. For H_2O_2, both cell samples did not survive this treatment. The percent average of BP and MS cells treated with Rx only was 86 % (2.3) and 94 % (1.0), correspondingly. Similar results were observed for cells exposed to the vehicle solution, DMSO. Percent average of cell viability for BP and MS cells was 96 % (1.0) and 99 % (0.3). A statistical significance was observed for all ($p < 0.05$), except for samples treated with DMSO ($p = 0.13$), see Figure 4.4 and Table 4.4.

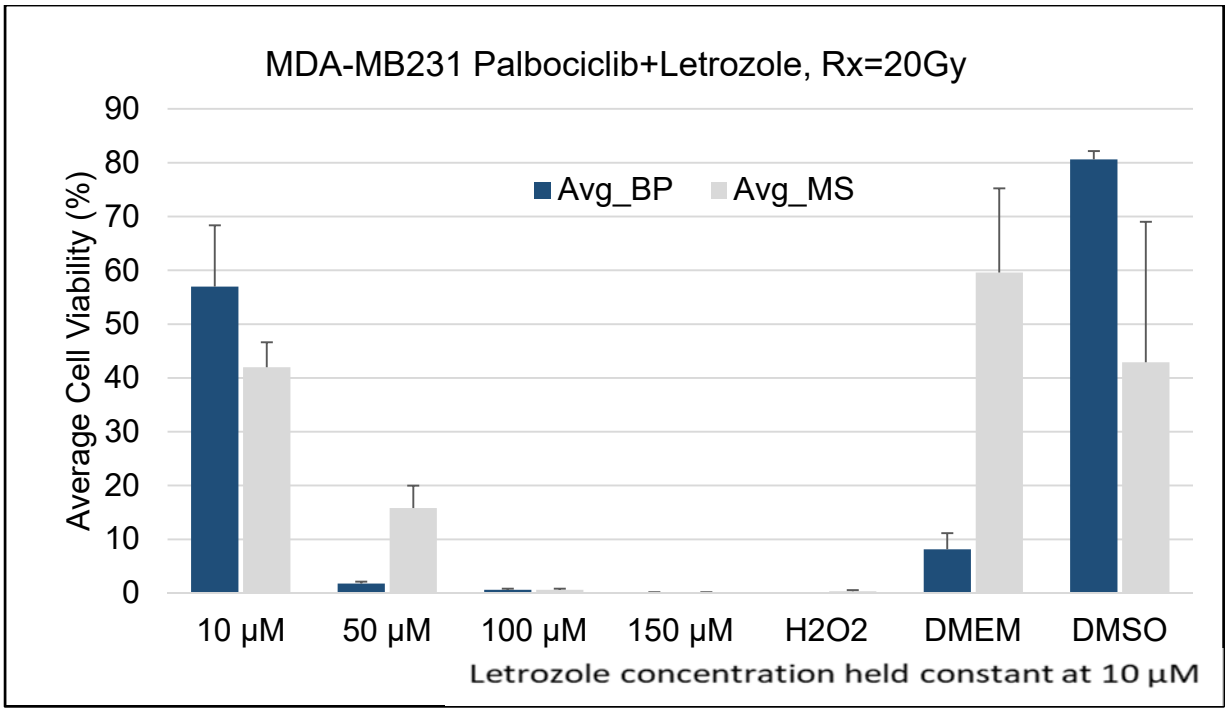

Figure 4.4 Percent cell viability of BP and MS MDA-MB-231 treated with palbociclib and letrozole (maintained at 10 µM, micro molar) in conjunction with radiation, cells evaluated at 20 Gy.

Table 4.4 – Paired T-test results from the cell viability of BP and MS MDA-MB-231 cells when treated with palbociclib and letrozole evaluated at 20 Gy.

Paired t-test			**Null hypothesis**		**H_0: $\mu_1 - \mu_2 = 0$**
	Estimation for Difference		**Alternative hypothesis**		**H_1: $\mu_1 - \mu_2 \neq 0$**
Conc. (BP Vs MS)	**Mean Difference**	**95% CI for Difference**	**T-Value**	**DF**	**P-Value**
10 µM	14.98	(0.83, 29.13)	2.72	5	**0.042**
50 µM	-14.04	(-19.23, -8.85)	-7.51	4	**0.002**
100 µM	-1.277	(-2.185, -0.368)	-3.9	4	**0.018**
150 µM	-1.278	(-2.444, -0.113)	-3.04	4	**0.038**
H_2O_2	-0.3618	(-0.5861, -0.1375)	-4.48	4	**0.011**
DMEM	-51.44	(-91.01, -11.87)	-5.59	2	**0.031**
DMSO	37.7	(-27.2, 102.7)	2.5	2	0.13

4.3.2.2 MCF7 Breast Cancer Cells

The average cell viability percentage from BP MCF7 BCCs at 100nM palbociclib + 10 μM letrozole was 97.5 % (1.7) whereas for the MS cells was at 88.4 % (4.6) with statistical significance of p = 0.03. At 1 μM palbociclib + 10 μM letrozole was 75.5 % (23.1) and 93.8 % (8.4) for the BP and MS cells, respectively, though no statistical significance was found, p > .05. At 10 μM palbociclib + 10 μM letrozole the average cell viability of the BP and MS cells was 59.4 % (4.8) and 38.1 % (12.6), respectively; this result was statistically significant p = 0.017. For the controls with the vehicle and media solutions average percentages were 86.21 % (9.8) and 93.5 % (7.5) for BP cells and 96.15 % (3.0) and 98.36 % (0.3) for MS cells, respectively. And for H_2O_2, average percentage for BP and MS cells was 22 % (9.0) and 6.4 % (6.0) with a statistical significance of p = 0.007.

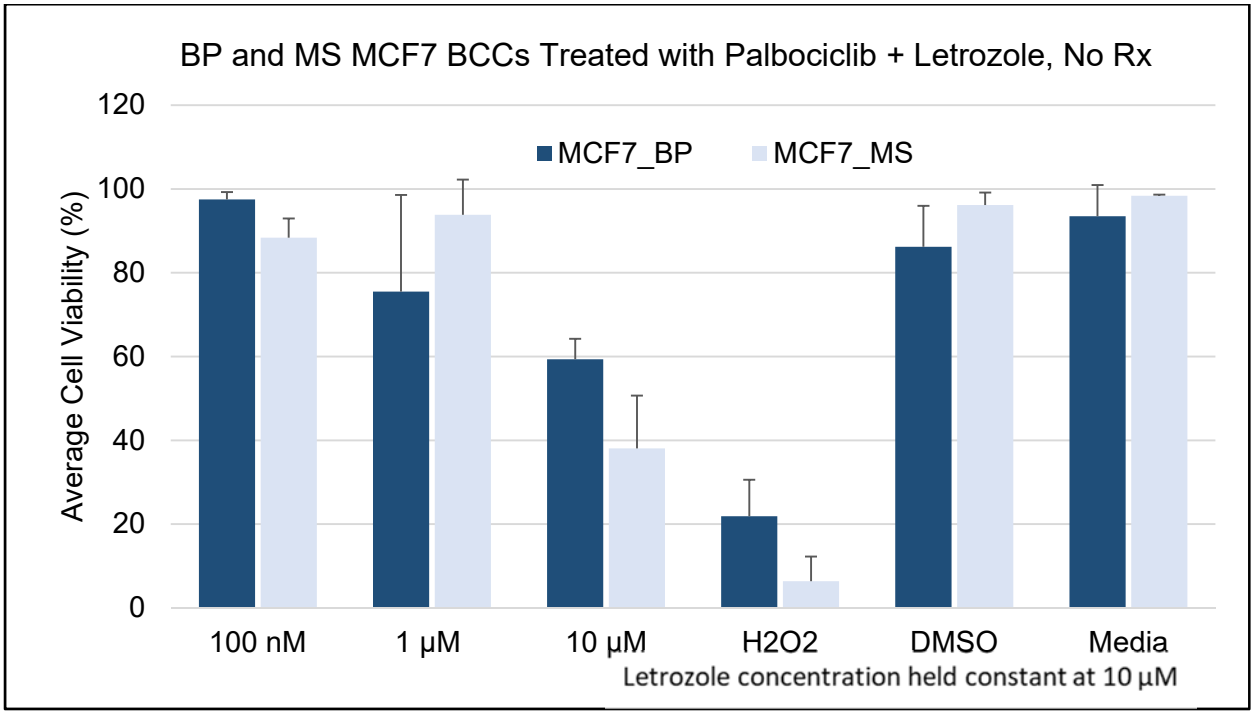

Figure 4.5 – Percent cell viability of Bioprinted and Manually Seeded MCF7 BCCs when treated with Palbociclib and letrozole.

Table 4.5 – Paired t-test results from the cell viability of BP and MS MCF7 BCCs when treated with palbociclib and letrozole at 100 nM, 1 µM, 10 µM, H_2O_2, Media, and DMSO.

Conc. (BP Vs MS)	Mean Difference	95% CI for Difference	T-Value	DF	P-Value
100 nM	-9.14	(-16.92, -1.36)	-3.74	3	**0.033**
1 µM	18.3	(-20.7, 57.4)	1.49	3	0.232
10 µM	-21.3	(-36.84, -5.76)	-3.52	5	**0.017**
H_2O_2	20.12	(7.85, 32.39)	5.01	4	**0.007**
Media	5	(-13.52, 23.52)	1.16	2	0.365
DMSO	9.93	(-15.40, 35.27)	1.69	2	0.234

Results from the BP and MS MCF7 BCCs post-treatment with the drug combination of palbociclib and letrozole given concurrently with radiation (Rx) therapy of 10 Gy given in 3 fractions, at 10 µM concentration of palbociclib +10 µM letrozole, the average percentage of the cell viability was 87 % (5.15) while the manually seeded cells was 60 % (5.3). This result was statistically significant, $p < 0.05$. The BP and MS cells at 50 µM palbociclib+10 µM letrozole was 38 % (3.5), and 30 % (5.5), respectively and statistical significance was found $p < 0.027$. At 100 µM palbociclib +10 µM letrozole, the average for the BP and MS cells was 14 % (2.5) and 18 % (2.9), respectively and no statistical significance was found, $p> 0.05$. At 150 µM palbociclib + 10 µM letrozole, mean cell viability was not evaluated due to cell segmentation. For H_2O_2, average percentage was 12 % (2.3) and 15 % (8.2) for both BP and MS cells respectively. The percent average of BP and MS cells only treated with Rx was 81 % (10.6) and 65 % (3.2), respectively. Similar results were observed for cells exposed to DMSO 84 % (4.0) and 69 % (9.6) for BP and MS MCF7 BCCs respectively; no statistical significance was found for all three, H_2O_2, media, and DMSO.

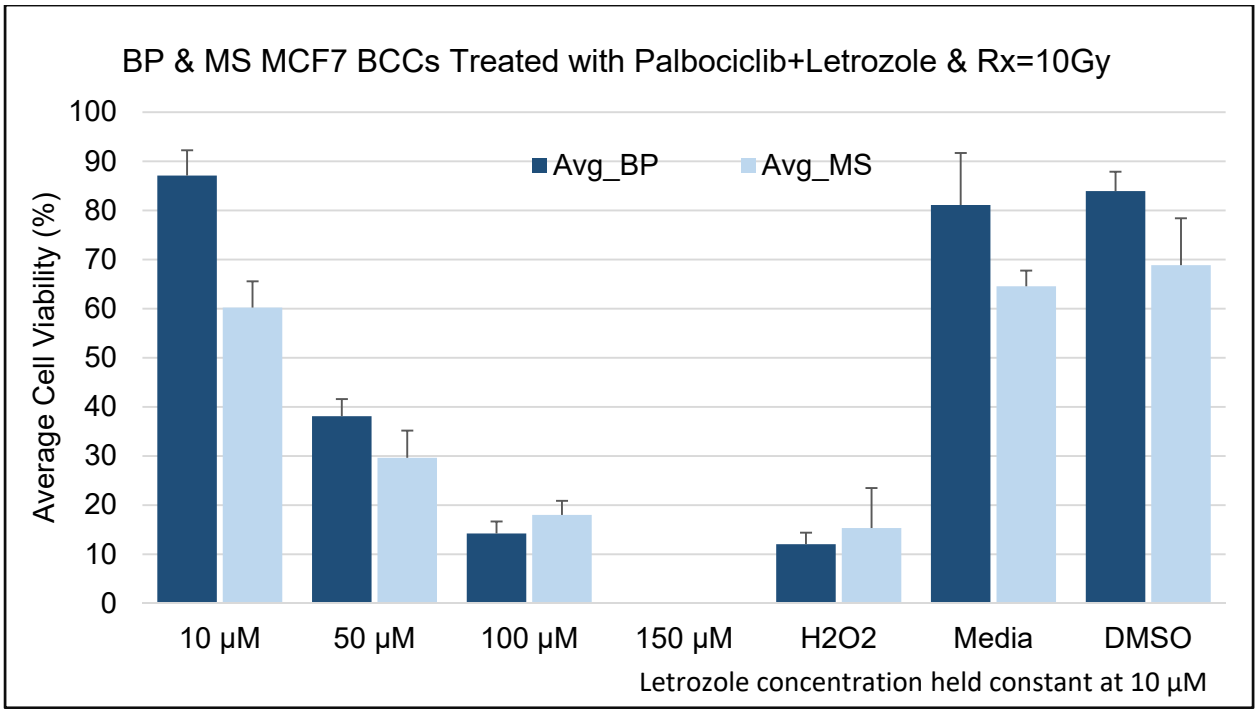

Figure 4.6 – Percent cell viability of Bioprinted and Manually Seeded MCF7 BCCs when treated with Palbociclib and letrozole and 10 grays of radiation given in 3 fractions. Treatments of palbociclib at 150 µM was not evaluated because cells could not be segmented due to the fact that no live cells remained post-treatment.

Table 4.6 – Paired t-test results from the cell viability of BP and MS MCF7 BCCs when treated with palbociclib + letrozole in conjunction with 10 grays of radiation given in 3fractions (Cell viability evaluation in the In Cell Analyzer was not possible at 150 µM, micro molar).

Paired t-test			**Null hypothesis**		**H_0: $\mu_1 - \mu_2 = 0$**
	Estimation for Difference		**Alternative hypothesis**		**H_1: $\mu_1 - \mu_2 \neq 0$**
Concentration (BP Vs MS)	**Mean Difference**	**95% CI for Difference**	**T-Value**	**DF**	**P-Value**
10 µM	26.89	(19.03, 34.74)	8.1	7	**0.0001**
50 µM	8.47	(1.32, 15.62)	2.9	6	**0.027**
100 µM	-3.77	(-7.77, 0.23)	-2.23	7	0.061
H_2O_2	-3.29	(-16.78, 10.19)	-0.78	3	0.494
Media	16.55	(-10.98, 44.07)	2.59	2	0.123
DMSO	15.1	(-10.59, 40.79)	2.53	2	0.127

The Results of the BP and MS MCF7 BCCs post-treatment of the drug combination of palbociclib and letrozole given concurrently with radiation (Rx) therapy of 20 grays given

in 5 fractions, at a concentration of 10 μM of palbociclib +10 μM letrozole, the average cell viability percentage was 71 % (6.8) and 67 % (18.0). This result was statistically significant, $p < 0.05$. The BP and MS cells at 50 μM palbociclib +10 μM letrozole was 5 % (5.2), and 8 % (2.1), respectively and no statistical significance was found $p > 0.05$. At 100 μM palbociclib +10 μM letrozole, the average for the BP and MS cells was 0 % and 1 % (1.0), respectively and no statistical significance was found, $p > 0.05$. At 150 μM palbociclib + 10 μM letrozole, mean cell viability was not evaluated due to cell segmentation. For H_2O_2, average percentage was 0 % (0.0) and 0 % (0.2) for both BP and MS cells respectively. The average viability of BP and MS cells only treated with Rx was 18 % (7.2) and 37 % (28.8), respectively. MCF7 cells treated with DMSO was 84 % (3.6) and 85 % (10.7) for BP and MS MCF7 BCCs respectively; no statistical significance was found for both, untreated and treated with DMSO.

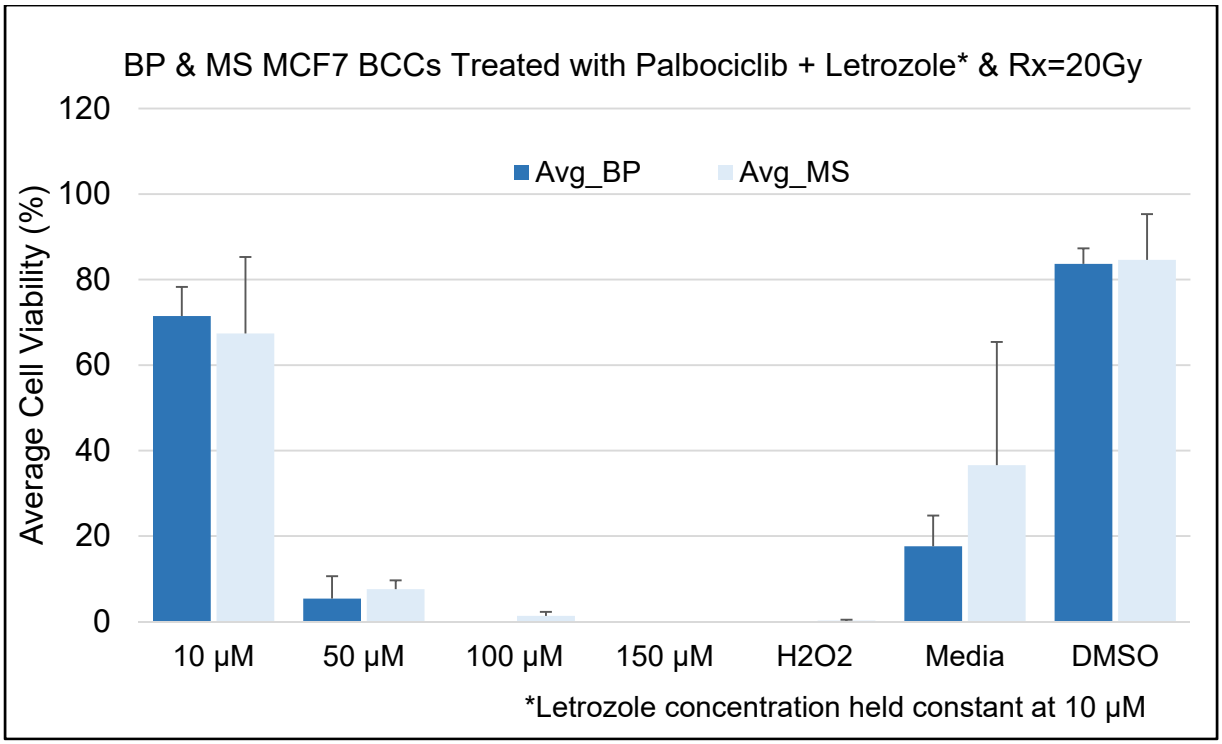

Figure 4.7 – Percent cell viability of Bioprinted and Manually Seeded MCF7 BCCs when treated with Palbociclib and letrozole and 20 grays of radiation given in 5 fractions. Treatments of palbociclib at 100 and 150 µM was not evaluated because cells could not be segmented due to the fact that no live cells remained post-treatment.

Table 4.7 – Paired t-test results from the cell viability of BP and MS MCF7 BCCs when treated with palbociclib + letrozole in conjunction with 20 grays of radiation given in 5 fractions (Cell viability evaluation in the In Cell Analyzer was not possible at 100 and 150 µM, micro-molar).

Paired t-test			Null hypothesis		H_0: $\mu_1 - \mu_2 = 0$
	Estimation for Difference		Alternative hypothesis		H_1: $\mu_1 - \mu_2 \neq 0$
Concentration	**Mean Difference**	**95% CI for Difference**	**T-Value**	**DF**	**P-Value**
10 µM	4.08	(-17.92, 26.07)	0.48	5	0.654
50 µM	-2.21	(-8.67, 4.25)	-0.88	5	0.419
H_2O_2	-0.2844	(-0.4810, -0.0877)	-4.01	4	**0.016**
DMEM	-18.9	(-92.6, 54.7)	-1.11	2	0.384
DMSO	-0.95	(-29.05, 27.16)	-0.15	2	0.898

4.3.2.3 MCF-10A Breast Cells

When BP MCF-10As were treated with palbociclib and letrozole concomitantly with radiation we observed the following: at a concentration of 10 μM of PD and Letrozole, BP and MS cells had a cell viability of 99 % (0.3 and 0.5), respectively. At 50 μM of PD plus letrozole and a radiation exposure of 10 grays, the average cell viability was 71 % (1.6) and 69 % (2.2) for both cell samples, the BP and MS cells. At a concentration of 100 μM and 150 μM palbociclib plus 10 μM of letrozole and a radiation of 10 grays the average cell viabilities is below 0.3 % for both sample types, BP and MS. BP and MS cells exposed to H_2O_2, the average cell viability was 2.9 % (1.1) and 2.8 % (0.9), respectively. The cells treated only with 10 grays had a 99 % (0.04) and 99 % (0.3) average cell viability in the BP and MS cells respectively. Similarly, cells treated with the solvent (DMSO) had an average cell viability of 97 % (0.2) and 98 % (0.03), for the BP and MS MCF-10A breast cells, see *Figure 4.8*. A statistical significance was not observed, see *Table 4.8*.

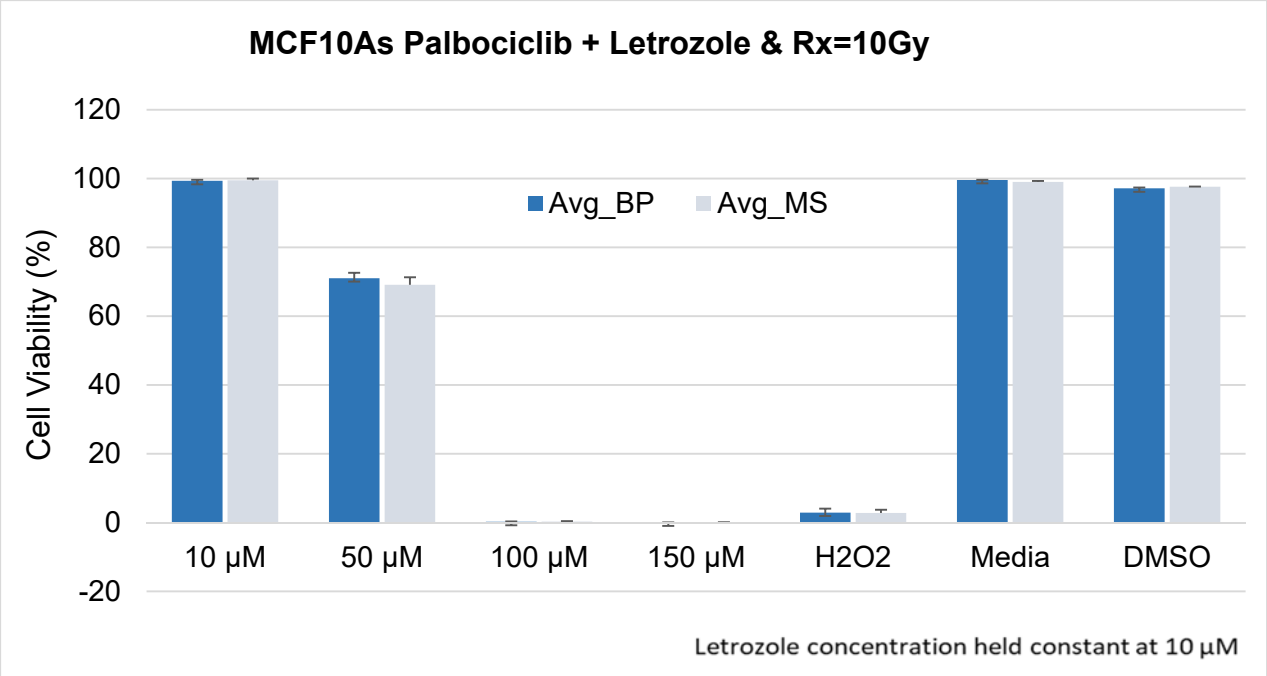

Figure 4.8 – Percent cell viability of Bioprinted and Manually Seeded MCF-10A breast cells when treated with Palbociclib + letrozole with a total radiation of 10 grays.

Table 4.8 – Paired T-test results from the cell viability of BP and MS MCF-10A breast cells when treated with palbociclib + letrozole in conjunction with 10 grays of radiation given in 3 fractions. µM = micro-molar.

Paired t-test			Null hypothesis		H_0: $\mu_1 - \mu_2 = 0$
	Estimation for Difference		Alternative hypothesis		H_1: $\mu_1 - \mu_2 \neq 0$
Drug Conc. (BP vs MS)	Mean Difference	95% CI for Difference	T-Value	DF	P-Value
10 µM	-0.145	(-0.811, 0.521)	-0.53	6	0.612
50 µM	1.93	(-0.93, 4.80)	1.6	7	0.155
100 µM	-0.0372	(-0.2482, 0.1738)	-0.45	5	0.669
150 µM	-0.0128	(-0.0776, 0.0520)	-0.47	7	0.655
H_2O_2	0.115	(-1.765, 1.996)	0.16	5	0.881
Media	0.577	(-0.146, 1.300)	3.44	2	0.075
DMSO	-0.483	(-1.101, 0.136)	-3.36	2	0.078

When BP and MS MCF-10A breast cells were treated with the drug combination of palbociclib and letrozole given concomitantly with radiation (Rx) therapy of 20 Gy given in 5 fractions, at 10 µM concentration of palbociclib + 10 µM letrozole, the average

percentage of live cells was 88.5 % (6.5) while the manually seeded cells was 87.6 % (3.5). This result was not statistically significant, $p > .05$. The BP and MS cells at 50 µM palbociclib+10 µM letrozole was 18 % (4.2), and 15.4 % (5.4), respectively and no statistical significance was found $p > .05$. At 100 µM palbociclib+10 µM letrozole, the average for the BP and MS cells was 0 % (0.0) and 3 % (3.0), respectively and no statistical significance was found $p > .05$. At 150 µM palbociclib + 10 µM letrozole, mean cell viability percentage was 5 % (11.2) and 2 % (4.1) for BP and MS cells, respectively, no statistical significance, see *table 4.9* below. Treatment with H_2O_2, the mean cell viability percentage was 0 % (0) and 2 % (3.4) for BP and MS MCF7 BCCs, respectively. The percent average of BP and MS cells only treated with Rx was 92 % (5.0) and 87 % (9.0), respectively. Similar results were observed for cells exposed to the vehicle solution, DMSO in this instance. Percent average of cell viability for BP and MS cells was 91 % (2.0) and 82 % (6.8), respectively though no statistical significance was seen for both, media and DMSO.

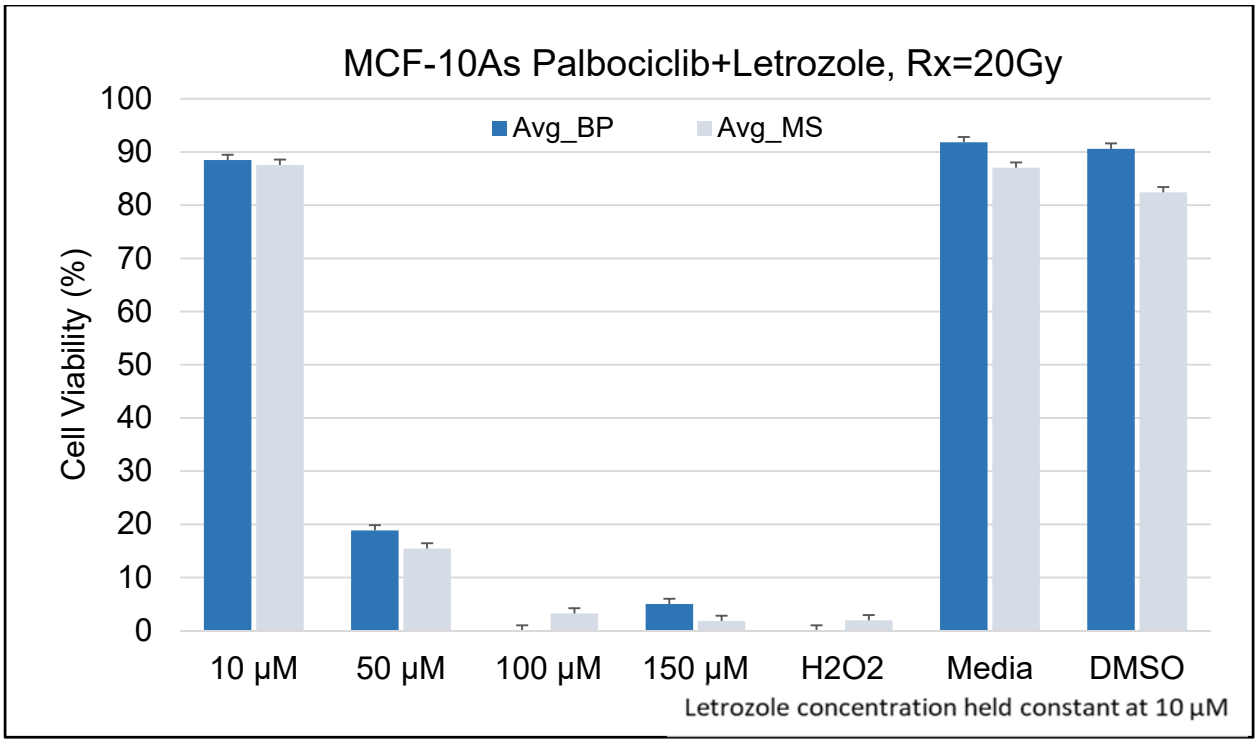

Figure 4.9 – Percent cell viability of Bioprinted and Manually Seeded MCF-10A breast cells when treated with Palbociclib + letrozole with a total radiation of 20 Grays.

Table 4.9 – Paired t-test results from the cell viability of BP and MS MCF-10A breast cells when treated with palbociclib + letrozole in conjunction with 20 grays of radiation given in 5 fractions. µM = micro-molar

Paired t-test			Null hypothesis		H_0: $\mu_1 - \mu_2 = 0$
	Estimation for Difference		Alternative hypothesis		H_1: $\mu_1 - \mu_2 \neq 0$
Drug Conc. (BP vs MS)	Mean Difference	95% CI for Difference	T-Value	DF	P-Value
10 µM	0.91	(-7.18, 8.99)	0.27	6	0.793
50 µM	3.4	(-3.81, 10.61)	1.11	7	0.302
100 µM	-3.23	(-6.91, 0.45)	-2.44	4	0.072
150 µM	-1.82	(-6.87, 3.23)	-1	4	0.374
H_2O_2	-1.95	(-7.43, 3.54)	-1.13	3	0.341
Media	4.77	(-14.03, 23.57)	0.81	3	0.479
DMSO	8.21	(-9.09, 25.50)	2.04	2	0.178

4.4 Discussion

These findings seem to indicate that bioprinting has an unanticipated effect on the viability of BP MCF7 cells when treated with tamoxifen. At ≥ 90 μM concentrations of tamoxifen, approximately 10% survived this treatment, appearing to develop some type of drug resistance. Though this characteristic is only observed in the bioprinted cells. This effect is known as the hormesis effect, it seems that the bioprinted cells develop a biphasic response when exposed to an increased concentration of this drug [113]. Another reason for this outcome may also be due to the activation of kinases and chaperone proteins, e.g., HSP27 and HSP70 as it was observed in the phospho-MAPK array assay. The fact that BP MCF7 BCCs significantly upregulated LUCAT1, CYP1A1 and other genes explains this drug resistance, which was found in the RNA seq analysis previously conducted. LUCAT1 is a protein found in breast cancer cells with stem cell properties and it has been linked to cell survival [20].

In the palbociclib-letrozole + radiation treatments, we observed that at 10 μM drug concentration, both the BP and MS MDA-MB231 cells survived the overall treatment for more than 5 days post-irradiation, this also included cells treated only with radiation and cells treated with the vehicle control. On the other hand, BP and MS MCF7 BCCs and MCF-10A breast cells did not survive these same treatment when given in conjunction with radiation, at 10 and 20 grays, post 24 h. At 10 grays of radiation exposure, both BP and MS MCF7 cells survived the treatment combination; however, at 10 and 50 μM concentrations, the mean viability of the BP cells was significantly higher than the MS MCF7 cells. These results indicate that the treatment combination (including radiation) further affects cell viability as anticipated. This is expected due to the fact that

palbociclib, a CDK4/6 inhibitor, halts cell division in G1 phase, then radiation exposure performs as intended, by killing the majority of cells that were unable to divide. The percentage of cells that were not affected by the palbociclib + letrozole treatments are theoretically, the cells that also survived radiation. It is possible that bioprinting is provoking the generation of cancer cells with stem cell properties, which according to Zheng, et al., are regarded as cells with drug resistant attributes [203].

In the BP and MS MCF-10A breast cells at a concentration of 50 μM of PD + 10 μM of letrozole, a statistical significance was observed between the two radiation treatments, at 10 grays and 20 grays ($p < .001$). The average percentage of viable cells decreased by 3 fold between the cells exposed to 10 grays and the cells exposed to 20 grays. Additionally, both radiation exposures, at 10 and 20 grays, had very little effect on cell toxicity of untreated and cells treated with the vehicle. However, in the BP samples, cell viability was, again, higher than the MS cell samples, suggesting once more that the biochemical properties of the bioprinted cells considerably affect their reaction to these treatments.

The same trend as the BP MCF7 BCCs is observed with the non-cancerous MCF-10A cells: a higher average cell viability was found in the BP MCF-10As when exposed to 150 μM concentrations and a radiation of 20 grays; though the percent cell viability was lower than the MCF7 cells. This effect might be due to the biphasic response as observed in many cancer cells [234]. This effect is a desired characteristic for the proposed tumor models. This characteristic of the BP cells could be further utilized to represent actual tumor environments because these results suggest an ordinary response to drug treatments of actual breast tumors *in vivo*.

When visually observed under the microscope 36 h later, 100 % of the MCF7 and MCF-10A cells did not survive either radiation exposures, 10 or 20 grays. Treatments with 10 μM drug concentrations of palbociclib + letrozole given concomitantly with radiation, showed significantly higher cell viability of both BP MCF7, and MCF-10A cells. The short term response of bioprinted MCF7 and MCF-10A cells was somewhat affected, viability was reduced approximately by 16 and 11% respectively. On the other hand, MDA-MB-231 was not significantly affected by either level of radiation exposure with similar drug concentrations in the short and long terms post-treatments.

This investigation was designed to analyze the short term drug response, 8 - 24 h posttreatments, of the BP models when exposed to drug treatments (previously mentioned). It may also be possible that 5 % or a higher percentage of the cells may have been able to survive longer if the assay was conducted 48 h or later following the treatments. The exact mechanism of such responses remains to be elucidated, though cell survival of the bioprinted models is a desired property of in vitro models used in preclinical research. The hormetic dose-response is a controversial model because it challenges the interpretation and modeling of threshold values of dose-response interactions. The later model is used by drug agencies, FDA and EPA, to stablish acceptable drug exposures [234]. This bioprinted model could be further explored by adding other type of cells if one can overcome the challenge of identifying which cells remain viable.

4.5 Conclusion

Overall, in this experiment we presented results of two drug treatments in bioprinted cell samples, tamoxifen and the combination of palbociclib plus letrozole alone and when

given concomitantly with radiation. Cells were treated with varied concentrations of palbociclib (10, 50, 100 and 150 μM), and 10 μM letrozole in combination with radiation, 10 and 20 grays, given in three and five fractions. Cells were evaluated at 8 - 10 hours post-radiation exposure. BP MCF7 BCCs displayed a biphasic response at higher concentrations of tamoxifen, which was not the case with MS MCF7 BCCs. This hormetic response observed in the BP cells offers a great opportunity in drug discovery for it provides a more realistic model that can mimic *in vivo* environments. Additionally, RNA seq results of BP MCF7 cells further explain these findings, when several of the genes that were upregulated are associated with many diseases, like breast cancer, DM, and many others [141, 144]. Future research should include RNA seq studies conducted in BP cells post-treatments, with similar or new drugs. In general, the bioprinting approach will likely set a precedent in the future of drug discovery.

Chapter 5

5.1 Introduction

The objective of this study was to confirm our hypothesis that bioprinted (BP) breast cancer cells developed *in vitro* provide better tumor models or similar to manually seeded (MS) cells, which can be used for drug discovery. BP breast cancer cells cultured *in vitro* can be used to represent actual tissue environments because cell arrangement can be better controlled and manipulated than in the MS method. The overarching goal is to offer a breast tumor model based on bioprinting technology that can be customized for phenotypic and target drug discovery. This model can potentially be used to predict a better response to breast cancer treatments of aggressive or with rare biomarkers. Furthermore, through bioprinting cells can be structured in diverse patterns that could ultimately be assembled in 3D models.

In this chapter, we presented the results obtained by testing the biological response of BP MCF7 and MCF10A cells when implanted in immunocompromised mice. Tissue analysis is normally used to identify the biomarkers and characteristics of tumors in patients diagnosed with cancer. We hypothesized that bioprinting will allow better tumor formation when implanted in mice because we discovered that bioprinting is activating pathways that have been associated tumor development. Through the phospho-MAPK array assay, we learned that bioprinting is phosphorylating 21 kinases that have been associated with cancer development, like Akt2/pan, MKK3/6, ERK1/2 and other pathways, see *Figure 3.3*. Additionally, through RNA Seq analysis, we confirmed that

bioprinting further suppresses p53, which is a known tumor suppressor gene. This model may be able to identify novel breast cancer treatment regimens.

5.2 Materials and Methods

5.2.1 Implantation process

For the bioprinted tumor implants, the same bioprinting process was followed except, for a square mesh pattern drawn in Microsoft word that was used for bioprinting the bioink (cell solution) over a 48 well-plate. Cells were incubated in a humidified incubator maintained at 37°C, in 5 % CO_2 for 6-8 days. Triplicate samples of each configuration in two separate experiments was prepared with bioprinted (BP) and manually seeded (MS) MCF7 cells. After bioprinting and creating a working model, tumor growths were incubated for 8-10 days to allow tumor formation prior to implanting them in Severe Combined Immunodeficiency (SCID) mice. Mice were followed for 5-6 weeks and then euthanized in order to analyze the tissue.

A total of 40 C.B-17SCID mice (eight-week old females), were used. 13 mice were implanted subcutaneously with BP MCF7 BCC samples, 10 were implanted with MS MCF7 cell samples, 6 mice were implanted with MS MCF10A cell samples, 9 mice were implanted with BP MCF-10A cell samples, and 2 mice were used for controls with no implants. All animal procedures were performed under approved protocol by the Institutional Animal Care and Use Committee (IACUC) at the University of Texas at El Paso (UTEP), protocol # A-201701-4. Mice were anesthetized with isoflurane kept at 3 % and maintained in a 37^{o}C pad throughout the implantation process. An 8-10 mm subcutaneous incision was carefully made in the left ventral region, in the inguinal

mammary fat pad vicinity. The samples were carefully inserted and then immediately sutured.

Table 5.1 Quantity of mice and the type of implants used

Quantity	Type of implant
13	Bioprinted MCF7s
10	Manually Seeded MCF7
9	Bioprinted MCF10A
6	Manually Seeded MCF10A
2	No implant

5.2.2 Tissue Process

Mice were followed for 5-6 weeks at which point they were euthanized to harvest the tissue where samples were implanted (n = 40). Next, tissue samples from the implant site and non-implant site were harvested and fixed in 10% formalin solution. Samples were dehydrated in ethanol (50 %, 60 %, 70 %, 90 % and 100 %), twice in xylene and paraffin in a MICROM STP 120 Tissue Processor, see protocol in Appendix II. Tissue samples were immediately embedded in single cassettes with paraffin in the HistoStar (Thermo Scientific). Embedded tissue blocks from the implant and non-implant site were sectioned (4 μm) in the Finesse ME + Microtome from Thermo-Scientific and mounted in plus microscope slides. Single slides were de-paraffinized and stained in hematoxylin and eosin (H & E) per mouse protocol in the Varistar tissue stainer. Mounting medium was immediately applied, covered with a glass coverslip and allowed to dry. Afterwards, the stained microscope slides were observed under the microscope

for image analysis. Immunohistochemistry (IHC) was completed per protocol, from Santa Cruz technologies.

5.3 Results

Tissue slides from the BP implants were identified with hyperplasia and carcinomas in situ. In figure 5.1, tissue image showing part of the skin area near the implant site, this sample came from manually seeded MCF7 cells. In figure 5.2, a comparison of two similar tissue areas from two different mice, the image to the left came from a sample with manually seeded MCF10A cells. The image to the right is from a tissue with bioprinted MCF7 cells. Figure 5.3 is a tissue sample of the spleen from M19-S5, some areas in the spleen were identified with oncocytic cells showing abundant heterogeneous enlarged mitotic figures with enlarged nuclei, cytoplasm and pleomorphic carcinomas displaying enlarged nuclei, and few mitotic figures depicted by the arrows, see area depicted by a rectangle in Figure 5.4.

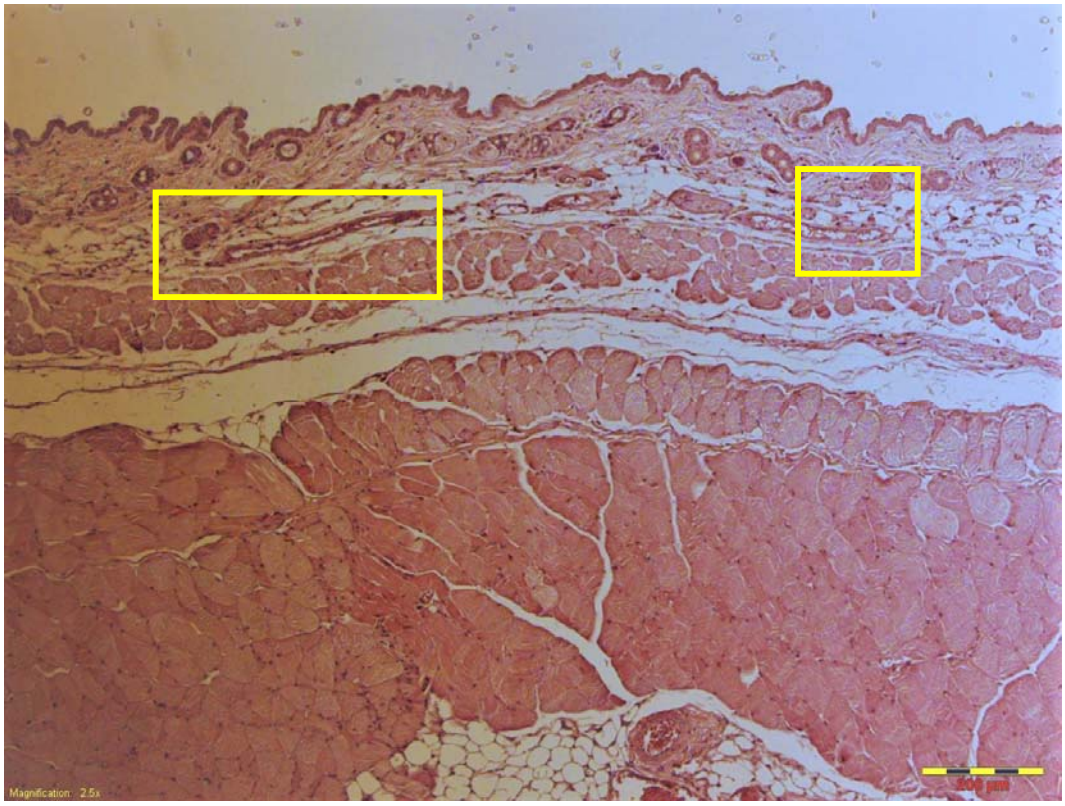

Figure 5.1 (M1S4) Image of tissue implanted with manually seeded MCF7 sample, showing the skin area, the stroma and muscle tissue. Few cells scarcely appear to what we believe is hyperplasia.

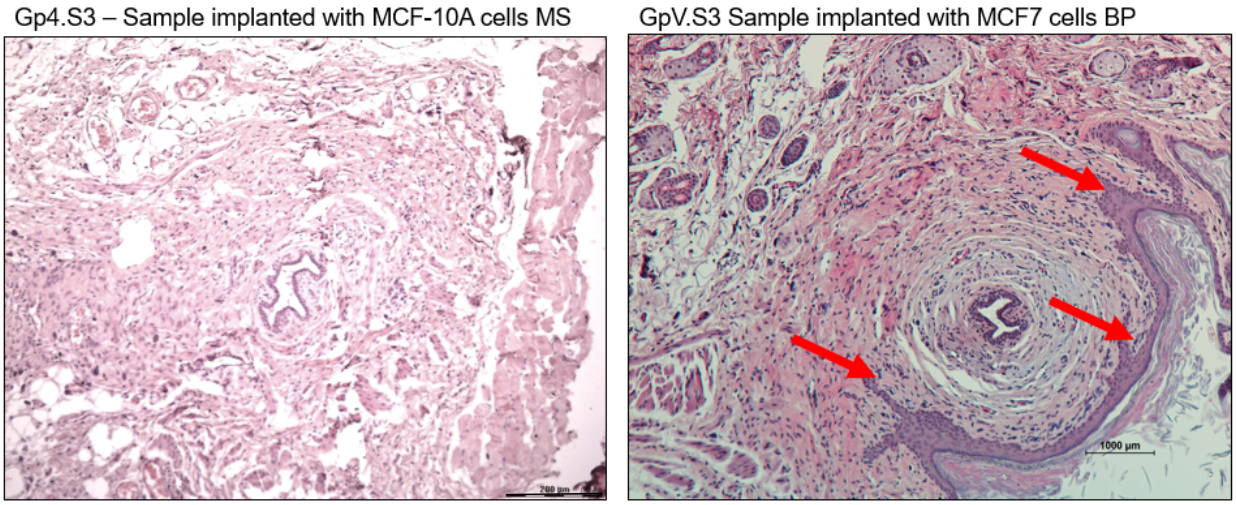

Figure 5.2 Image from two different samples compared side-by-side. Tissue of manually seeded MCF10A sample and tissue from bioprinted MCF7 cells. In the image to the right we identified cancer cells infiltrating the stroma. Both tissues were stained with Hematoxylin and Eosin (H & E).

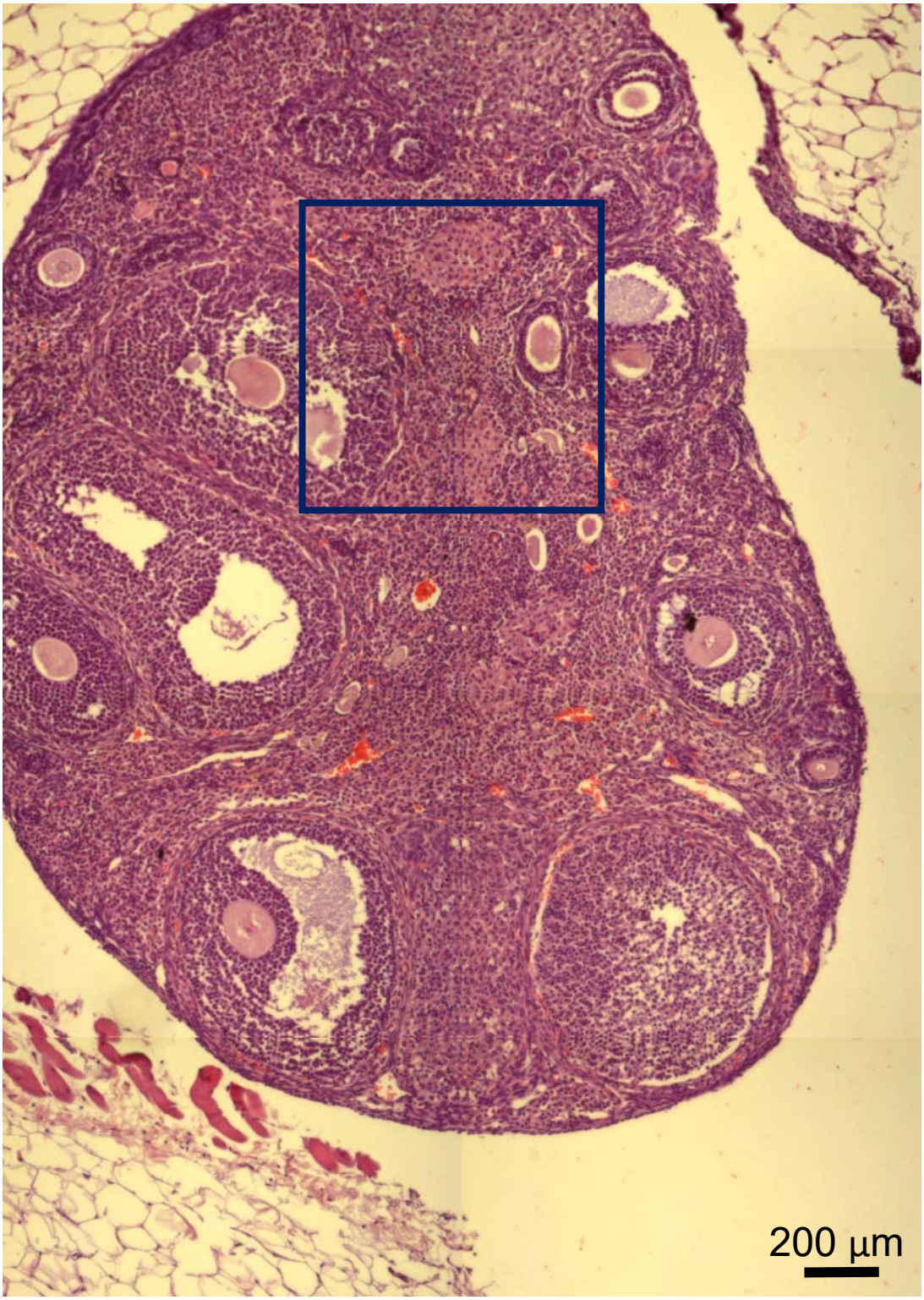

Figure 5.3 – M19.S5 Image at 20X from spleen, sample is from a bioprinted MCF7 cell sample

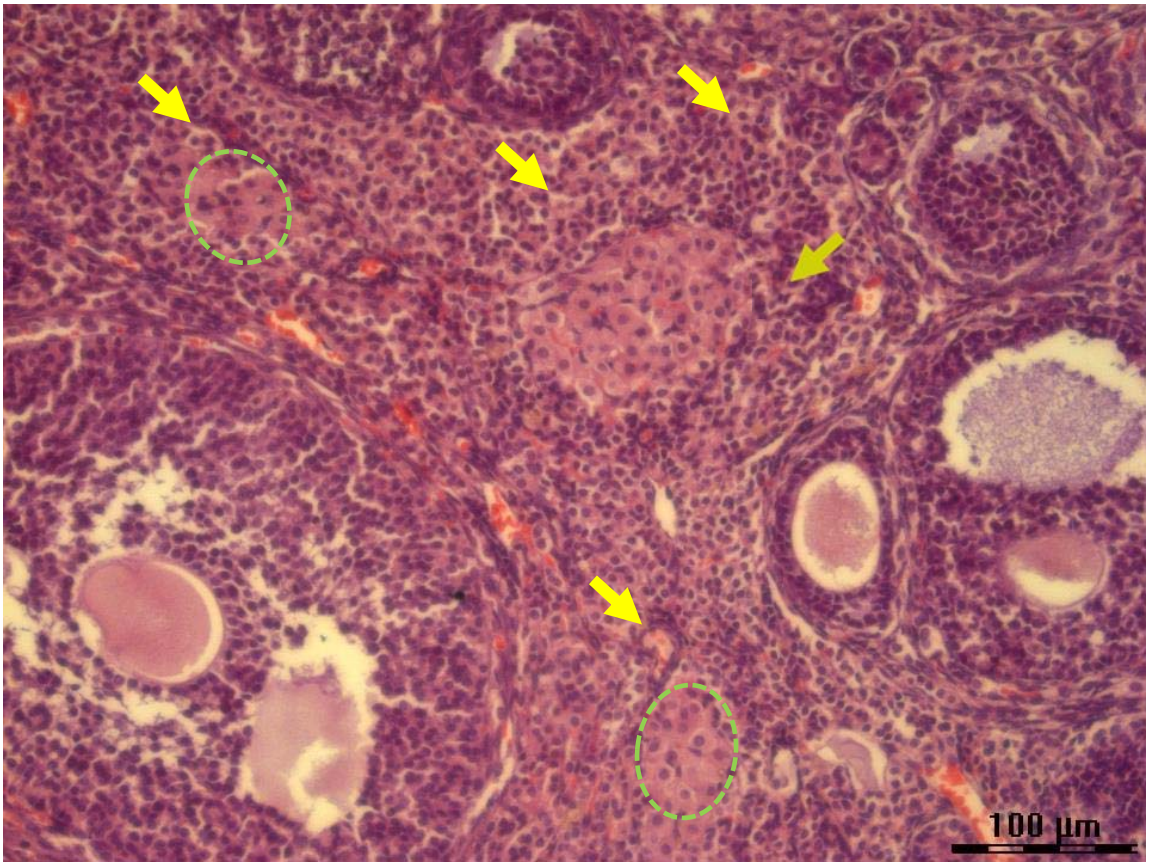

Figure 5.4 Close up of the area enclosed by the square in figure 5.2, this image shows abundant granular cytoplasm (green circles) and pleomorphic carcinomas depicted by arrows.

5.4 Discussion

This part of the analysis presented several challenges because, it was challenging to match different samples with another sample from the same area. In the area near the implants, we observed hyperplasia and carcinoma in situ, which are signs of cancer development. Some metastasis were detected in some of the bioprinted samples, cells invading the stroma, right side of Figure 5.2. We believe that the invasive behavior of the cells may be due to LUCAT1 and IL6. LUCAT1 has been implicated in breast cancer metastasis and cell survival [235].

In tissues coming from the lining of the stomach section of bioprinted cell samples, we observed higher cellular conglomerations suggesting the development of pathogenic diseases or cancer metastasis. In other areas near the implant site, some cells with stellate appearance are observed starting to migrate to the inner core of the ductal unit in one of the lobular ducts of a mammary gland, see appendix II. Undifferentiated cancer cells are associated with malignant cancers. Cells found in this states are known to be anaplastic.

5.5 Conclusion

In this chapter, we presented the results from the bioprinted implants and showed that tissues from the bioprinted samples appeared to have developed more cancer cells than the tissue samples coming from the MS cell implants. Undoubtedly, tissue analysis provided insightful information of the advantage of using BP models to evaluate new drugs *in vivo* and *in vitro* as it was observed in the tissues. We were able to analyze and identify the biological response of this model. The biological response of the BP implants *in vivo* suggests that the bioprinted MCF7 model is a better model for drug discovery than the MS sample models. Additionally, substantial physiological and biochemical differences were found between the BP and the MS cell samples, like the type of upregulated genes LUCAT1, IL6, CYP1A1 and many others. The migratory, replicative, and ability to survive drug treatments are characteristics attributed to the bioprinting process. Evidently, bioprinting causes massive gene alterations and large kinase phosphorylations which make this cancer model an ideal and realistic model for drug discovery.

References

1. Nelson, C.M. and M.J. Bissell. *Modeling dynamic reciprocity: engineering three-dimensional culture models of breast architecture, function, and neoplastic transformation*. in *Seminars in cancer biology*. 2005. Elsevier.
2. Breastcancer.org. *Mammography Technique and Types*. 2013 06/2016]; Breast cancer modalities]. Available from: https://www.breastcancer.org/symptoms/testing/types/mammograms/types.
3. Weinberg, R., *The biology of cancer*. 2013: Garland science.
4. Mayr, L.M. and P. Fuerst, *The future of high-throughput screening.* Journal of biomolecular screening, 2008. **13**(6): p. 443-448.
5. Yamada, K.M. and E. Cukierman, *Modeling tissue morphogenesis and cancer in 3D.* Cell, 2007. **130**(4): p. 601-610.
6. Wilson, W.C., Jr. and T. Boland, *Cell and organ printing 1: protein and cell printers.* Anat Rec A Discov Mol Cell Evol Biol, 2003. **272**(2): p. 491-6.
7. Tavassoli, F.A. and P. Devilee, *Pathology and genetics of tumours of the breast and female genital organs*. 2003: Iarc.
8. Parise, C.A. and V. Caggiano, *Disparities in race/ethnicity and socioeconomic status: risk of mortality of breast cancer patients in the California Cancer Registry, 2000–2010.* BMC cancer, 2013. **13**(1): p. 449.
9. Torre, L.A., R.L. Siegel, E.M. Ward, et al., *Global cancer incidence and mortality rates and trends—an update.* Cancer Epidemiology and Prevention Biomarkers, 2016. **25**(1): p. 16-27.
10. *U.S. Breast Cancer Statistic*. Electronic Article [Electronic Article] 2018; https://www.breastcancer.org/symptoms/understand_bc/statistics:[Available from: https://www.breastcancer.org/symptoms/understand_bc/statistics.
11. Cronin, K.A., A.J. Lake, S. Scott, et al., *Annual Report to the Nation on the Status of Cancer, part I: National cancer statistics.* Cancer, 2018.
12. Shiels, M.S., J.Y. Islam, P.S. Rosenberg, et al., *Projected Cancer Incidence Rates and Burden of Incident Cancer Cases in HIV-Infected Adults in the United States Through 2030.* Annals of internal medicine, 2018.
13. Swinney, D.C. and J. Anthony, *How were new medicines discovered?* Nature Reviews Drug Discovery, 2011. **10**: p. 507.
14. Bissell, M.J., A. Rizki, and I.S. Mian, *Tissue architecture: the ultimate regulator of breast epithelial function.* Current opinion in cell biology, 2003. **15**(6): p. 753.
15. Gassmann, O., A. Schuhmacher, M. von Zedtwitz, et al., *Future Directions and Trends*, in *Leading Pharmaceutical Innovation*. 2018, Springer. p. 155-163.
16. Kim, J.B., R. Stein, and M.J. O'hare, *Three-dimensional in vitro tissue culture models of breast cancer—a review.* Breast cancer research and treatment, 2004. **85**(3): p. 281-291.
17. Moroni, L., T. Boland, J.A. Burdick, et al., *Biofabrication: a guide to technology and terminology.* Trends in biotechnology, 2017.
18. Imamura, Y., T. Mukohara, Y. Shimono, et al., *Comparison of 2D-and 3D-culture models as drug-testing platforms in breast cancer.* Oncology reports, 2015. **33**(4): p. 1837-1843.
19. Finn, R.S., M. Martin, H.S. Rugo, et al., *PALOMA-2: Primary results from a phase III trial of palbociclib (P) with letrozole (L) compared with letrozole alone in postmenopausal women with ER+/HER2– advanced breast cancer (ABC).* Journal of Clinical Oncology, 2016. **34**(15_suppl): p. 507-507.

20. Campbell, A., A. Philipovskiy, R. Heydarian, et al., *2D and 3D thermally bioprinted human MCF-7 breast cancer cells: A promising model for drug discovery.* Journal of Clinical Oncology, 2019. **37**(15_suppl): p. 2605-2605.
21. Lu, J., H. Guo, W. Treekitkarnmongkol, et al., *14-3-3ζ cooperates with ErbB2 to promote ductal carcinoma in situ progression to invasive breast cancer by inducing epithelial-mesenchymal transition.* Cancer cell, 2009. **16**(3): p. 195-207.
22. Holliday, D.L. and V. Speirs, *Choosing the right cell line for breast cancer research.* Breast cancer research, 2011. **13**(4): p. 215.
23. Walker, K.S., D. Maria, A. Paterson, et al., *Activation of protein kinase B β and γ isoforms by insulin in vivo and by 3-phosphoinositide-dependent protein kinase-1 in vitro: comparison with protein kinase B α.* Biochemical Journal, 1998. **331**(1): p. 299-308.
24. Forbes, L.J., F. Warburton, M. Richards, et al., *Risk factors for delay in symptomatic presentation: a survey of cancer patients.* British journal of cancer, 2014. **111**(3): p. 581-588.
25. Bower, J.E., *Behavioral symptoms in breast cancer patients and survivors: fatigue, insomnia, depression, and cognitive disturbance.* Journal of clinical oncology: official journal of the American Society of Clinical Oncology, 2008. **26**(5): p. 768.
26. Apter, D. and R. VIHKO, *Early menarche, a risk factor for breast cancer, indicates early onset of ovulatory cycles.* The Journal of Clinical Endocrinology & Metabolism, 1983. **57**(1): p. 82-86.
27. McPherson, K., C. Steel, and J. Dixon, *ABC of breast diseases: breast cancer—epidemiology, risk factors, and genetics.* BMJ: British Medical Journal, 2000. **321**(7261): p. 624.
28. Koo, M.M., W. Hamilton, F.M. Walter, et al., *Symptom signatures and diagnostic timeliness in cancer patients: a review of current evidence.* Neoplasia, 2018. **20**(2): p. 165-174.
29. Rohan, T. and C. Bain, *Diet in the etiology of breast cancer.* Epidemiologic reviews, 1987. **9**(1): p. 120-145.
30. Williams, C.P., A. Azuero, M. Pisu, et al., *Abstract PD7-01: Impact of guideline concordant treatment on cost and health care utilization in early stage breast cancer patients*. 2018, AACR.
31. Cserni, G., E. Chmielik, B. Cserni, et al., *The new TNM-based staging of breast cancer.* Virchows Archiv, 2018. **472**(5): p. 697-703.
32. Cancer, A.J.C.o., *Breast*, in *AJCC cancer staging manual*. 2002, Springer. p. 223-240.
33. Giuliano, A.E., J.L. Connolly, S.B. Edge, et al., *Breast cancer—major changes in the American Joint Committee on Cancer eighth edition cancer staging manual.* CA: a cancer journal for clinicians, 2017. **67**(4): p. 290-303.
34. Rezo, A., J. Dahlstrom, B. Shadbolt, et al., *Tumor size and survival in multicentric and multifocal breast cancer.* The Breast, 2011. **20**(3): p. 259-263.
35. Edge, S.B. and A.J.C.o. Cancer, *AJCC cancer staging handbook: from the AJCC cancer staging manual*. Vol. 2010. 2010: Springer New York.
36. Sanders, M.A., S.M. Wong, J.B. Iorgulescu, et al., *Changes and clarifications in the eighth edition of the AJCC cancer staging system for breast cancer.* Ajsp: Reviews & Reports, 2018. **23**(3): p. 113-117.
37. Amin, M.B., F.L. Greene, S.B. Edge, et al., *The Eighth Edition AJCC Cancer Staging Manual: Continuing to build a bridge from a population-based to a more "personalized" approach to cancer staging.* CA: a cancer journal for clinicians, 2017. **67**(2): p. 93-99.
38. Eble, J.N., F.A. Tavassoli, and P. Devilee, *Pathology and Genetics of Tumours of the Breast and Female Genital Organs*. 2003: Iarc.
39. Lee, C.H., D.D. Dershaw, D. Kopans, et al., *Breast cancer screening with imaging: recommendations from the Society of Breast Imaging and the ACR on the use of mammography, breast MRI, breast ultrasound, and other technologies for the detection of clinically occult breast cancer.* Journal of the American college of radiology, 2010. **7**(1): p. 18-27.

40. Sameer Gupta, M.D., M.P.H. *Breast Self-Exam*. breastcancer.org [website] 2010 [cited Webpage 2017]; 2010:[Available from: https://www.breastcancer.org/symptoms/testing/types/self_exam.
41. Kremkau, F.W., *Diagnostic ultrasound: principles and instruments*. 2001: WB Saunders Company.
42. Stavros, A.T., D. Thickman, C.L. Rapp, et al., *Solid breast nodules: use of sonography to distinguish between benign and malignant lesions.* Radiology, 1995. **196**(1): p. 123-134.
43. Zhi, H., B. Ou, B.-M. Luo, et al., *Comparison of ultrasound elastography, mammography, and sonography in the diagnosis of solid breast lesions.* Journal of ultrasound in medicine, 2007. **26**(6): p. 807-815.
44. Jaffer, F.A. and R. Weissleder, *Molecular imaging in the clinical arena.* Jama, 2005. **293**(7): p. 855-862.
45. Drukteinis, J.S., B.P. Mooney, C.I. Flowers, et al., *Beyond mammography: new frontiers in breast cancer screening.* The American journal of medicine, 2013. **126**(6): p. 472-479.
46. Blaus, B., *Mammogram*, in *WikiJournal of Medicine*. 2014.
47. Kelly, K.M., J. Dean, W.S. Comulada, et al., *Breast cancer detection using automated whole breast ultrasound and mammography in radiographically dense breasts.* European radiology, 2010. **20**(3): p. 734-742.
48. Costelloe, C.M., H.H. Chuang, J.E. Madewell, et al., *Cancer response criteria and bone metastases: RECIST 1.1, MDA and PERCIST.* Journal of Cancer, 2010. **1**: p. 80.
49. Dromain, C., F. Thibault, F. Diekmann, et al., *Dual-energy contrast-enhanced digital mammography: initial clinical results of a multireader, multicase study.* Breast Cancer Research, 2012. **14**(3): p. R94.
50. Hendrick, R.E., *Radiation doses and cancer risks from breast imaging studies.* Radiology, 2010. **257**(1): p. 246-253.
51. Lehman, C.D., C. Gatsonis, C.K. Kuhl, et al., *MRI evaluation of the contralateral breast in women with recently diagnosed breast cancer.* New England Journal of Medicine, 2007. **356**(13): p. 1295-1303.
52. Weissleder, R. and U. Mahmood, *Molecular imaging.* Radiology, 2001. **219**(2): p. 316-333.
53. Thakur, M.L. and B.C. Lentle, *Joint SNM/RSNA molecular imaging summit statement.* J Nucl Med, 2005. **46**(9): p. 11N-13N.
54. Blumen, H., K. Fitch, and V. Polkus, *Comparison of treatment costs for breast cancer, by tumor stage and type of service.* American health & drug benefits, 2016. **9**(1): p. 23.
55. Christiansen, P., S.L. Carstensen, B. Ejlertsen, et al., *Breast conserving surgery versus mastectomy: overall and relative survival—a population based study by the Danish Breast Cancer Cooperative Group (DBCG).* Acta Oncologica, 2018. **57**(1): p. 19-25.
56. Gradishar, W.J., B.O. Anderson, R. Balassanian, et al., *Breast cancer, version 4.2017, NCCN clinical practice guidelines in oncology.* Journal of the National Comprehensive Cancer Network, 2018. **16**(3): p. 310-320.
57. Murphy, C.C., L.K. Bartholomew, M.Y. Carpentier, et al., *Adherence to adjuvant hormonal therapy among breast cancer survivors in clinical practice: a systematic review.* Breast cancer research and treatment, 2012. **134**(2): p. 459-478.
58. Hammond, M.E.H., D.F. Hayes, M. Dowsett, et al., *American Society of Clinical Oncology/College of American Pathologists guideline recommendations for immunohistochemical testing of estrogen and progesterone receptors in breast cancer (unabridged version).* Archives of pathology & laboratory medicine, 2010. **134**(7): p. e48-e72.
59. Carlson, R.W., B.O. Anderson, H.J. Burstein, et al., *The NCCN. Invasive breast cancer: Clinical practice guidelines in oncology™.* JNCCN Journal of the National Comprehensive Cancer Network, 2007. **5**(3): p. 246-312.

60. Burstein, H.J., J.J. Griggs, A.A. Prestrud, et al., *American society of clinical oncology clinical practice guideline update on adjuvant endocrine therapy for women with hormone receptor–positive breast cancer.* Journal of oncology practice, 2010. **6**(5): p. 243-246.
61. Partridge, S.C., J.E. Gibbs, Y. Lu, et al., *Accuracy of MR imaging for revealing residual breast cancer in patients who have undergone neoadjuvant chemotherapy.* American Journal of Roentgenology, 2002. **179**(5): p. 1193-1199.
62. Lacroix, M. and G. Leclercq, *Relevance of breast cancer cell lines as models for breast tumours: an update.* Breast cancer research and treatment, 2004. **83**(3): p. 249-289.
63. Ouwens, D.M., N.D. de Ruiter, G.C. van der Zon, et al., *Growth factors can activate ATF2 via a two-step mechanism: phosphorylation of Thr71 through the Ras–MEK–ERK pathway and of Thr69 through RalGDS–Src–p38.* The EMBO journal, 2002. **21**(14): p. 3782-3793.
64. Hanahan, D. and R.A. Weinberg, *Hallmarks of cancer: the next generation.* cell, 2011. **144**(5): p. 646-674.
65. Karp, G., *Cell and molecular biology: concepts and experiments*. 2009: John Wiley & Sons.
66. Andrade, E., A. Bento, J. Cavalli, et al., *Non-clinical studies required for new drug development-Part I: early in silico and in vitro studies, new target discovery and validation, proof of principles and robustness of animal studies.* Brazilian Journal of Medical and Biological Research, 2016. **49**(11).
67. Hevener, K.E., *Computational Toxicology Methods in Chemical Library Design and High-Throughput Screening Hit Validation*, in *Computational Toxicology*. 2018, Springer. p. 275-285.
68. Bleicher, K.H., H.-J. Böhm, K. Müller, et al., *A guide to drug discovery: hit and lead generation: beyond high-throughput screening.* Nature reviews Drug discovery, 2003. **2**(5): p. 369.
69. Klumpp, M., A. Boettcher, D. Becker, et al., *Readout technologies for highly miniaturized kinase assays applicable to high-throughput screening in a 1536-well format.* Journal of biomolecular screening, 2006. **11**(6): p. 617-633.
70. Voskoglou-Nomikos, T., J.L. Pater, and L. Seymour, *Clinical predictive value of the in vitro cell line, human xenograft, and mouse allograft preclinical cancer models.* Clinical Cancer Research, 2003. **9**(11): p. 4227-4239.
71. FDA. *Development & Approval Process (Drugs)*. FDA Webpage 2017; Available from: https://www.fda.gov/drugs/developmentapprovalprocess/default.htm.
72. FDA. *Guidance for Industry Developing Medical Imaging Drug and Biological Products*. [Website fda.gov] 2004 [cited 2017 09/2018]; Clinical Medical]. Available from: http://www.fda.gov/cder/guidance/index.htm.
73. Adams, C.P. and V.V. Brantner, *Spending on new drug development 1.* Health economics, 2010. **19**(2): p. 130-141.
74. Arora, T., A. Mehta, V. Joshi, et al., *Substitute of animals in drug research: an approach towards fulfillment of 4R's.* Indian journal of pharmaceutical sciences, 2011. **73**(1): p. 1.
75. FDA. *The Drug Development Process*. [Webpage] 2018 10/2018]; Jan/4/2018:[Available from: https://www.fda.gov/ForPatients/Approvals/Drugs/default.htm.
76. Hausheer, F.H., H. Kochat, A.R. Parker, et al., *New approaches to drug discovery and development: a mechanism-based approach to pharmaceutical research and its application to BNP7787, a novel chemoprotective agent.* Cancer chemotherapy and pharmacology, 2003. **52**(1): p. 3-15.
77. Ma, Y., Y. Ji, G. Huang, et al., *Bioprinting 3D cell-laden hydrogel microarray for screening human periodontal ligament stem cell response to extracellular matrix.* Biofabrication, 2015. **7**(4): p. 044105.
78. Elliott, N.T. and F. Yuan, *A review of three-dimensional in vitro tissue models for drug discovery and transport studies.* Journal of pharmaceutical sciences, 2011. **100**(1): p. 59-74.

79. Begley, C.G. and L.M. Ellis, *Drug development: Raise standards for preclinical cancer research.* Nature, 2012. **483**(7391): p. 531.
80. Richard A. Lehne, P., Jacqueline Burchum, DNSc, APRN, BC and Laura Rosenthal, DNP, ACN, *Pharmacology for Nursing Care*. 8th ed. 2013: Saunders/Elsevier.
81. Quirk, R.A., R.M. France, K.M. Shakesheff, et al., *Supercritical fluid technologies and tissue engineering scaffolds.* Current Opinion in Solid State and Materials Science, 2004. **8**(3-4): p. 313-321.
82. Focht, D.D., *Biodegradation.* Access Science, 2019.
83. Haider, T.P., C. Völker, J. Kramm, et al., *Plastics of the future? The impact of biodegradable polymers on the environment and on society.* Angewandte Chemie International Edition, 2019. **58**(1): p. 50-62.
84. Bartis, D. and J. Pongrácz, *Three dimensional tissue cultures and tissue engineering.* Teach. Mater. Med. Biotechnol. Master's Program. Univ. Pécs Univ. Debrecen, 2011. **15**.
85. Bajaj, P., R.M. Schweller, A. Khademhosseini, et al., *3D biofabrication strategies for tissue engineering and regenerative medicine.* Annual review of biomedical engineering, 2014. **16**: p. 247-276.
86. Hutmacher, D.W., *Biomaterials offer cancer research the third dimension.* Nature materials, 2010. **9**(2): p. 90.
87. Lv, Q. and Q. Feng, *Preparation of 3-D regenerated fibroin scaffolds with freeze drying method and freeze drying/foaming technique.* Journal of Materials Science: Materials in Medicine, 2006. **17**(12): p. 1349-1356.
88. Yanez, M., J. Rincon, A. Dones, et al., *In vivo assessment of printed microvasculature in a bilayer skin graft to treat full-thickness wounds.* Tissue Engineering Part A, 2014. **21**(1-2): p. 224-233.
89. Pham, C., J. Greenwood, H. Cleland, et al., *Bioengineered skin substitutes for the management of burns: a systematic review.* Burns, 2007. **33**(8): p. 946-957.
90. Falanga, V. and M. Sabolinski, *A bilayered living skin construct (APLIGRAF®) accelerates complete closure of hard-to-heal venous ulcers.* Wound Repair and Regeneration, 1999. **7**(4): p. 201-207.
91. Morgan, J.R. and M.L. Yarmush, *Bioengineered skin substitutes.* Sci. Med, 1997. **4**: p. 6-15.
92. Zhang, K., C.-K. Chou, X. Xia, et al., *Block-Cell-Printing for live single-cell printing.* Proceedings of the National Academy of Sciences, 2014. **111**(8): p. 2948-2953.
93. Catros, S., F. Guillemot, A. Nandakumar, et al., *Layer-by-layer tissue microfabrication supports cell proliferation in vitro and in vivo.* Tissue Engineering Part C: Methods, 2011. **18**(1): p. 62-70.
94. Deitzel, J.M., J. Kleinmeyer, D. Harris, et al., *The effect of processing variables on the morphology of electrospun nanofibers and textiles.* Polymer, 2001. **42**(1): p. 261-272.
95. Freeman, A.E. and R.M. Hoffman, *In vivo-like growth of human tumors in vitro.* Proceedings of the National Academy of Sciences, 1986. **83**(8): p. 2694-2698.
96. Boland, T., T. Xu, B. Damon, et al., *Application of inkjet printing to tissue engineering.* Biotechnology Journal: Healthcare Nutrition Technology, 2006. **1**(9): p. 910-917.
97. Catros, S., B. Guillotin, M. Bačáková, et al., *Effect of laser energy, substrate film thickness and bioink viscosity on viability of endothelial cells printed by Laser-Assisted Bioprinting.* Applied Surface Science, 2011. **257**(12): p. 5142-5147.
98. Mironov, V., T. Boland, T. Trusk, et al., *Organ printing: computer-aided jet-based 3D tissue engineering.* TRENDS in Biotechnology, 2003. **21**(4): p. 157-161.
99. Xu, T., W. Zhao, J.-M. Zhu, et al., *Complex heterogeneous tissue constructs containing multiple cell types prepared by inkjet printing technology.* Biomaterials, 2013. **34**(1): p. 130-139.
100. Le, H.P., *Progress and trends in ink-jet printing technology.* Journal of Imaging Science and Technology, 1998. **42**(1): p. 49-62.

101. Singh, M., H.M. Haverinen, P. Dhagat, et al., *Inkjet printing—process and its applications.* Advanced materials, 2010. **22**(6): p. 673-685.
102. Xu, T., J. Jin, C. Gregory, et al., *Inkjet printing of viable mammalian cells.* Biomaterials, 2005. **26**(1): p. 93-99.
103. Cui, X. and T. Boland, *Human microvasculature fabrication using thermal inkjet printing technology.* Biomaterials, 2009. **30**(31): p. 6221-6227.
104. Murphy, S.V. and A. Atala, *3D bioprinting of tissues and organs.* Nature biotechnology, 2014. **32**(8): p. 773.
105. Francia, G., Shane K. Green, Guido Bocci, Shan Man, Urban Emmenegger, John ML Ebos, Adina Weinerman, Yuval Shaked, and Robert S. Kerbe, *Down-regulation of DNA mismatch repair proteins in human and murine tumor spheroids: implications for multicellular resistance to alkylating agents.* Molecular cancer therapeutics, 2005. **4**(10): p. 10.
106. Hribar, K.C., Darren Finlay, Xuanyi Ma, Xin Qu, Matthew G. Ondeck, Peter H. Chung, Fabian Zanella et al, *Nonlinear 3D projection printing of concave hydrogel microstructures for long-term multicellular spheroid and embryoid body culture.* Lab on a Chip, 2015. **15**(11): p. 6.
107. Zhang, W., C. Li, B.C. Baguley, et al., *Optimization of the formation of embedded multicellular spheroids of MCF-7 cells: How to reliably produce a biomimetic 3D model.* Analytical biochemistry, 2016. **515**: p. 47-54.
108. Timmins, N.E. and L.K. Nielsen, *Generation of multicellular tumor spheroids by the hanging-drop method*, in *Tissue Engineering*. 2007, Springer. p. 141-151.
109. Peng, W., P. Datta, B. Ayan, et al., *3D bioprinting for drug discovery and development in pharmaceutics.* Acta biomaterialia, 2017. **57**: p. 26-46.
110. Peng, W., D. Unutmaz, and I.T. Ozbolat, *Bioprinting towards physiologically relevant tissue models for pharmaceutics.* Trends in Biotechnology, 2016. **34**(9): p. 722-732.
111. Miri, A.K., A. Khalilpour, B. Cecen, et al., *Multiscale bioprinting of vascularized models.* Biomaterials, 2019. **198**: p. 204-216.
112. Yerneni, S.S., T.L. Whiteside, L.E. Weiss, et al., *Bioprinting exosome-like extracellular vesicle microenvironments.* Bioprinting, 2019. **13**: p. e00041.
113. Gudapati, H., M. Dey, and I. Ozbolat, *A comprehensive review on droplet-based bioprinting: past, present and future.* Biomaterials, 2016. **102**: p. 20-42.
114. Cui, X., K. Breitenkamp, M. Finn, et al., *Direct human cartilage repair using three-dimensional bioprinting technology.* Tissue Engineering Part A, 2012. **18**(11-12): p. 1304-1312.
115. Chen, F., L. Lin, J. Zhang, et al., *Single-cell analysis using drop-on-demand inkjet printing and probe electrospray ionization mass spectrometry.* Analytical chemistry, 2016. **88**(8): p. 4354-4360.
116. Phamduy, T.B., R.S. Sweat, M.S. Azimi, et al., *Printing cancer cells into intact microvascular networks: a model for investigating cancer cell dynamics during angiogenesis.* Integrative Biology, 2015. **7**(9): p. 1068-1078.
117. Campbell, A., Mohl, Jonathon E., Gutierrez, Denisse A., Varela-Ramirez, Armando , Boland, Thomas*, *Thermal Bioprinting Causes Ample Alterations of Expression of LUCAT1, IL6, CCL26 and NRN1L Genes and Massive Phosphorylation of Critical Oncogenic Drug Resistance Pathways in Breast Cancer Cells.* Frontiers in Bioengineering and Biotechnology, 2019. **TBD**.
118. De Maria, C., J. Rincon, A.A. Duarte, et al., *A new approach to fabricate agarose microstructures.* Polymers for Advanced Technologies, 2013. **24**(10): p. 895-902.
119. Robles-Escajeda, E., U. Das, N.M. Ortega, et al., *A novel curcumin-like dienone induces apoptosis in triple-negative breast cancer cells.* Cellular oncology, 2016. **39**(3): p. 265-277.

120. Santiago-Vázquez, Y., U. Das, A. Varela-Ramirez, et al., *Tumor-selective cytotoxicity of a novel pentadiene analogue on human leukemia/lymphoma cells.* Clinical cancer drugs, 2016. **3**(2): p. 138-146.
121. Iglesias-Figueroa, B.F., T.S. Siqueiros-Cendón, D.A. Gutierrez, et al., *Recombinant human lactoferrin induces apoptosis, disruption of F-actin structure and cell cycle arrest with selective cytotoxicity on human triple negative breast cancer cells.* Apoptosis, 2019: p. 1-16.
122. Bolger, A.M., M. Lohse, and B. Usadel, *Trimmomatic: a flexible trimmer for Illumina sequence data.* Bioinformatics, 2014. **30**(15): p. 2114-2120.
123. Langmead, B. and S. Salzberg, *Langmead. 2013. Bowtie2.* Nature Methods, 2013. **9**: p. 357-359.
124. Trapnell, C., A. Roberts, L. Goff, et al., *Differential gene and transcript expression analysis of RNA-seq experiments with TopHat and Cufflinks.* Nature protocols, 2012. **7**(3): p. 562.
125. Wickman, G., L. Julian, K. Mardilovich, et al., *Blebs produced by actin–myosin contraction during apoptosis release damage-associated molecular pattern proteins before secondary necrosis occurs.* Cell death and differentiation, 2013. **20**(10): p. 1293.
126. Kolesky, D.B., K.A. Homan, M.A. Skylar-Scott, et al., *Three-dimensional bioprinting of thick vascularized tissues.* Proceedings of the national academy of sciences, 2016. **113**(12): p. 3179-3184.
127. Cui, X., K. Breitenkamp, M. Lotz, et al., *Synergistic action of fibroblast growth factor-2 and transforming growth factor-beta1 enhances bioprinted human neocartilage formation.* Biotechnology and bioengineering, 2012. **109**(9): p. 2357-2368.
128. Chang, R., J. Nam, and W. Sun, *Direct cell writing of 3D microorgan for in vitro pharmacokinetic model.* Tissue Engineering Part C: Methods, 2008. **14**(2): p. 157-166.
129. Kim, Y.K., J.A. Park, W.H. Yoon, et al., *Drop-on-demand inkjet-based cell printing with 30-μ m nozzle diameter for cell-level accuracy.* Biomicrofluidics, 2016. **10**(6): p. 064110.
130. Calvert, P., *Inkjet printing for materials and devices.* Chemistry of materials, 2001. **13**(10): p. 3299-3305.
131. Roth, E.A., T. Xu, M. Das, et al., *Inkjet printing for high-throughput cell patterning.* Biomaterials, 2004. **25**(17): p. 3707-3715.
132. Moroi, J., S. Kashiwagi, S. Kim, et al., *Regional differences in apoptosis in murine gliosarcoma (T9) induced by mild hyperthermia.* International journal of hyperthermia, 1996. **12**(3): p. 345-354.
133. Milisav, I., B. Poljšak, and S. Ribarič, *Reduced risk of apoptosis: mechanisms of stress responses.* Apoptosis, 2017. **22**(2): p. 265-283.
134. Ugolkov, A., I. Gaisina, J.-S. Zhang, et al., *GSK-3 inhibition overcomes chemoresistance in human breast cancer.* Cancer letters, 2016. **380**(2): p. 384-392.
135. Di Paolo, G. and P. De Camilli, *Phosphoinositides in cell regulation and membrane dynamics.* Nature, 2006. **443**(7112): p. 651.
136. Arcaro, A. and A.S. Guerreiro, *The phosphoinositide 3-kinase pathway in human cancer: genetic alterations and therapeutic implications.* Current genomics, 2007. **8**(5): p. 271-306.
137. Mattson, M.P., *Hormesis defined.* Ageing research reviews, 2008. **7**(1): p. 1-7.
138. Brembeck, F.H., M. Rosário, and W. Birchmeier, *Balancing cell adhesion and Wnt signaling, the key role of β-catenin.* Current opinion in genetics & development, 2006. **16**(1): p. 51-59.
139. Woodgett, J.R., *Recent advances in the protein kinase B signaling pathway.* Current opinion in cell biology, 2005. **17**(2): p. 150-157.
140. Alonso, M. and A. Martinez, *GSK-3 inhibitors: discoveries and developments.* Current medicinal chemistry, 2004. **11**(6): p. 755-763.
141. Pap, M. and G.M. Cooper, *Role of glycogen synthase kinase-3 in the phosphatidylinositol 3-kinase/Akt cell survival pathway.* Journal of Biological Chemistry, 1998. **273**(32): p. 19929-19932.

142. Wang, Q., X. Wang, A. Hernandez, et al., *Regulation of TRAIL expression by the phosphatidylinositol 3-kinase/Akt/GSK-3 pathway in human colon cancer cells.* Journal of Biological Chemistry, 2002. **277**(39): p. 36602-36610.
143. Alvarez, E., I.C. Northwood, F.A. Gonzalez, et al., *Pro-Leu-Ser/Thr-Pro is a consensus primary sequence for substrate protein phosphorylation. Characterization of the phosphorylation of c-myc and c-jun proteins by an epidermal growth factor receptor threonine 669 protein kinase.* Journal of Biological Chemistry, 1991. **266**(23): p. 15277-15285.
144. Okazaki, K. and N. Sagata, *The Mos/MAP kinase pathway stabilizes c-Fos by phosphorylation and augments its transforming activity in NIH 3T3 cells.* The EMBO journal, 1995. **14**(20): p. 5048-5059.
145. Hibi, M., A. Lin, T. Smeal, et al., *Identification of an oncoprotein-and UV-responsive protein kinase that binds and potentiates the c-Jun activation domain.* Genes & development, 1993. **7**(11): p. 2135-2148.
146. Mantawy, E.M., A. Esmat, W.M. El-Bakly, et al., *Mechanistic clues to the protective effect of chrysin against doxorubicin-induced cardiomyopathy: Plausible roles of p53, MAPK and AKT pathways.* Scientific reports, 2017. **7**(1): p. 4795.
147. Dai, R., W. Frejtag, B. He, et al., *c-Jun NH2-terminal kinase targeting and phosphorylation of heat shock factor-1 suppress its transcriptional activity.* Journal of Biological Chemistry, 2000. **275**(24): p. 18210-18218.
148. Kurokawa, M., K. Mitani, T. Yamagata, et al., *The evi-1 oncoprotein inhibits c-Jun N-terminal kinase and prevents stress-induced cell death.* The EMBO Journal, 2000. **19**(12): p. 2958-2968.
149. Robinson, M.J. and M.H. Cobb, *Mitogen-activated protein kinase pathways.* Current opinion in cell biology, 1997. **9**(2): p. 180-186.
150. Shimamura, A., B.A. Ballif, S.A. Richards, et al., *Rsk1 mediates a MEK–MAP kinase cell survival signal.* Current Biology, 2000. **10**(3): p. 127-135.
151. Hu, Y., X. Fang, S.M. Dunham, et al., *90-kDa ribosomal S6 kinase is a direct target for the nuclear fibroblast growth factor receptor 1 (FGFR1) ROLE IN FGFR1 SIGNALING.* Journal of Biological Chemistry, 2004. **279**(28): p. 29325-29335.
152. Dalby, K.N., N. Morrice, F.B. Caudwell, et al., *Identification of regulatory phosphorylation sites in mitogen-activated protein kinase (MAPK)-activated protein kinase-1a/p90 rsk that are inducible by MAPK.* Journal of Biological Chemistry, 1998. **273**(3): p. 1496-1505.
153. Hartman, K.G., M.I. Vitolo, A.D. Pierce, et al., *Complex formation between S100B protein and the p90 ribosomal S6 kinase (RSK) in malignant melanoma is calcium-dependent and inhibits extracellular signal-regulated kinase (ERK)-mediated phosphorylation of RSK.* Journal of Biological Chemistry, 2014. **289**(18): p. 12886-12895.
154. Rogalla, T., M. Ehrnsperger, X. Preville, et al., *Regulation of Hsp27 oligomerization, chaperone function, and protective activity against oxidative stress/tumor necrosis factor α by phosphorylation.* Journal of Biological Chemistry, 1999. **274**(27): p. 18947-18956.
155. Kato, K., K. Hasegawa, S. Goto, et al., *Dissociation as a result of phosphorylation of an aggregated form of the small stress protein, hsp27.* Journal of Biological Chemistry, 1994. **269**(15): p. 11274-11278.
156. Almeida-Souza, L., S. Goethals, V. De Winter, et al., *Increased monomerization of mutant HSPB1 leads to protein hyperactivity in Charcot-Marie-Tooth neuropathy.* Journal of biological chemistry, 2010. **285**(17): p. 12778-12786.
157. Vos, M.J., B. Kanon, and H.H. Kampinga, *HSPB7 is a SC35 speckle resident small heat shock protein.* Biochimica et Biophysica Acta (BBA)-Molecular Cell Research, 2009. **1793**(8): p. 1343-1353.

158. Bryantsev, A.L., S.Y. Kurchashova, S.A. Golyshev, et al., *Regulation of stress-induced intracellular sorting and chaperone function of Hsp27 (HspB1) in mammalian cells.* Biochemical Journal, 2007. **407**(3): p. 407-417.
159. Concannon, C.G., S. Orrenius, and A. Samali, *Hsp27 inhibits cytochrome c-mediated caspase activation by sequestering both pro-caspase-3 and cytochrome c.* Gene Expression, The Journal of Liver Research, 2001. **9**(4-5): p. 195-201.
160. Hurwitz, M. and P. Stauffer. *Hyperthermia, radiation and chemotherapy: the role of heat in multidisciplinary cancer care*. in *Seminars in oncology*. 2014. Elsevier.
161. Mazaira, G.I., C. Daneri-Becerra, N.R. Zgajnar, et al., *Gene expression regulation by heat-shock proteins: the cardinal roles of HSF1 and Hsp90.* Biochemical Society Transactions, 2018. **46**(1): p. 51-65.
162. Chatterjee, B.K., S. Puri, A. Sharma, et al., *Molecular Chaperones: Structure-Function Relationship and their Role in Protein Folding*, in *Regulation of Heat Shock Protein Responses*. 2018, Springer. p. 181-218.
163. Plimpton, R.L., J.M. Valpuesta, and B.M. Willardson, *Mechanisms of Protein Folding by Type II Chaperonins.* Role of Molecular Chaperones in Structural Folding, Biological Functions, and Drug Interactions of Client Proteins, 2018. **1**: p. 190-213.
164. Tamura, K., T. Sudo, U. Senftleben, et al., *Requirement for p38α in erythropoietin expression: a role for stress kinases in erythropoiesis.* Cell, 2000. **102**(2): p. 221-231.
165. Sayed, M., S.O. Kim, B.S. Salh, et al., *Stress-induced activation of protein kinase CK2 by direct interaction with p38 mitogen-activated protein kinase.* Journal of Biological Chemistry, 2000. **275**(22): p. 16569-16573.
166. Mathew Loesch, G.C., *The p38 MAPK stress pathway as a tumor suppressor or more?* Frontiers in bioscience: a journal and virtual library, 2008. **13**: p. 3581.
167. Zlobin, A., J.C. Bloodworth, and C. Osipo, *Mitogen-Activated Protein Kinase.* Predictive Biomarkers in Oncology: Applications in Precision Medicine, 2018: p. 213.
168. Deak, M., A.D. Clifton, J.M. Lucocq, et al., *Mitogen-and stress-activated protein kinase-1 (MSK1) is directly activated by MAPK and SAPK2/p38, and may mediate activation of CREB.* The EMBO journal, 1998. **17**(15): p. 4426-4441.
169. Haleagrahara, N., K. Hodgson, S. Miranda-Hernandez, et al., *Flavonoid quercetin–methotrexate combination inhibits inflammatory mediators and matrix metalloproteinase expression, providing protection to joints in collagen-induced arthritis.* Inflammopharmacology, 2018. **26**(5): p. 1219-1232.
170. Zaka, M., B.H. Abbasi, and S. Durdagi, *Novel tumor necrosis factor-α (TNF-α) inhibitors from small molecule library screening for their therapeutic activity profiles against rheumatoid arthritis using target-driven approaches and binary QSAR models.* Journal of Biomolecular Structure and Dynamics, 2019. **37**(9): p. 2464-2476.
171. Pierrat, B., J. da Silva Correia, J.-L. Mary, et al., *RSK-B, a novel ribosomal S6 kinase family member, is a CREB kinase under dominant control of p38α mitogen-activated protein kinase (p38αMAPK).* Journal of Biological Chemistry, 1998. **273**(45): p. 29661-29671.
172. Soloaga, A., S. Thomson, G.R. Wiggin, et al., *MSK2 and MSK1 mediate the mitogen-and stress-induced phosphorylation of histone H3 and HMG-14.* The EMBO journal, 2003. **22**(11): p. 2788-2797.
173. Tomás-Zuber, M., J.-L. Mary, F. Lamour, et al., *C-terminal elements control location, activation threshold, and p38 docking of ribosomal S6 kinase B (RSKB).* Journal of Biological Chemistry, 2001. **276**(8): p. 5892-5899.
174. Ferrari, S. and G. Thomas, *S6 Phosphorylation and the p70s6k/p85s6k.* Critical reviews in biochemistry and molecular biology, 1994. **29**(6): p. 385-413.

175. Kozma, S. and G. Thomas. *p70s6k/p85s6k: Mechanism of activation and role in mitogenesis*. in *Seminars in cancer biology*. 1994.
176. Cross, D.A., D.R. Alessi, P. Cohen, et al., *Inhibition of glycogen synthase kinase-3 by insulin mediated by protein kinase B.* Nature, 1995. **378**(6559): p. 785.
177. Wang, X., J. Yao, J. Wang, et al., *Targeting aberrant p70S6K activation for estrogen receptor–negative breast cancer prevention.* Cancer Prevention Research, 2017. **10**(11): p. 641-650.
178. Knowlton, D.L., K. Tang, P.V. Henstock, et al., *miRNA alterations modify kinase activation in the IGF-1 pathway and correlate with colorectal cancer stage and progression in patients.* Journal of Cancer, 2011. **2**: p. 490.
179. Edelmann, H.M., C. Kühne, C. Petritsch, et al., *Cell cycle regulation of p70 S6 kinase and p42/p44 mitogen-activated protein kinases in Swiss mouse 3T3 fibroblasts.* Journal of Biological Chemistry, 1996. **271**(2): p. 963-971.
180. Schachner, M., I. Leshchyns' ka, and V. Sytnyk, *Functions of the Neural Cell Adhesion Molecule (NCAM) at the Synapse.* 2017.
181. Stirling, J. and P. O'Hare, *CREB4, a transmembrane bZip transcription factor and potential new substrate for regulation and cleavage by S1P.* Molecular biology of the cell, 2006. **17**(1): p. 413-426.
182. Son, J., J.-H. Lee, H.-N. Kim, et al., *cAMP-response-element-binding protein positively regulates breast cancer metastasis and subsequent bone destruction.* Biochemical and biophysical research communications, 2010. **398**(2): p. 309-314.
183. Roskoski Jr, R., *ERK1/2 MAP kinases: structure, function, and regulation.* Pharmacological research, 2012. **66**(2): p. 105-143.
184. Neise, D., D. Sohn, A. Stefanski, et al., *The p90 ribosomal S6 kinase (RSK) inhibitor BI-D1870 prevents gamma irradiation-induced apoptosis and mediates senescence via RSK-and p53-independent accumulation of p21 WAF1/CIP1.* Cell death & disease, 2013. **4**(10): p. e859.
185. Niu, H., H.Y. Bihui, and R. Dalla-Favera, *Antigen receptor signaling induces MAP kinase-mediated phosphorylation and degradation of the BCL-6 transcription factor.* Genes & development, 1998. **12**(13): p. 1953-1961.
186. Williams, S.F. and R.C. Smallridge, *Targeting the ERK pathway: novel therapeutics for thyroid cancer.* Current Drug Targets-Immune, Endocrine & Metabolic Disorders, 2004. **4**(3): p. 199-220.
187. Laine, J., G. Künstle, T. Obata, et al., *The protooncogene TCL1 is an Akt kinase coactivator.* Molecular cell, 2000. **6**(2): p. 395-407.
188. Cheng, J.Q., A.K. Godwin, A. Bellacosa, et al., *AKT2, a putative oncogene encoding a member of a subfamily of protein-serine/threonine kinases, is amplified in human ovarian carcinomas.* Proceedings of the National Academy of Sciences, 1992. **89**(19): p. 9267-9271.
189. Noguchi, M., N. Hirata, and F. Suizu, *The links between AKT and two intracellular proteolytic cascades: ubiquitination and autophagy.* Biochimica et Biophysica Acta (BBA)-Reviews on Cancer, 2014. **1846**(2): p. 342-352.
190. Ruiz-Medina, B.E., D. Lerma, M. Hwang, et al., *Green barley mitigates cytotoxicity in human lymphocytes undergoing aggressive oxidative stress, via activation of both the Lyn/PI3K/Akt and MAPK/ERK pathways.* Scientific reports, 2019. **9**(1): p. 6005.
191. Martini, M., M.C. De Santis, L. Braccini, et al., *PI3K/AKT signaling pathway and cancer: an updated review.* Annals of medicine, 2014. **46**(6): p. 372-383.
192. Delcommenne, M., C. Tan, V. Gray, et al., *Phosphoinositide-3-OH kinase-dependent regulation of glycogen synthase kinase 3 and protein kinase B/AKT by the integrin-linked kinase.* Proceedings of the National Academy of Sciences, 1998. **95**(19): p. 11211-11216.
193. Bond, G.L., W. Hu, and A.J. Levine, *MDM2 is a central node in the p53 pathway: 12 years and counting.* Current cancer drug targets, 2005. **5**(1): p. 3-8.

194. Vaseva, A.V., N.D. Marchenko, K. Ji, et al., *p53 opens the mitochondrial permeability transition pore to trigger necrosis.* Cell, 2012. **149**(7): p. 1536-1548.
195. Ghosh, A., D. Stewart, and G. Matlashewski, *Regulation of human p53 activity and cell localization by alternative splicing.* Molecular and cellular biology, 2004. **24**(18): p. 7987-7997.
196. Yamasaki, S., N. Yagishita, T. Sasaki, et al., *Cytoplasmic destruction of p53 by the endoplasmic reticulum-resident ubiquitin ligase 'Synoviolin'.* The EMBO journal, 2007. **26**(1): p. 113-122.
197. Zhao, Y., R.B. Katzman, L.M. Delmolino, et al., *The notch regulator MAML1 interacts with p53 and functions as a coactivator.* Journal of Biological Chemistry, 2007. **282**(16): p. 11969-11981.
198. Raingeaud, J., A.J. Whitmarsh, T. Barrett, et al., *MKK3-and MKK6-regulated gene expression is mediated by the p38 mitogen-activated protein kinase signal transduction pathway.* Molecular and cellular biology, 1996. **16**(3): p. 1247-1255.
199. Moriguchi, T., N. Kuroyanagi, K. Yamaguchi, et al., *A novel kinase cascade mediated by mitogen-activated protein kinase kinase 6 and MKK3.* Journal of Biological Chemistry, 1996. **271**(23): p. 13675-13679.
200. Stein, B., H. Brady, M.X. Yang, et al., *Cloning and characterization of MEK6, a novel member of the mitogen-activated protein kinase kinase cascade.* Journal of Biological Chemistry, 1996. **271**(19): p. 11427-11433.
201. Goedert, M., A. Cuenda, M. Craxton, et al., *Activation of the novel stress-activated protein kinase SAPK4 by cytokines and cellular stresses is mediated by SKK3 (MKK6); comparison of its substrate specificity with that of other SAP kinases.* The EMBO journal, 1997. **16**(12): p. 3563-3571.
202. Watson, G., A.R. Ze'ev, and E. Lau, *ATF2, a paradigm of the multifaceted regulation of transcription factors in biology and disease.* Pharmacological research, 2017. **119**: p. 347-357.
203. Ben-Levy, R., S. Hooper, R. Wilson, et al., *Nuclear export of the stress-activated protein kinase p38 mediated by its substrate MAPKAP kinase-2.* Current Biology, 1998. **8**(19): p. 1049-1057.
204. Park, I.-H., R. Bachmann, H. Shirazi, et al., *Regulation of ribosomal S6 kinase 2 by mammalian target of rapamycin.* Journal of Biological Chemistry, 2002. **277**(35): p. 31423-31429.
205. Kim, D.-H., D.D. Sarbassov, S.M. Ali, et al., *mTOR interacts with raptor to form a nutrient-sensitive complex that signals to the cell growth machinery.* Cell, 2002. **110**(2): p. 163-175.
206. Inoki, K., T. Zhu, and K.-L. Guan, *TSC2 mediates cellular energy response to control cell growth and survival.* Cell, 2003. **115**(5): p. 577-590.
207. Brugarolas, J., K. Lei, R.L. Hurley, et al., *Regulation of mTOR function in response to hypoxia by REDD1 and the TSC1/TSC2 tumor suppressor complex.* Genes & development, 2004. **18**(23): p. 2893-2904.
208. Lane, M.T., T.J. Herda, A.C. Fry, et al., *Endocrine responses and acute mTOR pathway phosphorylation to resistance exercise with leucine and whey.* Biology of sport, 2017. **34**(2): p. 197.
209. Jacinto, E., R. Loewith, A. Schmidt, et al., *Mammalian TOR complex 2 controls the actin cytoskeleton and is rapamycin insensitive.* Nature cell biology, 2004. **6**(11): p. 1122.
210. Koren, I., E. Reem, and A. Kimchi, *DAP1, a novel substrate of mTOR, negatively regulates autophagy.* Current Biology, 2010. **20**(12): p. 1093-1098.
211. Habash, R.W., R. Bansal, D. Krewski, et al., *Thermal therapy, part 2: hyperthermia techniques.* Critical Reviews™ in Biomedical Engineering, 2006. **34**(6).
212. Tonelli, C., I.I.C. Chio, and D.A. Tuveson, *Transcriptional regulation by Nrf2.* Antioxidants & redox signaling, 2018. **29**(17): p. 1727-1745.
213. Thai, P., S. Statt, C.H. Chen, et al., *Characterization of a novel long noncoding RNA, SCAL1, induced by cigarette smoke and elevated in lung cancer cell lines.* American journal of respiratory cell and molecular biology, 2013. **49**(2): p. 204-211.

214. Ma, Q., *Role of nrf2 in oxidative stress and toxicity.* Annual review of pharmacology and toxicology, 2013. **53**: p. 401-426.
215. Zheng, A., X. Song, L. Zhang, et al., *Long non-coding RNA LUCAT1/miR-5582-3p/TCF7L2 axis regulates breast cancer stemness via Wnt/β-catenin pathway.* Journal of Experimental & Clinical Cancer Research, 2019. **38**(1): p. 305.
216. Zheng, Z., F. Zhao, D. Zhu, et al., *Long non-coding RNA LUCAT1 promotes proliferation and invasion in clear cell renal cell carcinoma through AKT/GSK-3β signaling pathway.* Cellular Physiology and Biochemistry, 2018. **48**(3): p. 891-904.
217. Kitaura, M., N. Suzuki, T. Imai, et al., *Molecular cloning of a novel human CC chemokine (Eotaxin-3) that is a functional ligand of CC chemokine receptor 3.* Journal of Biological Chemistry, 1999. **274**(39): p. 27975-27980.
218. Marijani, R., T. Mathews, H. McGann, et al., *Regulatory Effect of CCL26 on Cancer Related Genes during Inflammation*. 2011, Federation of American Societies for Experimental Biology.
219. Lin, Z.-Y., Y.-H. Chuang, and W.-L. Chuang, *Cancer-associated fibroblasts up-regulate CCL2, CCL26, IL6 and LOXL2 genes related to promotion of cancer progression in hepatocellular carcinoma cells.* Biomedicine & Pharmacotherapy, 2012. **66**(7): p. 525-529.
220. Thomas, J.K., H. Mir, N. Kapur, et al., *CC chemokines are differentially expressed in Breast Cancer and are associated with disparity in overall survival.* Scientific reports, 2019. **9**(1): p. 4014.
221. Liang, Q., X. Shen, and G. Sun, *Precision Medicine: Update on Diagnosis and Therapeutic Strategies of Hepatocellular Carcinoma.* Current medicinal chemistry, 2018. **25**(17): p. 1999-2008.
222. Ota, T., Y. Suzuki, T. Nishikawa, et al., *Complete sequencing and characterization of 21,243 full-length human cDNAs.* Nature genetics, 2004. **36**(1): p. 40.
223. *NRN1L neuritin 1 like [(human)] - NCBI.* NCBI, 2019.
224. Ellyard, J.I., D.T. Avery, T.G. Phan, et al., *Antigen-selected, immunoglobulin-secreting cells persist in human spleen and bone marrow.* Blood, 2004. **103**(10): p. 3805-3812.
225. Hirano, T., K. Yasukawa, H. Harada, et al., *Complementary DNA for a novel human interleukin (BSF-2) that induces B lymphocytes to produce immunoglobulin.* Nature, 1986. **324**(6092): p. 73.
226. Calderón-Garcidueñas, L., J.V. Cross, M. Franco-Lira, et al., *Brain immune interactions and air pollution: macrophage inhibitory factor (MIF), prion cellular protein (PrPC), Interleukin-6 (IL-6), interleukin 1 receptor antagonist (IL-1Ra), and interleukin-2 (IL-2) in cerebrospinal fluid and MIF in serum differentiate urban children exposed to severe vs. low air pollution.* Frontiers in neuroscience, 2013. **7**: p. 183.
227. Badawi, A.F., E.L. Cavalieri, and E.G. Rogan, *Role of human cytochrome P450 1A1, 1A2, 1B1, and 3A4 in the 2-, 4-, and 16 [alpha]-hydroxylation of 17 [beta]-estradiol.* Metabolism-Clinical and Experimental, 2001. **50**(9): p. 1001-1003.
228. Kobayashi, R., L.Z. Rassenti, G. Meisenholder, et al., *Autoantigen inhibits apoptosis of a human B cell leukemia that produces pathogenic rheumatoid factor.* The Journal of Immunology, 1993. **151**(12): p. 7273-7283.
229. Feitelson, M.A., A. Arzumanyan, R.J. Kulathinal, et al. *Sustained proliferation in cancer: Mechanisms and novel therapeutic targets*. in *Seminars in cancer biology*. 2015. Elsevier.
230. Weledji, E. and J. Tambe, *Breast Cancer Detection and Screening.* Med Clin Rev, 2018. **4**(2): p. 8.
231. Marmot, M., D. Altman, D. Cameron, et al., *The benefits and harms of breast cancer screening: an independent review.* British journal of cancer, 2013. **108**(11): p. 2205.
232. Cianfrocca, M. and L.J. Goldstein, *Prognostic and predictive factors in early-stage breast cancer.* The oncologist, 2004. **9**(6): p. 606-616.

233. Carolina, L., A. VARELA-RAMIREZ, and R.J. AGUILERA, *Differential nuclear staining assay for high-throughput screening to identify cytotoxic compounds.* Current cellular biochemistry, 2011. **1**(1): p. 1.
234. Calabrese, E.J. and L.A. Baldwin, *The hormetic dose-response model is more common than the threshold model in toxicology.* Toxicological Sciences, 2003. **71**(2): p. 246-250.
235. Bauer, K.R., M. Brown, R.D. Cress, et al., *Descriptive analysis of estrogen receptor (ER)-negative, progesterone receptor (PR)-negative, and HER2-negative invasive breast cancer, the so-called triple-negative phenotype: a population-based study from the California cancer Registry.* Cancer, 2007. **109**(9): p. 1721-1728.

Glossary

List of Abbreviations

BP: Bioprinted
MS: Manually Seeded
BCCs: Breast cancer cells
Ser: Serine
Thr: Threonine
Gly: Glycine
Tyr: Tyrosine
HER2: Human epidermal growth factor receptor 2
VEGF: Vascular Endothelial Growth Factor
EDTA: Ethylenediaminetetraacetic acid
Chr: Chromosome
GO: Gene ontology
ECM: Extracellular Matrix
ml(s): Milliliter(s)
h: Hours
min(s): minute(s)
RT: Room Temperature

Appendix I

Upregulated genes from BP MCF7 Cell samples

Gene Name	Chromosome	Sample1	Sample2	Status	Value1	Value2
FBLI+A2:B208M1	chr1	MS	BP	OK	3.9267	8.67642
GRHL3	chr1	MS	BP	OK	3.29011	6.94756
SERINC2	chr1	MS	BP	OK	9.74637	20.6255
MAP7D1	chr1	MS	BP	OK	10.16	23.6725
ARTN	chr1	MS	BP	OK	1.5177	4.39928
PLEKHO1	chr1	MS	BP	OK	2.81658	5.9777
SPRR1B	chr1	MS	BP	OK	7.09732	23.4578
IL6R	chr1	MS	BP	OK	0.571878	1.68307
TGFB2	chr1	MS	BP	OK	0.882809	3.16345
SCCPDH	chr1	MS	BP	OK	80.7339	168.403
DHRS3	chr1	MS	BP	OK	3.81449	9.18426
NBPF1	chr1	MS	BP	OK	8.54178	17.3376
IFFO2	chr1	MS	BP	OK	1.87258	6.81221
RAP1GAP	chr1	MS	BP	OK	6.16587	12.6189
MOB3C	chr1	MS	BP	OK	2.04389	5.11261
LRP8	chr1	MS	BP	OK	4.87216	14.3562
GBP2	chr1	MS	BP	OK	2.19287	4.65244
BCAR3	chr1	MS	BP	OK	2.64507	7.35811
GCLM	chr1	MS	BP	OK	2.81418	18.8373
PHTF1	chr1	MS	BP	OK	6.51986	13.4194
S100A7	chr1	MS	BP	OK	7.57309	23.0667
S100A6	chr1	MS	BP	OK	98.0374	218.226
SELL	chr1	MS	BP	OK	0.544378	2.25969
C1orf116	chr1	MS	BP	OK	0.334591	1.10439
DUSP10	chr1	MS	BP	OK	1.55605	3.68708
CAPN8	chr1	MS	BP	OK	1.74393	5.16656
SIPA1L2	chr1	MS	BP	OK	8.07156	18.341
AKR1C1	chr10	MS	BP	OK	1.07195	9.54644
AKR1C3	chr10	MS	BP	OK	11.6188	42.3069
ZNF365	chr10	MS	BP	OK	0.849057	2.18741
DDX21	chr10	MS	BP	OK	37.974	77.6104
PLAU	chr10	MS	BP	OK	0.313335	1.84237
PAPSS2	chr10	MS	BP	OK	14.2134	55.2579
HHEX	chr10	MS	BP	OK	3.54901	8.56703
AKR1C2	chr10	MS	BP	OK	34.2073	95.7251
NRP1	chr10	MS	BP	OK	10.1657	22.535
LINC01468	chr10	MS	BP	OK	18.3678	36.9121
AIFM2	chr10	MS	BP	OK	7.42538	17.1477

IDE	chr10	MS	BP	OK	11.5125	26.4017
CD44	chr11	MS	BP	OK	12.3171	37.9679
FJX1	chr11	MS	BP	OK	1.08285	3.42577
STX3	chr11	MS	BP	OK	5.95664	16.0924
PPP2R5B	chr11	MS	BP	OK	4.14014	8.63395
EHBP1L1	chr11	MS	BP	OK	7.02437	14.5089
KLC2	chr11	MS	BP	OK	20.7968	42.3771
GAL	chr11	MS	BP	OK	24.6209	50.766
MYEOV	chr11	MS	BP	OK	0.828166	2.28295
P2RY6	chr11	MS	BP	OK	0.472887	4.02792
TMEM45B	chr11	MS	BP	OK	4.07134	14.3443
DUSP8	chr11	MS	BP	OK	3.6054	7.56771
FOSL1	chr11	MS	BP	OK	1.69298	6.26689
PGM2L1	chr11	MS	BP	OK	0.846247	2.38704
ARRB1	chr11	MS	BP	OK	3.85802	9.66131
GDPD5	chr11	MS	BP	OK	3.04446	6.84893
CHORDC1	chr11	MS	BP	OK	4.50579	10.1885
GPRC5A	chr12	MS	BP	OK	46.3074	93.3704
EMP1	chr12	MS	BP	OK	0.651206	2.9149
TXNRD1	chr12	MS	BP	OK	24.5197	138.037
TRAFD1	chr12	MS	BP	OK	27.6589	56.7056
VDR	chr12	MS	BP	OK	2.48182	5.57566
KRT80	chr12	MS	BP	OK	106.467	289.256
KRT4	chr12	MS	BP	OK	11.9124	33.8798
B4GALNT1	chr12	MS	BP	OK	6.38962	21.1578
PHLDA1	chr12	MS	BP	OK	7.91885	27.231
NTN4	chr12	MS	BP	OK	2.94066	11.1099
SLC41A2	chr12	MS	BP	OK	1.36069	4.61989
NAA25	chr12	MS	BP	OK	7.8605	17.5864
CLIP1	chr12	MS	BP	OK	11.3662	28.7336
PITPNM2	chr12	MS	BP	OK	2.04813	5.40764
RGCC	chr13	MS	BP	OK	2.47291	6.91797
LMO7	chr13	MS	BP	OK	2.82787	6.74994
HS6ST3	chr13	MS	BP	OK	1.59923	4.12876
HSPH1	chr13	MS	BP	OK	30.8636	71.2378
LIG4	chr13	MS	BP	OK	1.99654	4.57396
ABHD4	chr14	MS	BP	OK	7.01526	17.6609
SAMD4A	chr14	MS	BP	OK	0.471884	1.65447
TTC9	chr14	MS	BP	OK	4.22494	8.522
BATF	chr14	MS	BP	OK	17.5846	36.9939
EIF5	chr14	MS	BP	OK	55.3639	118.778
CEP170B	chr14	MS	BP	OK	17.2999	35.9811

FERMT2	chr14	MS	BP	OK	10.6225	24.8597
MAP3K9	chr14	MS	BP	OK	2.43629	5.11886
PTPN21	chr14	MS	BP	OK	1.28898	2.87999
C15orf48	chr15	MS	BP	OK	1.58688	104.926
TMOD2	chr15	MS	BP	OK	0.320378	1.1494
FURIN	chr15	MS	BP	OK	5.51565	12.3625
SYNM	chr15	MS	BP	OK	0.719497	2.15163
ALDH1A3	chr15	MS	BP	OK	0.961502	30.0029
MYO1E	chr15	MS	BP	OK	3.96969	8.41733
STRA6	chr15	MS	BP	OK	0.711044	5.31797
SEMA7A	chr15	MS	BP	OK	1.07136	2.84316
CYP1A1	chr15	MS	BP	OK	0.473783	162.495
TNFRSF12A	chr16	MS	BP	OK	115.755	339.236
PDP2	chr16	MS	BP	OK	0.900458	1.91502
NRN1L	chr16	MS	BP	OK	0	1.66808
GAN	chr16	MS	BP	OK	2.483	7.27378
OSGIN1	chr16	MS	BP	OK	15.4532	43.6306
CRISPLD2	chr16	MS	BP	OK	2.6012	5.71324
KIAA0513	chr16	MS	BP	OK	3.86037	10.6516
ZNF469	chr16	MS	BP	OK	0.282562	1.80382
UNKL	chr16	MS	BP	OK	5.23298	19.9733
NQO1	chr16	MS	BP	OK	148.241	459.875
WSCD1	chr17	MS	BP	OK	0.731905	2.12065
ADORA2B	chr17	MS	BP	OK	4.0263	8.48186
TRIM16L	chr17	MS	BP	OK	6.54778	35.3976
ABCC3	chr17	MS	BP	OK	9.07609	32.9125
PRKCA	chr17	MS	BP	OK	1.95754	4.28213
SPHK1	chr17	MS	BP	OK	7.89098	20.8223
MIR22,MIR22HG	chr17	MS	BP	OK	3.36959	18.3256
ZNF594	chr17	MS	BP	OK	1.62913	3.28566
ALOXE3	chr17	MS	BP	OK	1.19859	2.60834
TRIM16	chr17	MS	BP	OK	15.1544	67.3261
FLII	chr17	MS	BP	OK	30.453	62.5339
ALDH3A1	chr17	MS	BP	OK	0.426173	6.16126
KRT13	chr17	MS	BP	OK	41.3909	95.5392
KRT17	chr17	MS	BP	OK	15.0591	61.8858
MPP3	chr17	MS	BP	OK	1.47728	3.04837
MAP3K14	chr17	MS	BP	OK	2.20055	5.32242
MAFG	chr17	MS	BP	OK	4.00078	11.8508
RBBP8	chr18	MS	BP	OK	17.5174	61.1022
LAMA3	chr18	MS	BP	OK	2.12918	6.1523
DTNA	chr18	MS	BP	OK	8.83981	17.7691

MAPK4	chr18	MS	BP	OK	1.6854	3.99929
FSTL3	chr19	MS	BP	OK	5.57192	11.5771
CNN2	chr19	MS	BP	OK	8.91239	19.124
TRIP10	chr19	MS	BP	OK	6.30853	13.0079
ICAM1	chr19	MS	BP	OK	0.97607	2.5496
KLF2	chr19	MS	BP	OK	6.2465	14.946
GDF15	chr19	MS	BP	OK	183.783	389.011
PLEKHF1	chr19	MS	BP	OK	0.810554	3.2911
CEACAM5	chr19	MS	BP	OK	21.8139	58.4458
CEACAM6	chr19	MS	BP	OK	26.1622	69.5711
BCL3	chr19	MS	BP	OK	13.5606	42.5235
IGFL1	chr19	MS	BP	OK	6.9717	15.2322
ZNF823	chr19	MS	BP	OK	2.63809	5.38673
PSG9	chr19	MS	BP	OK	1.0937	3.40133
KCNN4	chr19	MS	BP	OK	7.92633	16.4709
KLK6	chr19	MS	BP	OK	5.39735	11.1568
CLIP4	chr2	MS	BP	OK	0.605059	1.86397
EPAS1	chr2	MS	BP	OK	5.66639	38.2454
ACTG2	chr2	MS	BP	OK	0.760415	9.54863
ATOH8	chr2	MS	BP	OK	0.641643	1.72547
SLC9A2	chr2	MS	BP	OK	4.82041	10.8723
INHBB	chr2	MS	BP	OK	5.11667	17.9087
FMNL2	chr2	MS	BP	OK	1.59372	3.51657
ITGAV	chr2	MS	BP	OK	13.4546	28.4109
MYO1B	chr2	MS	BP	OK	25.2997	82.3447
NABP1	chr2	MS	BP	OK	2.06958	5.55777
NRP2	chr2	MS	BP	OK	0.474819	1.51921
CCNYL1	chr2	MS	BP	OK	8.07904	18.2027
PSMD1	chr2	MS	BP	OK	26.5125	54.1969
UGT1A1,UGT1A10, UGT1A3,UGT1A4, UGT1A5,UGT1A6, UGT1A7,UGT1A8, UGT1A9	chr2	MS	BP	OK	5.0658	19.8994
CAPN13	chr2	MS	BP	OK	2.60465	5.78064
FAM98A	chr2	MS	BP	OK	11.757	23.8727
CYP1B1	chr2	MS	BP	OK	23.613	228.394
PSME4	chr2	MS	BP	OK	11.347	28.3384
ZNF514	chr2	MS	BP	OK	1.87928	4.28084
FHL2	chr2	MS	BP	OK	8.44464	21.3486
MALL	chr2	MS	BP	OK	20.1256	53.4318
TFPI	chr2	MS	BP	OK	20.808	42.2067
HECW2	chr2	MS	BP	OK	0.899767	3.26049

ABCB6	chr2	MS	BP	OK	19.3435	38.953
AP1S3	chr2	MS	BP	OK	2.95626	7.17909
BPIFB1	chr20	MS	BP	OK	1.59498	4.24173
SRXN1	chr20	MS	BP	OK	19.4243	48.558
LZTS3	chr20	MS	BP	OK	1.06546	2.36786
SLC4A11	chr20	MS	BP	OK	1.46539	3.74037
THBD	chr20	MS	BP	OK	7.35114	41.8345
TMPRSS2	chr21	MS	BP	OK	2.56091	9.32321
SEC14L2	chr22	MS	BP	OK	0.868236	1.9992
HMOX1	chr22	MS	BP	OK	5.84251	201.602
PANX2	chr22	MS	BP	OK	3.03106	9.74817
MAPK8IP2	chr22	MS	BP	OK	1.80286	3.89027
LIF	chr22	MS	BP	OK	0.749343	2.74565
TRNT1	chr3	MS	BP	OK	9.74565	21.0589
LMCD1	chr3	MS	BP	OK	7.21158	21.9387
PPARG	chr3	MS	BP	OK	2.97566	11.4772
SLC6A6	chr3	MS	BP	OK	5.9205	20.1752
ATP1B3	chr3	MS	BP	OK	41.6034	84.693
MFSD1	chr3	MS	BP	OK	20.17	50.4716
IQCJ,IQCJ-SCHIP1,SCHIP1	chr3	MS	BP	OK	0.171387	1.11321
KCCAT211	chr3	MS	BP	OK	0.677292	2.00285
ST6GAL1	chr3	MS	BP	OK	0.677894	1.95755
PRRT3	chr3	MS	BP	OK	13.9405	31.1358
SLC4A7	chr3	MS	BP	OK	4.00223	9.41642
MGLL	chr3	MS	BP	OK	7.97009	26.9347
LXN	chr3	MS	BP	OK	89.5214	508.933
TNFSF10	chr3	MS	BP	OK	3.16142	7.38347
LIPH	chr3	MS	BP	OK	1.1993	2.80271
CLDN1	chr3	MS	BP	OK	0.779283	3.01806
LRRC15	chr3	MS	BP	OK	0.529176	1.40771
PCYT1A	chr3	MS	BP	OK	17.3582	34.7983
NAT8L	chr4	MS	BP	OK	2.34295	6.12973
ANXA3	chr4	MS	BP	OK	11.1302	37.4839
AGPAT9	chr4	MS	BP	OK	2.47253	12.3157
TLR2	chr4	MS	BP	OK	0.42391	2.27692
PALLD	chr4	MS	BP	OK	4.93146	17.0556
SNX25	chr4	MS	BP	OK	1.66655	3.76409
ABCG2	chr4	MS	BP	OK	4.73625	11.359
GPRIN3	chr4	MS	BP	OK	1.70617	3.51854
SLC7A11	chr4	MS	BP	OK	2.89424	12.4918
UBE2QL1	chr5	MS	BP	OK	1.30279	2.71886

FAM105A	chr5	MS	BP	OK	1.69996	4.07136
RAI14	chr5	MS	BP	OK	1.96312	5.45221
MAP1B	chr5	MS	BP	OK	0.246746	1.5113
F2RL1	chr5	MS	BP	OK	6.48504	14.3494
SLC12A2	chr5	MS	BP	OK	17.3236	50.0921
TGFBI	chr5	MS	BP	OK	9.71995	32.1289
SQSTM1	chr5	MS	BP	OK	86.2463	230.256
PLCXD3	chr5	MS	BP	OK	1.21121	2.83627
FAM169A	chr5	MS	BP	OK	1.17512	2.39397
LHFPL2	chr5	MS	BP	OK	5.04067	14.7649
LUCAT1	chr5	MS	BP	OK	0	1.10202
RUNX2	chr6	MS	BP	OK	1.45249	4.50158
RAB32	chr6	MS	BP	OK	7.84253	19.4102
TUBB2A	chr6	MS	BP	OK	6.24215	12.6586
CCND3	chr6	MS	BP	OK	19.0876	43.0712
TNFRSF21	chr6	MS	BP	OK	9.51115	20.4019
SLC17A5	chr6	MS	BP	OK	2.19572	4.80176
ME1	chr6	MS	BP	OK	13.8616	40.2739
MAN1A1	chr6	MS	BP	OK	3.20384	7.06729
FAM20C	chr7	MS	BP	OK	4.95249	10.5661
IL6	chr7	MS	BP	OK	0	1.55178
UPP1	chr7	MS	BP	OK	1.29389	7.14638
EGFR	chr7	MS	BP	OK	0.653778	1.56561
CROT	chr7	MS	BP	OK	6.45404	13.2955
ORAI2	chr7	MS	BP	OK	4.7087	9.52508
IFRD1	chr7	MS	BP	OK	11.9044	29.4647
AKR1B10	chr7	MS	BP	OK	1.29262	11.4868
MTRNR2L6	chr7	MS	BP	OK	6.40841	13.7596
ZYX	chr7	MS	BP	OK	24.5634	85.3438
STX1A	chr7	MS	BP	OK	4.07382	9.91442
CCL26	chr7	MS	BP	OK	0	2.35941
KIAA1549	chr7	MS	BP	OK	1.27848	2.7176
KIAA1147	chr7	MS	BP	OK	3.21148	7.68911
CLN8	chr8	MS	BP	OK	2.04271	4.64113
SDCBP	chr8	MS	BP	OK	22.1265	49.5401
RDH10	chr8	MS	BP	OK	4.72441	11.931
PSCA	chr8	MS	BP	OK	5.03375	16.8819
CSGALNACT1	chr8	MS	BP	OK	0.70724	2.20623
TNFRSF10A	chr8	MS	BP	OK	2.94612	6.36065
LOXL2	chr8	MS	BP	OK	2.86447	10.2349
ANKRD46	chr8	MS	BP	OK	5.53676	11.2671
TNFRSF11B	chr8	MS	BP	OK	6.66592	17.6564

ST3GAL1	chr8	MS	BP	OK	7.51172	49.5783
JRK	chr8	MS	BP	OK	2.15416	4.69514
SCRIB	chr8	MS	BP	OK	52.3913	192.587
CPSF1	chr8	MS	BP	OK	44.2017	193.464
DNAJA1	chr9	MS	BP	OK	128.691	281.235
C9orf47,S1PR3	chr9	MS	BP	OK	8.33377	37.303
WNK2	chr9	MS	BP	OK	2.2052	5.22976
C9orf3	chr9	MS	BP	OK	3.2278	8.63392
CYSRT1	chr9	MS	BP	OK	3.77992	10.3557
AQP3	chr9	MS	BP	OK	68.5803	214.4
NOL6	chr9	MS	BP	OK	11.2893	24.1885
FAM219A	chr9	MS	BP	OK	3.38284	7.5568
AAED1	chr9	MS	BP	OK	5.24152	11.8392
PTGR1	chr9	MS	BP	OK	13.5847	29.9858
NHS	chrX	MS	BP	OK	0.949663	2.27104
FAM155B	chrX	MS	BP	OK	1.0138	2.2087
RAI2	chrX	MS	BP	OK	0.668556	2.048
LOC401585	chrX	MS	BP	OK	0	1.68228
RGAG4	chrX	MS	BP	OK	2.27254	6.62343
L1CAM	chrX	MS	BP	OK	9.61206	35.9803
G6PD	chrX	MS	BP	OK	156.183	389.463

Downregulated genes from BP MCF7 Cell samples

Gene Name	Chromosome	Sample1	Sample2	Status	Value1	Value2
GABRD	chr1	MS	BP	OK	4.18334	1.52249
MST1P2	chr1	MS	BP	OK	3.08416	0.938822
CYP4B1	chr1	MS	BP	OK	5.84513	2.17816
CDKN2C	chr1	MS	BP	OK	13.6464	6.16617
CYR61	chr1	MS	BP	OK	24.5933	6.14334
PHGDH	chr1	MS	BP	OK	101.985	37.3391
HIST2H2AC	chr1	MS	BP	OK	58.1329	18.1773
NOS1AP	chr1	MS	BP	OK	3.46963	1.55455
IER5	chr1	MS	BP	OK	241.474	67.3384
NR5A2	chr1	MS	BP	OK	4.51864	1.22575
PCAT6	chr1	MS	BP	OK	14.947	6.20795
PPFIA4	chr1	MS	BP	OK	4.26419	0.620876
LINC00467	chr1	MS	BP	OK	12.133	5.62009
ATF3	chr1	MS	BP	OK	10.4726	4.39502
SPATA17	chr1	MS	BP	OK	3.15287	1.23294
MEGF6	chr1	MS	BP	OK	4.68514	2.11089
MFAP2	chr1	MS	BP	OK	10.4649	4.74004

TCEA3	chr1	MS	BP	OK	2.94826	0.982456
STMN1	chr1	MS	BP	OK	212.359	100.532
FAM46B	chr1	MS	BP	OK	10.9507	4.2723
GRIK3	chr1	MS	BP	OK	1.09833	0.52017
JUN	chr1	MS	BP	OK	132.836	47.3111
ITGB3BP	chr1	MS	BP	OK	24.3197	12.0193
RORC	chr1	MS	BP	OK	9.16978	3.09762
TMEM254	chr10	MS	BP	OK	21.3221	10.5814
ADRA2A	chr10	MS	BP	OK	2.25403	0.58173
DPYSL4	chr10	MS	BP	OK	6.74005	2.34211
ST8SIA6	chr10	MS	BP	OK	6.07977	2.12308
EGR2	chr10	MS	BP	OK	1.58201	0.226436
AFAP1L2	chr10	MS	BP	OK	3.12862	1.05982
GFRA1	chr10	MS	BP	OK	86.8281	34.0098
BNIP3	chr10	MS	BP	OK	153.466	43.2274
IFITM1	chr11	MS	BP	OK	81.517	38.2896
ZBED5-AS1	chr11	MS	BP	OK	6.37813	2.30345
MIR210HG	chr11	MS	BP	OK	2.78569	0.911351
ASCL2	chr11	MS	BP	OK	14.9831	6.86148
LRP4	chr11	MS	BP	OK	2.27751	0.710483
PGR	chr11	MS	BP	OK	3.11174	1.04894
FXYD2,FXYD6, FXYD6-FXYD2	chr11	MS	BP	OK	3.40407	0.713029
TMEM218	chr11	MS	BP	OK	3.35879	1.39684
METTL7A	chr12	MS	BP	OK	3.34781	0.778493
NR4A1	chr12	MS	BP	OK	126.055	14.1987
LRP1	chr12	MS	BP	OK	1.72241	0.75432
ASCL1	chr12	MS	BP	OK	44.5909	10.7534
P2RX2	chr12	MS	BP	OK	6.88318	3.31773
ING4	chr12	MS	BP	OK	15.2971	7.12238
CIT	chr12	MS	BP	OK	9.41693	4.17416
SHISA2	chr13	MS	BP	OK	9.67634	4.45637
SMAD9	chr13	MS	BP	OK	2.50891	1.14589
ADPRHL1	chr13	MS	BP	OK	10.9736	4.90528
DHRS2	chr14	MS	BP	OK	118.068	53.1984
PCK2	chr14	MS	BP	OK	78.27	37.8394
FOS	chr14	MS	BP	OK	382.114	24.1615
EVL	chr14	MS	BP	OK	186.062	82.1148
LINC00641	chr14	MS	BP	OK	5.38252	2.09831
C14orf93	chr14	MS	BP	OK	6.29485	3.09345
SLC7A8	chr14	MS	BP	OK	3.12562	0.878977
ALDH6A1	chr14	MS	BP	OK	21.2597	9.97808

EFCAB11	chr14	MS	BP	OK	13.4397	6.45043
DEGS2	chr14	MS	BP	OK	99.4525	46.1673
LOC100288637	chr15	MS	BP	OK	3.33517	1.48111
GCHFR	chr15	MS	BP	OK	26.5647	12.889
RCCD1	chr15	MS	BP	OK	22.7276	10.422
RASGRP1	chr15	MS	BP	OK	2.37658	0.987498
PIF1	chr15	MS	BP	OK	12.2167	4.10977
DET1	chr15	MS	BP	OK	5.1818	2.20186
MT2A	chr16	MS	BP	OK	269.068	70.1977
MT1X	chr16	MS	BP	OK	96.0845	23.8757
LINC01569	chr16	MS	BP	OK	3.7919	1.33683
LDHD	chr16	MS	BP	OK	12.6483	5.53366
SLC22A31	chr16	MS	BP	OK	4.64439	1.59544
FAM64A	chr17	MS	BP	OK	34.6993	15.3769
RAPGEFL1	chr17	MS	BP	OK	7.60472	3.6864
FZD2	chr17	MS	BP	OK	6.97954	3.08869
MAP2K6	chr17	MS	BP	OK	2.85528	0.350778
YBX2	chr17	MS	BP	OK	27.8528	8.56321
TP53	chr17	MS	BP	OK	88.398	43.3077
TMEM107	chr17	MS	BP	OK	11.5152	4.23188
HS3ST3A1	chr17	MS	BP	OK	14.0584	5.94986
LYRM9	chr17	MS	BP	OK	8.53619	2.59917
ALDOC	chr17	MS	BP	OK	84.1698	24.9848
PROCA1	chr17	MS	BP	OK	2.38614	0.788064
PRR15L	chr17	MS	BP	OK	42.4576	20.6772
TEX14	chr17	MS	BP	OK	6.32742	1.34961
AMZ2P1	chr17	MS	BP	OK	6.73802	3.27233
SDK2	chr17	MS	BP	OK	1.15632	0.418855
GADD45B	chr19	MS	BP	OK	53.533	17.6947
TNFAIP8L1	chr19	MS	BP	OK	3.13223	1.35613
IER2	chr19	MS	BP	OK	148.94	63.7485
CASP14	chr19	MS	BP	OK	2.70725	0.558583
ARHGAP33	chr19	MS	BP	OK	13.8803	3.54188
BCKDHA	chr19	MS	BP	OK	77.2719	37.9797
FOSB	chr19	MS	BP	OK	21.1927	1.21848
CCDC61	chr19	MS	BP	OK	9.14431	4.05778
PPP1R15A	chr19	MS	BP	OK	25.1424	11.3631
GAMT	chr19	MS	BP	OK	11.2322	4.78495
PLIN5	chr19	MS	BP	OK	4.41387	0.595951
EPOR	chr19	MS	BP	OK	5.99449	2.8713
ZNF850	chr19	MS	BP	OK	1.16992	0.507407

ZNF541	chr19	MS	BP	OK	1.39232	0.23604
TMEM143	chr19	MS	BP	OK	7.05567	2.86225
DBP	chr19	MS	BP	OK	27.5578	9.7823
KLK11	chr19	MS	BP	OK	185.482	87.1279
ZSCAN18	chr19	MS	BP	OK	4.54405	1.03901
KLF11	chr2	MS	BP	OK	9.47856	3.98721
GREB1	chr2	MS	BP	OK	133.213	64.6052
THNSL2	chr2	MS	BP	OK	10.1042	4.75317
SLC4A10	chr2	MS	BP	OK	1.5541	0.452234
PDK1	chr2	MS	BP	OK	13.8402	3.35931
FAM117B	chr2	MS	BP	OK	3.64823	1.81157
KCNE4	chr2	MS	BP	OK	33.3998	15.2768
SLC8A1	chr2	MS	BP	OK	1.62183	0.804317
LINC00342	chr2	MS	BP	OK	2.15022	0.797151
CXCR4	chr2	MS	BP	OK	61.2078	19.7941
RBM43	chr2	MS	BP	OK	3.14798	1.40896
NR4A2	chr2	MS	BP	OK	18.7457	4.73589
ABCA12	chr2	MS	BP	OK	16.3762	5.45275
SPAG4	chr20	MS	BP	OK	9.00511	3.05557
FAM83D	chr20	MS	BP	OK	46.8096	23.399
LINC00494	chr20	MS	BP	OK	18.1711	6.69982
MAFB	chr20	MS	BP	OK	35.5737	8.91101
LINC01522	chr20	MS	BP	OK	46.9755	20.9059
SYCP2	chr20	MS	BP	OK	12.395	5.95311
DSCR8	chr21	MS	BP	OK	45.2552	21.6431
PCP4	chr21	MS	BP	OK	246.032	113.592
TMPRSS3	chr21	MS	BP	OK	7.84049	2.61118
SIK1	chr21	MS	BP	OK	92.6307	27.3325
C21orf58	chr21	MS	BP	OK	15.2283	7.11415
ADM2	chr22	MS	BP	OK	1.56427	0.585045
PLA2G6	chr22	MS	BP	OK	3.36233	1.44814
DNAL4	chr22	MS	BP	OK	7.99405	3.88174
TTLL1	chr22	MS	BP	OK	3.42668	1.08357
DZIP3	chr3	MS	BP	OK	6.48244	2.11853
HES1	chr3	MS	BP	OK	561.124	65.8732
SRGAP3	chr3	MS	BP	OK	1.7744	0.645666
CSRNP1	chr3	MS	BP	OK	28.3925	5.92274
MST1	chr3	MS	BP	OK	2.76242	0.970352
CISH	chr3	MS	BP	OK	5.93475	1.98184
KIAA1407	chr3	MS	BP	OK	1.26329	0.459686
ALG1L	chr3	MS	BP	OK	23.3139	10.343
H1FX	chr3	MS	BP	OK	418.621	184.062

FRAS1	chr4	MS	BP	OK	1.51871	0.733811
ENPEP	chr4	MS	BP	OK	2.3647	1.1697
NMU	chr4	MS	BP	OK	6.35144	1.86006
UGT2B15	chr4	MS	BP	OK	9.28986	3.8664
HMGB2	chr4	MS	BP	OK	135.241	55.4489
FBXO4	chr5	MS	BP	OK	11.424	5.45482
GPX8	chr5	MS	BP	OK	2.3849	1.00286
CENPH	chr5	MS	BP	OK	33.259	15.4582
KIF20A	chr5	MS	BP	OK	34.0579	15.3945
EGR1	chr5	MS	BP	OK	68.0053	8.71083
PTTG1	chr5	MS	BP	OK	131.73	64.1339
HMMR	chr5	MS	BP	OK	26.7794	11.8342
SEPP1	chr5	MS	BP	OK	3.24463	1.19927
ARRDC3	chr5	MS	BP	OK	20.9876	9.96209
NREP	chr5	MS	BP	OK	6.99479	2.00517
FAXDC2	chr5	MS	BP	OK	8.2826	3.61634
DUSP1	chr5	MS	BP	OK	122.164	18.5287
DEF6	chr6	MS	BP	OK	7.16188	2.65631
PNRC1	chr6	MS	BP	OK	39.2521	18.8556
KCNK5	chr6	MS	BP	OK	5.65367	2.74678
CTGF	chr6	MS	BP	OK	26.3828	5.214
SGK1	chr6	MS	BP	OK	12.4451	5.80545
CITED2	chr6	MS	BP	OK	87.2873	34.8481
RAMP3	chr7	MS	BP	OK	18.5495	8.2339
RADIL	chr7	MS	BP	OK	3.11282	0.943617
LINC00174	chr7	MS	BP	OK	3.32227	1.11814
SEMA3A	chr7	MS	BP	OK	2.67903	1.1395
ASNS	chr7	MS	BP	OK	101.083	45.77
RASA4	chr7	MS	BP	OK	2.54205	1.05561
PLXNA4	chr7	MS	BP	OK	3.86009	1.7385
BNIP3L	chr8	MS	BP	OK	28.5755	12.5097
EPHX2	chr8	MS	BP	OK	3.4071	1.41557
C8orf46	chr8	MS	BP	OK	1.49584	0.369966
DEPTOR	chr8	MS	BP	OK	32.0459	11.6247
TRIB1	chr8	MS	BP	OK	45.7739	19.7385
MYC	chr8	MS	BP	OK	220.035	64.9307
EGR3	chr8	MS	BP	OK	21.4058	4.84159
PLAT	chr8	MS	BP	OK	3.82108	1.32667
GEM	chr8	MS	BP	OK	6.87955	2.87395
NDRG1	chr8	MS	BP	OK	69.3947	14.5765
TSNARE1	chr8	MS	BP	OK	7.13581	3.48226
LINC01604	chr8	MS	BP	OK	40.2464	13.2547

PARP10	chr8	MS	BP	OK	9.89325	4.37687
CA9	chr9	MS	BP	OK	18.2881	3.00862
TMEM8B	chr9	MS	BP	OK	3.23207	1.14022
GADD45G	chr9	MS	BP	OK	27.794	12.0449
NR4A3	chr9	MS	BP	OK	2.75911	1.02708
ZNF618	chr9	MS	BP	OK	2.43296	1.19579
COL27A1	chr9	MS	BP	OK	1.77041	0.532446
CNTRL	chr9	MS	BP	OK	3.03353	1.29765
OLFML2A	chr9	MS	BP	OK	1.19375	0.480089
ASS1	chr9	MS	BP	OK	121.428	53.4167
PTPRD	chr9	MS	BP	OK	1.38105	0.56444
ANKRD18A	chr9	MS	BP	OK	4.75748	2.22779
C5	chr9	MS	BP	OK	2.63997	0.97612
GYG2	chrX	MS	BP	OK	3.04484	1.37653
KLHL4	chrX	MS	BP	OK	12.6037	6.12868
TMEM187	chrX	MS	BP	OK	27.825	10.8771
PNPLA4	chrX	MS	BP	OK	3.07345	1.22027
MID1	chrX	MS	BP	OK	2.06519	0.982998
ZMAT1	chrX	MS	BP	OK	2.33809	0.601946
GPC3	chrX	MS	BP	OK	4.0926	1.66341
SOX3	chrX	MS	BP	OK	25.8994	7.9881
CH17-340M24.3	chrX	MS	BP	OK	18.2155	8.40622

Appendix II

Tissue Processing Protocol used in the MICROM STP 120 Tissue Processor

Step	Solution	Time (minutes)	Temperature (°C)	Stirring Rate (RPM)
1	50% Ethanol	5	25	60
2	60% Ethanol	5	25	60
3	70% Ethanol	5	25	60
4	70% Ethanol	5	25	60
5	95% Ethanol	5	25	60
6	95% Ethanol	5	25	60
7	100% Ethanol	5	25	60
8	100% Ethanol	5	25	60
9	Xylene	5	25	60
10	Xylene	5	25	60
11	Paraffin	15	60	60
12	Paraffin	30	60	60

Appendix III

Figure of tissue sample from a manually seeded MCF7 cell sample

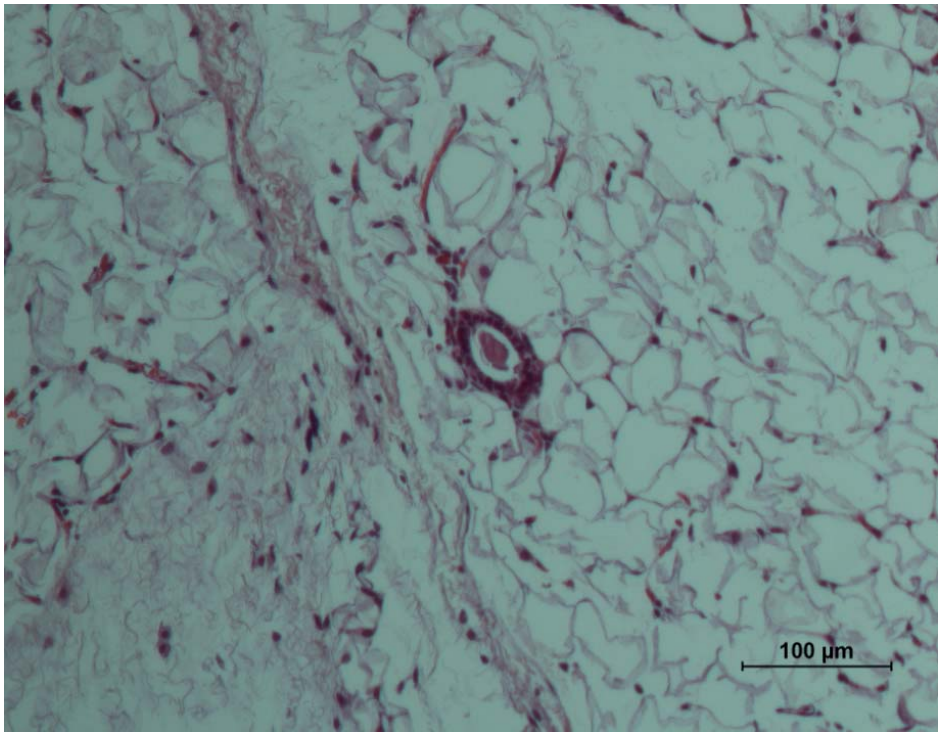

Figure of tissue sample from a BP MCF7 cell sample

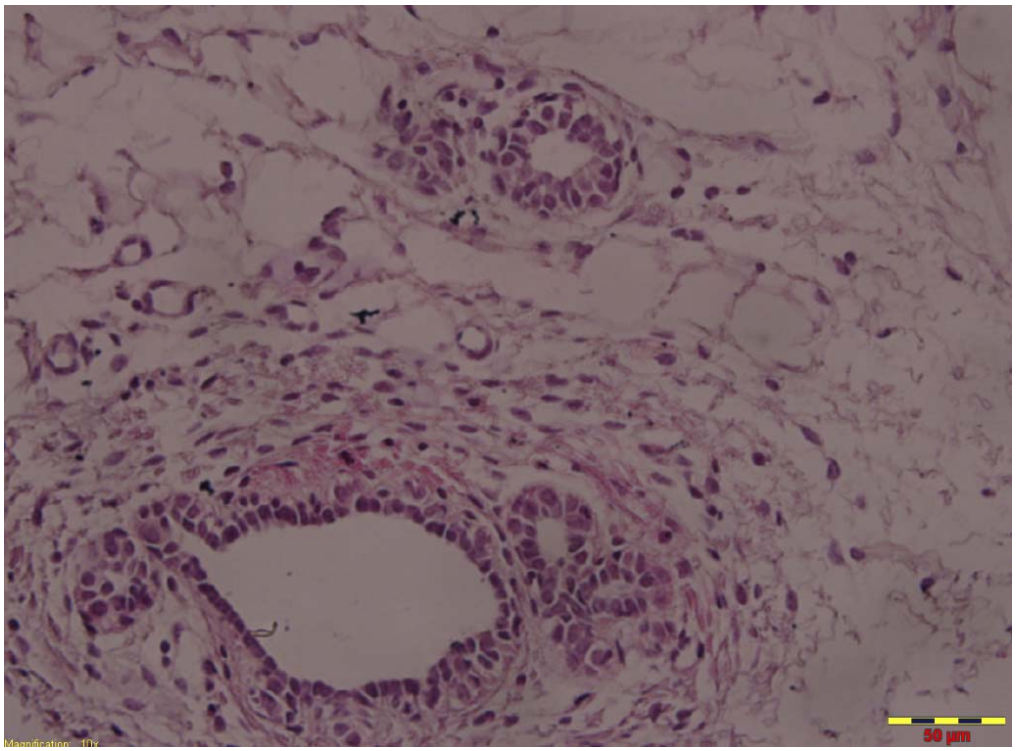

Figure of tissue sample from BP MCF7 cell sample

Curriculum Vitae

Aleli obtained a B.S. degree in Electrical Engineering, from the University of Texas at El Paso and a M.S. degree in Engineering Management from Dayton University. She has over 14 years of experience in the manufacturing industry, 11 years in advanced manufacturing (automotive field) and 3 years in the Medical Industry field, in program management. Aleli is known as an inspirational team leader, recognized for achieving measurable and significant results by effectively completing compliant manufacturing production transfers and setups from the ground up working collaboratively with employees locally and globally. She has held several positions, each with increasing responsibilities, including management positions. She started the Doctoral Program in Biomedical Engineering at The University of Texas at El Paso in the spring of 2014. During her doctoral studies she submitted 3 publications to high quality peer reviewed journals; in 2 of them, she has been first author and co-author in 1 publication. To date, 2 of her publications have been published and 2 of them are in peer review status and also another manuscript is in process. She also served as a Research Coordinator where she coordinated 10 Clinical Trials at Texas Tech University Health Sciences Center El Paso (TTUHSC El Paso): Celldex Study, A011106 Study, S1207 Study, E2112 Study, S0221 Study, S1007 Study, Coping with Cancer III Study (collaboration between TTUHSC El Paso and UTEP), B12 Study, ALPA Study and Neoadjuvant Study. Results of the phase II B12 clinical study were published in Feb/2018 where she was first author, and results from the ALPA study have been submitted for publication and it is in peer review status, she is second author.

During her undergraduate work she was awarded a grant to participate in a Research Experience for Undergraduates (REU) funded by the National Science Foundation at Michigan Technological University, where she designed and simulated GaAs-based Integrated Circuits.

- Aleli is a member of the American Society of Clinical Oncology (ASCO)
- The Golden Key International Honor Society (member by invitation only)

This Thesis was written by Aleli Campbell